INFORMATION TO USERS

This manuscript has been reproduced from the microfilm master. UMI films the text directly from the original or copy submitted. Thus, some thesis and dissertation copies are in typewriter face, while others may be from any type of computer printer.

The quality of this reproduction is dependent upon the quality of the copy submitted. Broken or indistinct print, colored or poor quality illustrations and photographs, print bleedthrough, substandard margins, and improper alignment can adversely affect reproduction.

In the unlikely event that the author did not send UMI a complete manuscript and there are missing pages, these will be noted. Also, if unauthorized copyright material had to be removed, a note will indicate the deletion.

Oversize materials (e.g., maps, drawings, charts) are reproduced by sectioning the original, beginning at the upper left-hand corner and continuing from left to right in equal sections with small overlaps. Each original is also photographed in one exposure and is included in reduced form at the back of the book.

Photographs included in the original manuscript have been reproduced xerographically in this copy. Higher quality 6" x 9" black and white photographic prints are available for any photographs or illustrations appearing in this copy for an additional charge. Contact UMI directly to order.

UMI

A Bell & Howell Information Company
300 North Zeeb Road, Ann Arbor MI 48106-1346 USA
313/761-4700 800/521-0600

Downloaded from SHAREOK. Persistent Handle URL: https://hdl.handle.net/11244/5747

THE UNIVERSITY OF OKLAHOMA

GRADUATE COLLEGE

SIMULTANEOUS DETERMINATION OF RELATIVE PERMEABILITY AND CAPILLARY PRESSURE FROM DISPLACEMENT DATA BY SIMULATED ANNEALING

A DISSERTATION

SUBMITTED TO THE GRADUATE FACULTY

in partial fulfillment of the requirements for the

degree of

DOCTOR OF PHILOSOPHY

by

Sezai Ucan

Norman, Oklahoma

1998

UMI Number: 9914400

Copyright 1998 by
Ucan, Sezai

All rights reserved.

UMI Microform 9914400
Copyright 1999, by UMI Company. All rights reserved.

This microform edition is protected against unauthorized
copying under Title 17, United States Code.

UMI
300 North Zeeb Road
Ann Arbor, MI 48103

Copyright © by SEZAI UCAN 1998

All Rights Reserved

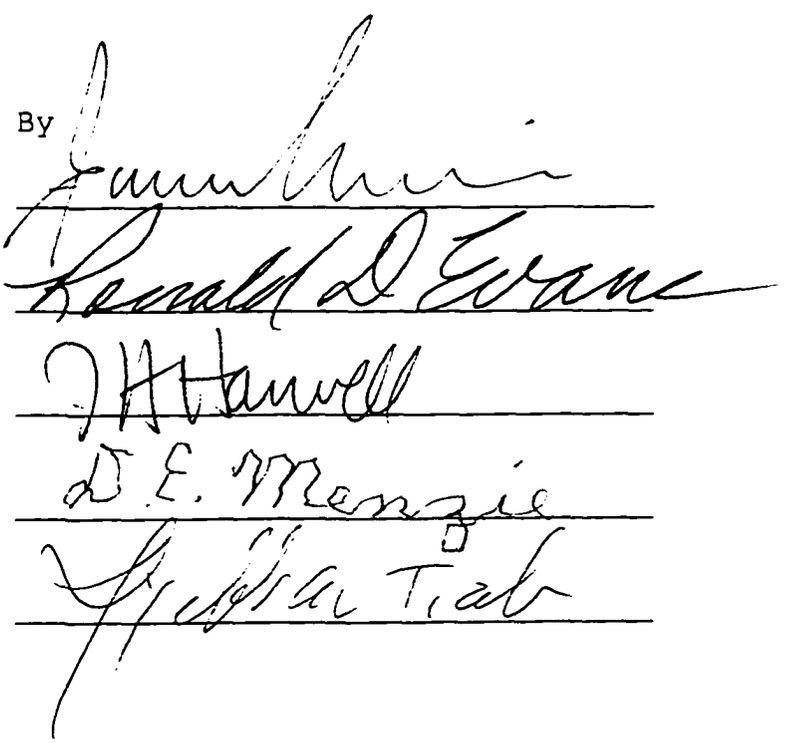
SIMULTANEOUS DETERMINATION OF RELATIVE PERMEABILITY AND CAPILLARY PRESSURE FROM DISPLACEMENT DATA BY SIMULATED ANNEALING

A DISSERTATION

APPROVED FOR THE SCHOOL OF

PETROLEUM AND GEOLOGICAL ENGINEERING

By



DEDICATION

To my dear parents, Kemal and Imhan, my brother Cemal, and my sisters Sultan and Nihal for their love and patience.

ACKNOWLEDGEMENTS

I would like to extend my sincere thanks to my advisor Dr. Faruk Civan for his continuos guidance, encouragement and comment during entire period of this work. It has been a valuable experience to learn and work with him.

I am greatly indebted to Dr. Ronald D. Evans, Dr. Djebbar Tiab, Dr. Donald Menzie, and Dr. Jeffrey Harwell for serving on my advisory committee. Their advise, suggestions, and help are gratefully appreciated.

The financial support provided by theU.S. Department of Energy and School of Petroleum and Geological Engineering at the University of Oklahoma is gratefully acknowledged.

Finally, I would like to thank my friends for their encouragement and support.

TABLE OF CONTENTS

Page

ACKNOWLEDGEMENTS v

LIST OF TABLES xi

LIST OF FIGURES xiii

ABSTRACT xviii

CHAPTER

I. INTRODUCTION 1

1.1 Objectives of the Study 2

1.2 Scope of the Study 9

II. LITERATURE REVIEW 12

2.1 Methods for Determination of Relative Permeability Curves 12

2.2 Forward (Direct) Methods 14

2.2.1 Steady-State Methods 15

2.2.2 Unsteady-State Methods 18

2.3 Inverse (Indirect) Methods 20

2.4 Pore Network Modeling 24

III. FORMULATION OF MATHEMATICAL MODEL 28

3.1 Introduction 28

3.2 Differential Equations for Multiphase Flow 28

3.3 Model Assumptions 30

Page

3.4 Unsteady-State Gas/Liquid Flow 34

3.5 Non-Darcy Flow 35

3.6 Steady-State Gas/Liquid Flow 37

IV. DESCRIPTION OF FINITE-DIFFERENCE MODEL 39

4.1 Introduction 39

Numerical Solution for Pressure .....

Equations 39

Grid System 40

4.3 IMPES Formulation 41

4.4 Calculating Interblock Transmissibility 44

4.5 Semi-Implicit Method 45

4.6 Initial Conditions 46

4.7 Boundary Conditions 46

4.8 Steady-State 47

4.9 Description of Numerical Model

Stability 48

V. FUNCTIONAL REPRESENTATION OF FLOW FUNCTIONS ... 52

5.1 Introduction 52

5.2 Discrete Points Representation 53

5.3 Global Exponential Functions 53

5.4 Local Cubic Spline Functions 54

VI. HISTORY MATCHING BY SIMULATED ANNEALING 59

Page

6.1 Abstract 59

6.2 Introduction 59

6.3 Global Optimization 65

6.4 Simulated Annealing (SA)Method and Its Parameters 67

6.4.1 Physical Analogy and Theory 67

6.4.2 Simulated Annealing Algorithm.... 70

6.4.3 Initial Temperature..... 72

6.4.4 Number of Iterations 74

6.4.5 Temperature Reduction Schedule... 75

6.4.5 Stopping Criteria 76

6.5 Objective Function for Estimation of Flow Functions 77

6.6 Final Remarks 80

VII. MODEL VALIDATION AND DATA ANALYSES 86

7.1 Unsteady-State Systems 86

7.1.1 Drainage Displacement I, Oil/Water system..... 86

7.1.2 Imbibition Displacement..... 90

7.1.3 Non-Darcy Flow Regime..... 94

7.1.4 Drainage Displacement II, Gas/Water System 96

Page

7.2 Steady-State Gas-Liquid Systems 98

7.2.1 Steady-State Gas/Brine System.... 98

7.2.2 Steady-State Nitrogen/Water System..... 102

7.3 Discussion 103

VIII. CONCLUSIONS AND RECOMMENDATIONS 156

NOMENCLATURE 158

REFERENCES 160

LIST OF TABLES

Table Page

6.1 Simulated Annealing Parameter 81

6.2 Coefficients of relative permeability and first and second derivatives at different knots 82

7.1 Core Properties and Operating Conditions, Simulated Imbibition Waterflood (Richmond and Watson) 106

7.2 Core Properties and Operating Conditions, Drainage Waterflood Expeiment (Richmond and Watson) 107

7.3 Summary of Application 108

7.4 Core Properties and Operating Conditions, Actual Gas/Water Draining (Ouenes at al.) 110

7.5 Core Properties and Operating Conditions, Simulated Gas/Water flow (Christiansen and Howarth) 111

7.6 Core Properties and Operating Conditions, Nitrogen and Water flow (Satik and Horne) 112

LIST OF FIGURES

Figure Page

4.1 Grid definition 50

4.2 Dirichlet and Well Type Injection Saturation Boundary Conditions. 51

6.1 Global and local minima 83

6.2 Flow chart of simulated annealing algorithm 84

6.3 Affect of random number on the initial temperatures for a range of changes on the objective function values according to the Metropolis algorithm 85

7.1 Comparison of experimental (forward) and assumed global functional representation of flow function (n1=2., n2=2., n3=2.) 113

7.2 Pressure drop and cumulative production history for the drainage experiment by using global functional representation (n1=2., n2=2., n3=2.) 114

7.3 Saturation history profiles for the drainage experiment by using global functional representation (n1=2., n2=2., n3=2.) 115

7.4 Comparison of experimental (forward) and

LIST OF FIGURES (continued)

Figure Page

estimated (inverse) representation of flow function by simulated annealing method (n1=5.1444, n2=2.8326, n3=2.4857) 116

7.5 Pressure drop and cumulative production history for the drainage experiment by using global functional representation (n1=5.1444, n2=2.8326, n3=2.4857) 117

7.6 Comparison of experimental (forward) and estimated (inverse) global functional representation of flow function 118

7.7 Comparison of experimental (forward) and estimated (inverse) local functional representation of flow function by simulated annealing method 119

7.8 Pressure drop and cumulative production history for the drainage experiment by using global and local functional representation..... 120

7.9 Pressure history profiles before the breakthrough for the drainage experiment 121

7.10 Pressure history profiles after the breakthrough for the drainage experiment 122

LIST OF FIGURES (continued)

Figure Page

7.11 Comparison of saturation history profiles using the estimated and initial flow functions 123

7.12 Comparison of initial and estimated discrete representation of flow function by simulated annealing Method (Ucan et al.) 124

7.13 Pressure drop and cumulative production history for the drainage experiment by using discrete representation of flow functions 125

7.14 Comparison of saturation history profiles for the imbibition experiment by using experimental and discrete representation of flow functions (Ucan et al.) 126

7.15 Comparison of initial and estimated local functional representation of flow functions by using external core data 127

7.16 Pressure drop and cumulative production history for the imbibition experiment by using local functional representation 128

7.17 Comparison of saturation history profiles using the estimated and initial flow

LIST OF FIGURES (continued)

Figure Page

functions 129

7.18 Comparison of initial and estimated local functional representation of flow functions by using internal and external core data 130

7.19 Pressure drop and cumulative production history for the imbibition experiment by using local functional representation 131

7.20 Pressure history profiles after the breakthrough for the imbibition experiment 132

7.21 Pressure history profiles after the breakthrough for the imbibition experiment 133

7.22 Comparison of saturation history profiles using estimated and initial flow functions 134

7.23 Effect of the inertial flow coefficient on the pressure drop 135

7.24 Effect of the inertial flow coefficient on the cumulative production rate 136

7.25 Effect of the inertial flow coefficient of saturation history profiles for Darcy and non-Darcy flows 137

LIST OF FIGURES (continued)

Figure Page

7.26 Effect of inertial flow coefficient on the pressure history profiles before the breakthrough for the drainage experiment 138

7.27 Effect of inertial flow coefficient on the pressure history profiles after the breakthrough for the drainage experiment 139

7.28 Minimization of the objective function at thereduced temperature for the imbibition experiment 140

7.29 Pressure drop history for the gas drainage experiment (Ouenes at al.) 141

7.30 Cumulative production rate for the gas drainage II experiment (Ouenes at al.) 142

7.31 Estimated relative permeability and capillary pressure curves obtained for the gas drainage II experiment 143

7.32 Saturation history profiles obtained for gas drainage II experiment 144

7.33 Pressure history profiles before the breakthrough for the gas drainage II experiment 145

LIST OF FIGURES (continued)

Figure Page

7.34 Pressure history profiles after the breakthrough for the gas drainage II experiment 146

7.35 Minimization of the objective function at the reduced temperature for the gas drainage II experiment 147

7.36 Relative permeability and capillary pressure curves for the simulated Darcy and non-Darcy flow 148

7.37 Saturation profiles for different total flow rate 149

7.38 Two phase pressure profiles for wetting and non wetting phases at different flow rates. 150

7.39 Affect of non-Darcy flow on the two phase pressure profiles 151

7.40 Affect of non-Darcy on the saturation profiles 152

7.41 Affect of non-Darcy flow on the relative permeability and capillary pressure curves. 153

7.42 Affect of non-Darcy on the saturation profiles 154

7.43 Relative permeability and capillary pressure curves for nitrogen-water system 155

ABSTRACT

A method for simultaneous estimation of relative permeability and capillary pressure data from unsteady-state and steady-state laboratory core flow displacement data is presented. Internal core flow measurements data are incorporated into the estimation of the flow functions, and the effect of the non-Darcy flow on the flow functions is analyzed.

The requirements for unique estimation of the two-phase flow functions are investigated. The number of observable parameters is increased by including both the external and internal data. The flow functions are represented by global empirical functions, discrete values, and piece-wise local functions. The simulated annealing method is implemented for non-linear global optimization. Applications to unsteady-state drainage and imbibition, and steady-state core flood tests are presented. Global functional representations of the relative permeability and capillary pressure data are shown to be insufficient. Discrete representations of the flow functions yield non-smooth functions. A piece-wise functional representation is shown to lead to unique determination of the relative

permeability and capillary pressure data when the transient-state internal saturation profiles and the overall pressure differentials are used together for history matching.

The method presented in this study can be used for accurate determination of the flow functions which are necessary for accurate description of flow behavior in hydrocarbon reservoirs and effective reservoir exploitation and management.

CHAPTER I

INTRODUCTION

Multiphase flow is a very common phenomenon in production from petroleum reservoirs. As the primary oil recovery decreases, secondary and tertiary oil recovery processes become more important in the exploitation of petroleum reservoirs, multiphase flow is commonly involved in porous media. Key features that describe the multiphase flow in porous media are the relative permeability and capillary pressure curves.

Relative permeabilities have been used to predict reservoir productivity, to describe rock-fluid interactions and wettability status of the rock, and to identify formation damage and reasons for low productivity. Capillary pressures have been used to describe the pore level processes, including the adsorption or desorption phenomena, hydrocarbon distribution in porous media, and migration of hydrocarbon from the source rock to the reservoir rock. Due to their wide variety of use, their importance and

their interdependency to each other, new technologies in laboratory measurement have always been an interest of industry.

Numerous investigations have been reported for the simultaneous estimation of capillary pressure and relative permeability functions from laboratory core data. Efforts have been made to gather internal core data such as saturation and pressure history profiles. These can be measured along the core by various techniques including gamma-ray attenuation, CT scanning, or NMR imaging. In addition, the overall pressure drop across the core and core production data are also measured. As new laboratory equipment and experimental techniques become available, various functional representations of relative permeability and capillary pressure are being investigated with a variety of interpretation methods and optimization techniques.

1.1 OBJECTIVE OF THE STUDY

The aim of this study is to develop a method to estimate relative permeabilities and capillary pressure curves simultaneously by means of the history matching of

unsteady-state and steady-state displacement data obtained from laboratory core flow tests. The limitations of conventional methods to estimate relative permeabilities and capillary pressure curves are addressed, and internal core data measurements have been incorporated into the estimation of flow functions.

Traditional methods for interpretation of the simultaneous immiscible fluid flow data to generate relative permeability and capillary pressure curves facilitate the external core data such as the production/injection rates and pressure drop histories. Flow functions can be obtained by laboratory experiments through steady-state, unsteady-state methods, and centrifuge methods. All these methods have some limitations, advantages, and disadvantages. Steady-state methods are time consuming and usually require a long time to obtain stabilization, but this is the simplest method to determine relative permeability and capillary pressure. Whereas, the unsteady-state method requires numerical or graphical differentiation of experimental data, which amplifies the errors when inaccurate measurements are used. In this method, it is usually difficult to describe the flow functions over the entire

saturation range of interest for low mobility ratio cases. The centrifuge method provides the relative permeabilities of the displaced phase only. The majority of the interpretation methods assumes incompressible fluids and Darcy flow, and no capillary pressure. The results from these experiments are valid for the macroscopic flow description if the details of the physical process in the pore structure level are omitted. Most of the methods assume that porosity and permeabilty distribution along the core are constant, and homogenous and, that irreducible residual saturation has been attained throughout the core. The usual assumptions include that; each fluid remains continuous, all flow is in the same direction, there is no channeling and formation damage in heterogeneous cores, operational problems such as viscous fingering and capillary end effects are difficult to monitor and account for properly in the estimation of flow functions, the sample cores are representative of internal reservoir rock and fluid properties, and the reservoir conditions are similar to the laboratory conditions. All these assumptions occur only in rare instances.

Capillary pressure curves are especially important to determine the fluid distribution in the reservoir and capillary trapping mechanisms in the reservoir. However, capillary pressure is usually neglected in relative permeability measurements by conventional methods. Neglecting the capillary pressure make the relative permeability curves independent of the flow rate for the Darcy flow and no Klinkenberg effect cases. Capillary pressure may be neglected for non-Darcy flow because the viscous forces dominate over the capillary forces. But for special cases, such as during flow through tight gas reservoirs or naturally fractured reservoirs, capillary forces will be as important as other parameters.

Extensive literature on indirect methods is also available for unsteady-state methods, but not for steady-state methods. In the steady-state method, saturation profiles are flat except over a short region near the inlet and outlet ends of the core due to capillary effect. In absence of pressure profiles, flat saturation profiles do not have a significant role in the estimation of the flow functions by history matching. Therefore, special experimental set up is required to measure the saturation profiles accurately at both the inlet and

outlet ends.

For gas/liquid systems, the non-Darcy flow effects are important to determine the shape of the relative permeability and capillary pressure curves and to represent the real phenomena occurring at reservoir conditions. At high velocities around the wellbore in gas wells, accurate representation of in-situ dynamic behavior of immiscible fluid systems, such as pressure and saturation distributions which are important for design and operation of well performance and propped hydraulic fracture, requires the consideration of the non-Darcy effect. By incorporating the non-Darcy flow in the estimation of flow functions, non-Darcy flow around the wellbore does not need to be treated by a skin factor.

Petrophysical properties of multiphase flow systems in porous rock are complex functions of the morphology and topology of the porous medium, interactions between rock and fluids, phase distribution and flow patterns and regimes. It is impractical to deconvolute the effect of the individual factors and forces from the macroscopic petrophysical properties. Therefore, the effect of these

properties on the flow behavior is lumped in the form of empirically determined relative permeability and capillary pressure functions which are used as the primary flow parameters for the macroscopic description of multiphase flow in porous media. However, development of reliable methods for simultaneous determination of relative permeability and capillary pressure data from laboratory core flood tests is a challenging task and is of continuing interest to the oil and gas industry.

Description of fluid flow in porous media can be accomplished with three main categories: transport phenomena, interfacial effects, and pore structure. There is a strong interaction between these categories. Macroscopic transport properties are based on the continuum approach. Topology and morphology of porous media are neglected in the continuum approach. Because the pore space is highly chaotic, complex morphology and topology challenge the implementation of pore structure models into the continuum laws to predict macroscopic transport properties. Any naturally occurring porous medium cannot be described exactly. But some important features that are relevant to the multiphase flow can be described quantitatively. The topology and morphology of

a given piece of rock can be reduced to an analogue of a three dimensional network model systematically by direct and indirect visualization of its pore structure.

When a problem is ill-posed, its solution may not necessarily be unique, and therefore perturbation of any model parameters may lead to arbitrary variations of the solutions. As demonstrated in the present study, observed values are quite sensitive to flow functions. In reservoir simulation, the flow functions are usually chosen as the first model parameters to be tuned for history matching. Presently, there are no satisfactory general theoretical flow functions available. For the prediction of two phase relative permeabilities alone, over thirty different empirical models have been proposed (Honarpoor et al., and Siddiqui et al.). Although these empirical models are applicable only to specific conditions, they have been selected arbitrarily without any particular basis in many applications.

Reservoir simulators have been used as a major tool for reservoir characterization and management. Before making any future performance prediction of the reservoir, the common practice is to validate the geological,

petropysical, pressure-volume-temperature(pVT), reservoir, and numerical models and their model parameters by past performance of the reservoir. This procedure is known as history matching or inverse problem in mathematics. Due to the issue of uniqueness, the past performance of a field can be matched by using different models and data sets. In this process, relative permeabilities have been used carelessly or misused to match the history performance of the reservoir. Some engineers do not rely on relative permeabilities at all and use them as superficial factors for history matching. Therefore, the future simulated performance of the field can never match the actual future performance of the field. Accuracy and reliability of the flow functions can be increased by using in-situ saturation profiles, local functional representations of relative permeability, and capillary pressure curves with a global optimization technique for history matching.

1.2 SCOPE OF THE STUDY

This study addresses the issue of uniqueness in the determination of relative permeability and capillary pressure functions by means of the history matching of

unsteady-state and steady-state displacement data obtained from laboratory core flow tests. History matching (the inverse problem) requires a reliable porous media averaged, macroscopic flow description model (the forward problem) to predict the values of the observable parameters such as cumulative production, histories of the pressure drop, and saturation profiles so that the best estimates of the relative permeabilities and capillary pressure functions can be determined. However, some model parameters may be overdetermined while others are underdetermined, unless the method of interpretation is designed to assimilate a proper set of experimental data. Lack of intrinsic data, experimental uncertainties, and an accurate physical representation of the complex flow affect the reliability of the predictions.

In this study, the uniqueness and simultaneous predictability of the flow functions are investigated. For this purpose;

1) The flow functions are chosen as the only model parameters to be estimated.
2) The number of observable parameters is enlarged by using both the external and internal data.

3) The flow functions are represented by global empirical functions, discrete values, and piece-wise continuous local functions.

4) A finite difference solution of the model is used to solve the equations of the multiphase for laboratory core flow tests.

5) The simulated annealing method is used as a non-linear global optimization technique. This method does not require the evaluation of the first or second gradients of the objective function and it usually converges to the global optimum without increasing the computational effort significantly.

6) The inlet and outlet boundary conditions, and capillary end effects are accounted properly for a core flood simulation.

7) Flow functions are estimated under different flow processes, such as drainage and imbibition.

8) Non-Darcy, visco-inertial, flow resistance effects for the relative permeabilities of both gas and oil have been studied.

9) Automated core flood simulators for steady-state and unsteady-state core flood tests have been developed for the simultaneous estimation of relative permeability and capillary pressure curves.

CHAPTER II

LITERATURE REVIEW

2.1 Methods for Determination of Relative Permeability Curves.

Different approaches for the determination of relative permeability have been reported in the literature since 1950. Many comparative studies have been written about estimation of relative permeability curves (Amyx et al. and Honarpour et al.). Generally, the estimation of relative permeability was organized under two direct broad categories as steady-state and unsteady-state techniques. Different experimental and interpretation methods have been introduced in the literature to eliminate or reduce the influence of capillary forces and other simplifying assumptions. These efforts can be classified in three main categories;

1- Direct (Forward) Methods

2- Indirect (Inverse) Methods

3- Pore Network Models

In direct methods, special experimental set-ups have been designed. On the other hand, for indirect methods, different kinds of automated history matching methods have been used to overcome the difficulties of the assumptions of direct methods. Direct methods are based on integral formulations of the equations describing the fluid pressure and saturations for laboratory cores (Civan and Evans). However, the pore network models attempt to relate the multiphase flow at the microscopic pore scale to the macroscopic phenomena observed at the laboratory core scale.

Numerous investigations have been conducted to study the validity of these assumptions and to estimate the capillary pressure and relative permeability data simultaneously. Efforts have been made to gather internal core data information such as the initial permeability, porosity, and saturation distribution along the core, and saturation and pressure history profiles during displacement experiments. These information can be measured along the core by the gamma-ray attenuation technique, CT scanning (Eleri, et al, Satik et al), or

NMR imaging (Enwere and Archer) in addition to the usual overall pressure drop and production data. Indirect methods and pore network models are starting to incorporate the internally measured core data information. The direct methods are usually limited from the point of incorporating the internal core data information.

2.2 Forward (Direct) Methods

The steady-state method is reported to be the most direct way to determine the relative permeabilities from coreflow test (Marle). Each point on a relative permeability vs. saturation curve is obtained by one experiment. In order to obtain the whole curve, the experiment has to be repeated under different flow-rate fractions. The second most widely used direct method is the displacement of initially saturated single phase fluid by injecting another phase in a core. In the unsteady-state experiments, transient data are gathered and used to calculate the relative permeability curves.

2.2.1 Steady-State Methods

In steady-state experiments, time dependent data is not observed, fluids are injected at a constant rate and pressure drop and saturation are not recorded until they reach stable values. Then, the flow rates and the fractions of injected fluid are changed to obtain the data of different fluid saturations and pressure drops for stabilized flow. A sequence of experiments is performed over a range of discrete saturation values. Depending on the permeability and porosity of the core, experiments can take a very long time.

In order to eliminate the effect of capillary pressure, different experimental methods have been introduced in the literature, and classified in three main sub-groups.

In the multiple core method or the Penn-State method, (MacAllister et al), the effects of the inlet and outlet of core boundaries are eliminated by sandwiching the core sample with two other cores. Injected two phases are distributed over a cross section by the upstream core before reaching the test core sample. Capillary end effects are reduced by the downstream core.

In high rate methods, (Maini et al, and Braun and Blackwell), two fluid phases are simultaneously injected into the core sample at a high flow rate so that the capillary end effect can be eliminated and a uniform saturation distribution can be obtained from the inlet of the core to the outlet of the core. However, high flow rate may also cause viscous fingering for a highly permeable medium.

In the stationary-liquid method, (Ning and Holditch), the relative permeability of a nonwetting mobile gas is measured in the presence of a wetting immobile liquid phase saturation. When low pressure gradients are used, capillary pressure and saturations are uniform throughout the core and the wetting phase will not mobilized. Obtaining only mobile phase relative permeability is the main disadvantage of this method.

Ramakrishnan and Cappiello set up a special experimental method to assure zero capillary pressure for the outlet boundary condition of the steady-state method. In this study, they did not attempt to establish uniform saturation in the core, in contrast to the traditional

methods mentioned above. One of the main drawbacks of this method is that it allows for calculating of only the nonwetting phase relative permeability.

Mitlin et al have extended the original method developed by Ramakrishnan and Cappiello. In their experimental setup, individual phase pressures were measured by a customized endcap and experimental procedure was extended to include variations in both the total rate and the ratio of the individual phase flow rates. In their numerical solution, gravitational forces and compressibility of the fluids are also considered.

Recently, Huang and Honarpour reported a methodology to correct the relative permeability curves for the capillary end effects. These corrections require the priori capillary pressure curves. In their study, the relationship and functionality between the capillary pressure curves and relative permeabilities are assumed to be known and based on the Corey-Burdine equation which approximates the porous media as a bundle of capillary tubes. Relative permeability and capillary pressure curves are also limited to the Brooks and Corey type of functional representation.

2.2.2 Unsteady-State Methods

Unsteady-state methods require measuring the pressure drop and average fluid saturation while a fluid is injected into the rock sample with known initial saturation conditions. The calculation procedure is more rigorous compared to the steady-state case. Whereas, unsteady-state experiments can be completed very quickly compared to steady-state cases.

For an unsteady-state two phase gas displacement case, Welge has outlined the method for calculating of the ratio of the two-phase relative permeabilities from the gas displacement method by differentiating the cumulative brine production from a rock sample with respect to the cumulative gas volume injected. Then, Johnson, Bossler and Naumann (JBN) presented a methodology to calculate the individual relative permeability curves from displacement experiments. In this method, relative permeabilities are calculated at the outlet of the core from the cumulative volumes produced, the pressure drop, and the time derivative of cumulative volumes produced and pressure drop. Both methods require high injection

rates to reduce the effect of capillary pressure. Generally, high injection rates in core experiments do not resemble reservoir displacement rates and may cause viscous fingering. Therefore, low rate methods have been introduced to simultaneously estimate the capillary pressure and relative permeability. Numerical history matching techniques have been used to include the capillary effects in the displacement processes. Centrifuge methods for measuring relative permeability have been adapted from centrifuge capillary pressure methods. By measuring the rate of fluid drained from a rock various centrifuge speeds, the capillary pressure relationship can be calculated. To obtain the relative permeability, the transient fluid production data at various spin rates is recorded, (O'Meara and Crump).

Toth at al have developed an analytical interpretation method to determine the saturation along the core for constant pressure differences and constant injection rates. A quadratic function was introduced to represent the saturation profile along the cores. In this study, capillary pressure is neglected. For viscous dominated flow, a quadratic function approximation of the saturation distribution is the leading accurate average

saturation value. For the imbibition experiment, it may be correct to assume that the injected phase saturation reaches its maximum value for high injection flow rates.

2.3 Inverse (Indirect) Methods

The simultaneous measurement of capillary pressure and relative permeability is a new development in the area of two phase flow measurements. Performance of the one dimensional simulator is matched with non-linear regression techniques to extract the observed parameters from unsteady-state experiments.

Various functional representations of relative permeability and capillary pressure curves with a variety of interpretation methods and optimization techniques have also been investigated. Kerig and Watson used a regression based method to estimate the relative permeability curves using a spline function representation. Richmond and Watson extended this regression based method for the simultaneous estimation of a functional representation of capillary pressure and relative permeability curves. Chardaire et al. used piece-wise linear functions to determine the relative

permeabilities and capillary pressure simultaneously by using a multi-scale representation of the parameters. Chardaire et al. have proposed an automatic adjustment method to determine the capillary pressure and relative permeability by using the optimal control theory. Ouenes et al. used a discrete representation of the relative permeability and capillary pressure by applying the simulated annealing method for Darcy flow of incompressible fluids. In these studies, the internal core data information has not been incorporated into the history match.

Firoozabadi et al have shown that it is possible to match the saturation profiles and recovery curves from a laboratory test by means of different forms of relative permeability and capillary pressure curves. They have pointed out that entirely different relative permeability models could match the same recovery performance. Thus, using only the recovery curves and overall pressure differential data, referred to as the external data, to represent the flow functions by empirical global functions does not guarantee a unique set of relative permeability and capillary pressure curves. As demonstrated in this study, internal core data

(saturation and/or pressure profiles) along with the conventional external data (overall pressure and effluent fluid production data) can help achieve unique solutions provided that sufficient experimental data are available for the fluid/rock system of interest.

For gas/liquid systems, the non-Darcy flow effects are important to determine the shape of the relative permeability and capillary pressure curves and to represent the real phenomena occurring at reservoir conditions. At high velocities around the wellbore in gas wells, accurate representation of in-situ dynamic behavior of immiscible fluid systems, such as pressure and saturation distributions which are important for the design, performance and operation of wells and propped hydraulic fractures require the consideration of the non-Darcy effect. By incorporating the non-Darcy flow into the estimation of flow functions, non-Darcy flow around the wellbore does not need to be treated by a skin factor.

Extensive literature on indirect methods is also available for unsteady-state methods, but not for steady-state methods. In the steady-state methods, saturation

profiles are flat except over a short region near the inlet and outlet ends of the core due to the capillary effect. In the absence of pressure profiles, flat saturation profiles do not have a significant role in the estimation of the flow functions by history matching. Therefore, a special experimental set up is required to measure the saturation profiles accurately at both the inlet and outlet ends.

In this study, for a steady-state case, the flow functions are generated specifically also to represent the saturation and pressure profiles along the core by automatic history matching. For this purpose, first, the Forchheimer equation is incorporated for multiphase non-Darcy flow and the forward model is solved numerically by the finite-difference method. Second, the simulated annealing method is applied as the non-linear global optimization technique for history matching. The predictability and uniqueness of the flow functions are investigated by using various saturation and pressure profiles data. The methodology is tested by two examples. In the first case, a simulated gas/brine system is used to generate the flow functions under Darcy and non-Darcy flow conditions and the results are compared with each

other. In the second case, experimentally measured saturation distribution by CT equipment for a nitrogen/water system in Berea sandstone is used to generate the relative permeability and capillary pressure curves simultaneously. Required experimental data types and the limitations of the method presented are also discussed.

2.3 Pore Network Modeling

The key step to understanding the dynamics of multiphase fluid in porous media is to relate the physics at the microscopic scale to the macroscopic phenomena observed in laboratory core tests. A theoretical model which can be treated mathematically can be developed from the Navier-Stokes equations and boundary conditions in the pore space.

Several pore level models have been proposed in the literature. These models are usually modified with respect to dimensionality and connectivity of pore space. The simplest models of a porous medium are based on a bundle of straight and parallel capillary tubes with uniform diameters. Later, this model was extended to

considering tubes of different diameters and lengths, (Dullien). In both cases, the flow was assumed to be in one direction. The capillary tube models neglect the fact that the fluid path may branch and later on join together. Fatt was the first to discuss a two dimensional model. The pore throats are represented by cylindrical tubes. Fatt assumed that there were non-dead end pores in porous medium, and no simultaneous two phase flow in the capillary channels. This original model was later extended by other researchers in terms of the connectivity and the shape of the pores.

Recent developments in the modeling of the porous medium is in the application of the effective medium theory (E.M.T.) to the network models. Koplik applied E.M.T. to creeping incompressible fluid flow in two dimensional networks. Using the Stokes equation for the pressure difference between the centers of two neighboring pore bodies connected by a throat, Koplik has shown that E.M.T. provides a reasonable approximation to flow in a two dimensional network.

Heiba et al. used a Bethe tree as an approximation to a porous medium. They introduced the transport-path

accessibility and transport-path conductivity functions to derive the general formulae for the relative permeabilities of two-phase systems.

Dias and Payatakes developed a network model for the immiscible micro-displacement of two phase flow in a porous medium. The porous medium was modeled as a network of randomly sized unit cells of the constricted tube. Under creeping flow conditions, they studied the effects of the viscosity ratio and capillary number on the micro-displacement efficiency.

Mohanti et al conducted studies on a cubic network for given pore throat and pore body size distributions. Primary drainage and imbibition capillary pressure curves and the relative permeabilities resulting from fluid distribution were determined. They also studied the dispersivity by network modeling and compared it with the experimental results.

E.M.T. is also used to predict the permeability alteration by matrix damage in sandstone formations. Khatib and Vitthal used a three dimensional network to calculate the absolute permeability and reduction of

permeability by E.M.T. Rossen and Kumar used the E.M.T. to analyze the effect of the fracture aperture distribution on the relative permeability curves for single-phase and two-phase flows in a natural fracture. They also extended the E.M.T. to the fluid flow non-Newtonian fluids in a porous medium and pointed out that E.M.T. cannot be used for simultaneous multiphase flow in two dimensions.

CHAPTER III

FORMULATION OF MATHEMATICAL MODEL

3.1 Introduction

This chapter presents the general mass conservation equations for isothermal flow in porous media. All the necessary assumptions are stated to derive two phase unsteady-state and steady-state flow equations in the core scale. Then the working equations for non-Darcy multiphase flow are also incorporated into the steady-state and unsteady-state flows.

3.2 Differential Equations for Multiphase Flow

The mass balance for the species equation is given by Lake as:

$$\frac{\partial W_i}{\partial t} + \bar{\nabla}.\bar{N}_i - R_i = 0 \qquad (3.1)$$

where i=1,...,N_c and N_c is the number of components.
The overall concentration of the component i ,[M/L^3] is given by

$$W_i = \sum_{j=1}^{N_p} \phi \rho_j S_j w_{ij} + (1-\phi)\rho_s w_{is} \qquad j = 1,\ldots,N_p \tag{3.2}$$

where N_p is the number of phases, ϕ is the porosity, fraction, w_{ij} is the mass fraction of component i in the phase j, w_{is} is the stationary mass fraction of component i on the rock surface, ρ_j is the fluid density of phase j, (M/L^3), ρ_s is the density of the rock, (M/L^3), and S_j is the saturation of phase j, fraction.

The mass flux of the component species i , $[M/(L^2T)]$ is given by

$$N_i = \sum_{j=1}^{N_p} (\rho_j w_{ij} \vec{u}_j - \phi \rho_j S_j \bar{\bar{K}}_{ij} \cdot \vec{\nabla} w_{ij}) \tag{3.3}$$

where $\vec{u}_j$ is the Darcy's velocity of phase j, [L/T], $\bar{\bar{K}}_{ij}$ is the dispersion coefficient tensor of component i in phase j, $[L^2/T]$. The total reaction rate of component i, $[M/(L^2T)]$ is given by

$$R_i = \sum_{j=1}^{N_p} \phi S_j r_{ij} + (1-\phi) r_{is} \tag{3.4}$$

r_{ij} is the homogeneous kinetic reaction rate of the component i in the j phase, and r_{is} is the stationary phase reaction rates. Substituting Eqs. 3.2-3.3, Eq. 3.1 becomes:

$$\frac{\partial}{\partial t}\left[\sum_{j=1}^{Np}\phi\rho_j S_j w_{ij} - (1-\phi)\rho_s w_{is}\right] + \vec{\nabla}.\left[\sum_{j=1}^{Np}\rho_j w_{ij}\vec{u}_j - \phi\rho_j S_j \bar{\bar{K}}_{ij}.\vec{\nabla}w_{ij}\right] =$$

$$\sum_{j=1}^{Np}\phi S_j r_{ij} + (1-\phi)r_{is} \qquad (3.5)$$

Eq. 3.5 is the general form of multiphase and multicomponent flow in porous media.

3.3 Model Assumptions

The present research interest; the following assumptions for a gas/liquid or a liquid/liquid system are made:

1) No chemical reaction: $R_i = 0.$

2) No dispersion: $\bar{\bar{K}}_{ij} = 0.$

3) No adsorption: $w_{is} = 0.$

4) Gas exists only in gaseous phase. Water and oil do not vaporize in to the gas phase: $w_{11} = 1.$

5) Only the gaseous and the aqueous phases exist: $N_p = 2.$

6) Isothermal flow, density is only a function of pressure.

7) One dimensional flow and gravity forces are included in the flow direction.

8) Compressible fluids and rock.

9) Newtonian fluids and Darcy law are applicable. (Note that the correction for non-Darcy flow is given later).

10) Permeability and porosity distribution are known and there is no channeling due to permeability or porosity contrast.

11) No viscous fingering.

Based on these assumptions, Eq. 3.5 takes the following form for the liquid and gas phases. The water continuity equations is presented by:

$$\frac{\partial}{\partial t}(\phi \rho_l S_l) + \frac{\partial}{\partial x}(\rho_l u_l) = 0 \tag{3.6}$$

Similarly, for the gas, including an additional term for the dissolved gas:

$$\frac{\partial}{\partial t}[\phi(\rho_1 w_{2l} S_l + \rho_2 S_2)] + \frac{\partial}{\partial x}(\rho_l u_l w_{2l} + \rho_2 u_2) = 0 \tag{3.7}$$

The formation volume factors according to the Black-Oil assumptions are given by:

$$B_w = \frac{\rho_w^s}{\rho_w} = \frac{Volume\ of\ water\ at\ reservoir\ condition\ (P,T)}{Volume\ of\ water\ at\ standard\ condition\ (P_s,T_s)} \tag{3.8}$$

$$B_g = \frac{\rho_g^s}{\rho_g} = \frac{Volume\ of\ gas\ at\ reservoir\ condition\ (P,T)}{Volume\ of\ gas\ at\ standard\ condition\ (P_s,T_s)} \tag{3.9}$$

$$R_s = \frac{w_{21}\rho_w^s}{w_{11}\rho_g^s} = \frac{w_{21}\rho_w^s}{\rho_g^s} = \left[\frac{Volume\ of\ dissolved\ gas}{Volume\ of\ water\ phase}\right]_{(P_s,T_s)} \tag{3.10}$$

Substituting Eqs. 3.8, 3.9, and 3.10 into Eqs. 3.6 and 3.7 yields:

$$\frac{\partial}{\partial t}\left(\phi S_w \frac{\rho_w^s}{B_w}\right) + \frac{\partial}{\partial x}\left(\frac{\rho_w^s}{B_w} u_w\right) = 0 \tag{3.11}$$

$$\frac{\partial}{\partial t}\left[\phi\left(\frac{\rho_g^s R_s}{B_w} S_w + \frac{\rho_g^s}{B_g} S_g\right)\right] + \frac{\partial}{\partial x}\left(\frac{\rho_g^s R_s}{B_w} u_w + \frac{\rho_g^s}{B_g} u_g\right) = 0 \tag{3.12}$$

It assumed assume that $(\rho_{w,g})_{Ts,Ps}$ does not depend on time and space. Under this assumption, each term in Eqs. 3.11 and 3.12 is divided by their respective standard densities to obtain:

$$\frac{\partial}{\partial t}\left(\frac{\phi S_w}{B_w}\right) + \frac{\partial}{\partial x}\left(\frac{u_w}{B_w}\right) = 0 \tag{3.13}$$

$$\frac{\partial}{\partial t}\left(\frac{\phi R_s S_w}{B_w} + \frac{\phi S_g}{B_g}\right) + \frac{\partial}{\partial x}\left(\frac{R_s u_w}{B_w} + \frac{u_g}{B_g}\right) = 0 \tag{3.14}$$

Eqs. 3.13 and 3.14 are the continuity balances for water and gas expressed in standard volumes. If the mass conservation equations for water and gas components are written with the source and sink or production and injection well terms $[L^3/(L^3T)]$, the results are:

$$\frac{\partial}{\partial t}\left(\frac{\phi S_w}{B_w}\right) - \frac{\partial}{\partial x}\left(\frac{u_w}{B_w}\right) + Q_w = 0 \qquad (3.15)$$

and

$$\frac{\partial}{\partial t}\left(\frac{\phi R_s S_w}{B_w} - \frac{\phi S_g}{B_g}\right) - \frac{\partial}{\partial x}\left(\frac{R_s u_w}{B_w} + \frac{R_s u_g}{B_g}\right) + Q_g = 0 \qquad (3.16)$$

S_w and S_g are the saturations of water and gas respectively and u_w and u_g are the Darcy velocities of the water and gas, respectively. B_w, B_g and R_s are the formation volume factors of the gas and water, respectively. Q_w and Q_g denote water and gas sources. The following auxiliary relations are required to determine the solutions. The saturations add up to one:

$$S_w + S_g = 1 \qquad (3.17)$$

The capillary pressure is given by:

$$P_c(S_w) = P_g - P_w \qquad (3.18)$$

The Darcy equations for water and gas phases are given by:

$$u_g = \frac{kk_{rg}}{\mu_g}\left(\frac{\partial P_g}{\partial x} - \gamma_g \frac{\partial z}{\partial x}\right) \qquad (3.19)$$

$$u_w = \frac{kk_{rw}}{\mu_w}\left(\frac{\partial P_w}{\partial x} - \gamma_w \frac{\partial z}{\partial x}\right) \qquad (3.20)$$

In Eqs 3.19 and 3.20, μ_w and μ_g are the viscosities of water and gas; k_{rw} and k_{rg} are the relative permeabilities for the water and gas phases; P_w and P_g are the pressures of water and oil phases; and γ_w and γ_g are the specific weights of the water and gas; and k is the permeability of the porous medium, respectively. The formation volume factors and viscosities are only functions of pressure and are used in a table format.

The rock compressibility is defined as:

$$C_r = \frac{1}{\phi}\frac{\partial \phi}{\partial P}\bigg|_T \qquad (3.21)$$

Where P is the saturation weighted average pore fluid pressure, (Civan and Evans.). The porosity can be approximated from the rock compressibility:

$$\phi = \phi_b \exp\left[C_r\left(P_o - P_b\right)\right] \qquad (3.22)$$

where:

C_r is the rock compressibility, $[LT^2/M]$, and ϕ_b is the porosity at the base pressure.

3.4 Unsteady-State Gas/Liquid Flow

Combining the Darcy equations with the mass conservation equations for each phase yields the following pressure-saturation equations:

$$\frac{\partial}{\partial x}\left(K_w\frac{\partial P_w}{\partial x} - \gamma_w\frac{\partial z}{\partial x}\right) + Q_w = \frac{\partial}{\partial t}\left(\frac{\phi S_w}{B_W}\right) \tag{3.23}$$

and

$$\frac{\partial}{\partial x}\left(K_g\frac{\partial P_g}{\partial x} - \gamma_g\frac{\partial z}{\partial x}\right) + \frac{\partial}{\partial x}\left(K_w R_s\frac{\partial P_w}{\partial x} + \gamma_w\frac{\partial z}{\partial x}\right) + Q_g = \frac{\partial}{\partial t}\left(\frac{\phi S_g}{B_g} + \frac{\phi R_s S_w}{B_w}\right) \tag{3.24}$$

where K_w and K_g are the conductivity of water and gas, defined as:

$$K_g = \frac{kk_{rg}}{B_g\mu_g} \tag{3.25}$$

$$K_w = \frac{kk_{rw}}{B_w\mu_w} \tag{3.26}$$

3.5 Non-Darcy Flow

The additional pressure drop that occurs during the high-velocity flow of fluid in porous media is taken into account by a correction factor according to the Forchheimer equation. For single phase flow, this equation reads as:

$$-\frac{\partial P}{\partial x} = \frac{\mu}{k}u + \beta\rho u^2 \qquad (3.27)$$

To express the apparent pressure drop under the non-Darcy flow conditions, the non-Darcy flow number is used (Wattenbarger and Ramey):

$$F_{nd} = \left(1 + \frac{\beta k \rho u}{\mu}\right)^{-1} \qquad (3.28)$$

where β is the non-Darcy flow coefficient. If β or u approaches zero, then F_{nd} approaches 1, and the flow assumes Darcy flow. The lower value of F_{nd}, less than one, is an indication of the non-Darcy flow regime. This approach can be extended for multiphase flow as, following Schulenberg and Muller:

$$-\frac{\partial P_i}{\partial x} = \frac{\mu_i}{k k_{ri}}u_i + \frac{1}{\eta \eta_{ri}}\rho_i u_i^2 \quad ; i = g, w \qquad (3.29)$$

In Eq. 3.29, k_{ri} is relative permeability for the Darcy flow; η_{ri} is the relative non-Darcy flow coefficient for each phase. η is the inverse of β. Schulenberg and Muller assumed that η accounts for the inertial pressure drop of a single phase flow through porous media. They attributed this term to the passability of porous media. They then defined relative passabilities η_{rg} and η_{rw} as

functions of the effective saturation and particle shape. They approximated the relative passabilities of water and gas as:

$$\eta_{rw} = S_w^{5} \tag{3.30}$$

$$\eta_{rg} = (1-S_w)^{6} \tag{3.31}$$

where S_w is the water saturation. The non-Darcy flow number for multiphase flow can be given as:

$$(F_{nd})_e = \left(1 + \frac{kk_{ri}\rho_i u_i}{\eta\eta_{ri}\mu_i}\right)^{-1} \quad i = g,w \tag{3.32}$$

Chung and Catton considered that k_{ri} and η_{ri} are very close to each other and assumed they were equal. Invoking this assumption, the non-Darcy flow number for multiphase flow becomes:

$$(F_{nd})_i = \left(1 + \frac{k\rho_i u_i}{\eta\mu_i}\right)^{-1} \quad i = g,w \tag{3.33}$$

in which:

$$\eta = \frac{1}{\beta} \tag{3.34}$$

3.6 Steady-State Gas/Liquid Flow

By using the chain rule for Eq. 3.18, substituting Eq. 3.33, into Eqs. 3.19 and 3.20, and neglecting gravity forces, the saturation distribution along the core can be written as follows, modifying the equation by Richardson et al for the non-Darcy effect:

$$\frac{\partial S_w}{\partial x} = -\frac{\dfrac{\mu_w u_w}{k\, k_{rw} F_{ndw}} - \dfrac{\mu_g u_g}{k\, k_{rg} F_{ndg}}}{\dfrac{\partial P_c}{\partial S_w}} \qquad (3.35)$$

As demonstrated by Richardson et al, the initial value problem defined by Eq. 3.35 can be solved to obtain the saturation distribution. However, in this study, considering pressure dependent fluid properties, Eq. 3.35 is solved simultaneously along with the pressure equation, which is given by:

$$-\frac{\partial P_w}{\partial x} = \frac{\mu_w u_w}{F_{ndw} k k_{rw}} \qquad (3.36)$$

The two first order ordinary differential equations, 3.35 and 3.36, require a set of two boundary conditions to obtain saturation distribution along the core.

CHAPTER IV

DESCRIPTION OF FINITE-DIFFERENCE MODEL

4.1 Introduction

This chapter describes the numerical solution procedure for the two phase flow equations for unsteady and steady-state cases. The grid definition, the source and sink terms, transmissibility allocation and boundary conditions are presented. The impact of Dirichlet and well type boundary conditions on the injection and production boundary for pressure and saturation equations are discussed. Semi-implicit and IMPES numerical solutions are compared based on the stability and time execution in the inverse solution.

4.2 Numerical Solution for Pressure Equations

There are two nonlinear partial differential equations;

$$\frac{\partial}{\partial x}[K_w(\frac{\partial P_w}{\partial x}-\rho_w\frac{\partial z}{\partial x})]-q_w=\frac{\partial(\phi b_w S_w)}{\partial t} \tag{4.1}$$

$$\frac{\partial}{\partial x}[K_g(\frac{\partial P_g}{\partial x}-\rho_g\frac{\partial z}{\partial x})]+\frac{\partial}{\partial x}[K_w R_s(\Delta P_w-\rho_w\Delta z)]-q_g=\frac{\partial}{\partial t}(\phi b_w R_s S_w+\phi b_g S_g) \tag{4.2}$$

The solution of these equations is succeeded in two

stages for each time step. First, water and gas pressure equations are solved simultaneously over the grid points. Then, block saturation equation is solved by using the pressure values.

In Eqs 4.1 and 4.2, q_w and q_g are the source and sink terms and the water and gas formation volume factors are given by

$$b_w = \frac{1}{B_w} \tag{4.3}$$

$$b_g = \frac{1}{B_g} \tag{4.4}$$

and water and gas conductivites are given by

$$K_w = \frac{k\ k_{rw}\ b_w}{\mu_w} \tag{4.5}$$

and

$$K_g = \frac{k\ k_{rg}\ b_g}{\mu_g} \tag{4.6}$$

4.3 Grid System

The grid system is constructed based on the core length L and uniform cross-section. A block centered grid system is used. The first and last grid points are placed at x=0 and x=L, respectively. For a uniform N grid node distribution, the intervals are given by

$$\Delta x_{i+\frac{1}{2}} = x_{i+1} - x_i \qquad 1 \le i \le N-1 \tag{4.7}$$

In writing the difference equations, it is convenient to define;

$$\Delta x_i = x_{i-\frac{1}{2}} + \Delta x_{i-\frac{1}{2}} \qquad 1 \le i \le N \tag{4.8}$$

This grid system is illustrated in Figure 4.1.

4.4 IMPES Formulation

The objective of this method is to obtain a single pressure equation by a combination of the mass balance equations. The IMPES method has been originally proposed by the Sheldon et al and Stone and Garder. Multiply Eq. 4.1 and Eq. 4.2 by $\Delta_x A$, where, A is cross flow area to obtain:

$$\Delta_x[T_w(\Delta_x P_w - \gamma_w \Delta_x z)] - q_w = \frac{V}{\Delta t}\Delta_t(\phi b_w S_w) \tag{4.9}$$

$$\Delta_x[T_g(\Delta_x P_g - \gamma_g \Delta_x z)] + \Delta_x[T_w R_s(\Delta_x P_w - \gamma_w \Delta_x z] - q_g = \frac{V}{\Delta t}\Delta_t(\phi b_w R_s S_w + \phi b_g S_g) \tag{4.10}$$

where the volume of each grid block is,

$V_i = A.\Delta_x.$

and, the transmissibility of water and gas are given by

$$T_{w,i+1/2} = [\frac{k\ k_{rw} b_w}{\mu_w}\frac{A}{\Delta_x}]_{i+1/2}$$

and

$$T_{g,i-1/2} = [\frac{k\, k_{rg} b_g\ A}{\mu_g\ \ \Delta x}]_{i-1/2} \tag{4.11}$$

Expanding the time derivative of the right hand side of

Eqs. 4.9 and .4.10 in a consistent manner according to the implicit pressure and explicit saturation (IMPES)method; we obtain for water:

$$\Delta_t(\phi b_w S_w) = (\phi b_w)_{n-1}\Delta_t S_w - (S_w)_n \Delta_t(\phi b_w)$$

or

$$\Delta_t(\phi b_w S_w) = (\phi b_w)_{n-1}\Delta_t S_w + (S_w)_n \phi_{n-1}\Delta_t b_w + (S_w b_w)_n \Delta_t \phi \qquad (4.12)$$

where the slope of nonlinearity is defined as;

$$\Delta_t b_w = b'_w \ \Delta_t P_w \qquad (4.13)$$

$$b'_w = \frac{b_{w,n-1} - b_{w,n}}{P_{w,n-1} - P_{w,n}} \qquad (4.14)$$

Using the definition of the rock compressibility;

$$C_f = \frac{1}{\phi}\ \frac{d\phi}{dp} \qquad (4.15)$$

$$\phi = \phi_b[1 + C_f(P - P_b)\ ] \qquad (4.16)$$

$$\Delta_t \phi \cong \phi_b C_f \Delta_t P \qquad (4.17)$$

The porosity, ϕ_b, is defined at the base pressure, P_b. Similarly expanding gas equation in the time derivative; we obtain:

$$\Delta_t(\phi b_w R_s S_w + \phi b_g S_g) = (\phi b_g)_{n-1}\Delta_t S_g + S_{gn}\phi_{n-1}\Delta_t b_g + S_{gn} b_{gn}\Delta_t \phi +$$

or

$$(\phi b_w R_s)_{n-1}\Delta_t S_w + S_{wn}\phi_{n-1}\Delta_t(R_s b_w) + S_{wn}(R_s b_w)_n \Delta_t \phi \qquad (4.18)$$

where

$$\Delta_t b_g = b'_g \Delta_t P \qquad (4.19)$$

$$b'_g = \frac{b_{gn-1} - b_g}{P_{g,n+1} - P_{g,n}} \qquad (4.19)$$

$$\Delta_t(b_w R_s) = (b_w R_s)' \Delta_t P \qquad (4.20)$$

$$(b_w R_s)' = \frac{(b_w R_s)_{n-1} - (b_w R_s)_n}{P_{w,n+1} - P_{w,n}} \tag{4.20}$$

The capillary pressure does not change over a time step because of explicit assumptions for saturation. Thus,

$$\Delta_t P_w = \Delta_t P_g = \Delta_t P_{pore\ pressure} \tag{4.21}$$

and

$$\Delta_x P_w^{n+1} = \Delta_x P_g^{n+1} - \Delta_x P_c^n \tag{4.22}$$

Since $S_w + S_g = 1.0$;

$$\Delta_t S_w = -\Delta_t S_g \tag{4.23}$$

if we put the Eq. 4.12 - Eq. 4.31 into the Eq. 4.9 and Eq. 4.10 and eliminate the ΔS term. After rearranging, we obtain the following matrix form of pressure equation:

$$AA(P_{wt-1})_{n+1}^{k+1} - BB(P_{wt})_{n+1}^{k+1} + CC(P_{wt-1})_{n+1}^{k+1} = R.H.S \tag{4.24}$$

k is the iteration index and n is the time step level. The coefficients of pressure equations are defined in the following way;

$$AA = A T_{wt-1/2} + C_{11} T_{gt-1/2} \tag{4.25}$$

$$BB = A(T_{wt-1/2} + T_{wt-1/2}) + C_{11}(T_{gt-1/2} + T_{gt-1/2}) + CT \tag{4.26}$$

$$CC = A T_{wt-1/2} + C_{11} T_{gt-1/2} \tag{4.27}$$

$$A = C_{11} R_S - C_{21} + C_{22} \tag{4.28}$$

$$CT = C_{20} C_{11} - (C_{21} - C_{22}) C_{10} \tag{4.29}$$

$$C_{10} = \frac{V}{\Delta t} S_{wn} [\phi_{n-1} b'_w + b_{wn} \phi_b C_f] \tag{4.30}$$

$$C_{11} = \frac{V}{\Delta t} (\phi b_w)_{n-1} \tag{4.31}$$

$$C_{20} = \frac{V}{\Delta t} S_{gn}[\phi_{n-1} b'_g - b_{gn} \phi_b C_t] + S_{wn}[\phi_{n-1}(R_s b_w)' - (R_s b_w)_n \phi_b C_f] \quad (4.32)$$

$$C_{21} = \frac{V}{\Delta t}(\phi b_w R_s)_{n-1} \quad (4.33)$$

$$C_{22} = \frac{V}{\Delta t}(\phi b_g)_{n-1} \quad (4.34)$$

$$GR = C_{11}[T_{gi-1/2}\gamma_g(z_{i-1} - z_i) - T_{gi-1/2}\gamma_g(z_i - z_{i-1})] +$$

$$C_{11}[T_{wi-1/2} R_s \gamma_w(z_{i-1} - z_i) - T_{wi-1/2} R_s \gamma_w(z_i - z_{i-1}] -$$

$$(C_{21} - C_{22})[T_{wi-1/2}\gamma_w(z_{i-1} - z_i) - T_{wi-1/2}\gamma_w(z_i - z_{i-1})] \quad (4.35)$$

The right hand side of equation, RHS, is defined as:

$$RHS = C_{11}(q_{gi})_n - (C_{21} - C_{22})(q_{wi})_n - CT(P_w)_n -$$

$$C_{11}[T_{gi-1/2}(P_{cgw,i-1} - P_{cgw,i})_n - T_{gi-1/2}(P_{cgw,i} - P_{cgw,i-1})_n] + GR \quad (4.36)$$

After solving the pressure equation, the saturation equation , Eq. 4.24, is solved and the saturation values are updated. The explicit saturation equation for new time step;

$$(S_{wi})_{n-1} = (S_{wi})_n + \frac{1}{C_{11}} \{T_{wi-1/2}(P_{wi-1} - P_{wi})_{n-1} - T_{wi-1/2}(P_{wi} - P_{wi-1})_{n-1} - q_{wi} -$$

$$C_{10}[(P_{wi})_{n-1} - (P_{wi})_n] + (S_{wi})_n + GR\} \quad (4.37)$$

4.5 Calculating Interblock Transmissibilities

Interblock transmissibilities are calculated bye one point upstream weighting method.

$$T_{wi-1/2} = \left[\frac{kk_{rw}}{\mu_w} \frac{b_w}{\Delta x} \frac{A}{\Delta x}\right]_{i+1/2} \quad (4.38)$$

$$T_{gi-1/2} = \left[\frac{kk_{rg}}{\mu_g} \frac{b_g}{\Delta x} \frac{A}{\Delta x}\right]_{i+1/2} \quad (4.39)$$

$$k_{rw,i-1/2} = W k_{rw,upstream} + (1 - W) k_{rw,downstream} \quad (4.40)$$

$$k_{rg,i-1/2} = W\,k_{rg,upstream} + (1-W)\,k_{rg,downstream} \qquad (4.41)$$

For upstream weighting, transmissibility of the inter-bloc is;

$$T_{w,i-1/2} = \frac{2\,k_i\,k_{i-1}}{k_i\,\Delta x_{i-1} + k_{i-1}\,\Delta x_i}\,\frac{b_w}{\mu_w}\,.\,A.\,k_{rw,upstream}\,. \qquad (4.42)$$

4.6 Semi-Implicit Method

The semi-implicit method attempts to approximate the nonlinearity in the saturation dependent properties. In the saturation equation, Eq. 4.37, the technique employed to approximate the nonlinearity in the relative permeability and capillary pressure is given by Nolen at al;

$$k^{n+1}_{rw,i-1/2} = k^{n}_{rw,i-1/2} + \frac{\partial k_{rw}}{\partial S_w}\left(S^{n+1}_{wi} - S^{n}_{wi}\right) \qquad (4.43)$$

$$P^{n+1}_{c,i-1/2} = P^{n}_{c,i-1/2} + \frac{\partial P_c}{\partial S_w}\left(S^{n+1}_{wi} - S^{n}_{wi}\right) \qquad (4.44)$$

Slop of the flow functions can be calculated easily for functional representation. If a table format is used, the slope is calculated by adding the δS_w, where δS_w is an arbitrarily specified increment of saturation, in a corresponding saturation. By substitution of Eqs 4.43 and 4.44 in to the Eq. 4.37 for each grid blocks, the new time step saturation values are calculated.

High rate unsteady-state two phase gas displacement tests suffer from stability limitations. Thus, it is required to use a very low time step in the simulation. However, the semi-implicit method allows to use a large time step. Thus, the required computing time to obtain flow functions in history matching is reduced by using a large time step in the semi-implicit method.

4.7 Initial Conditions

The initial condition for the pressure and saturation equations are given by

$$P_w = P_{initial} \quad 0 \le x \le L, \quad t = 0 \tag{4.45}$$

$$S_w = S_{initial} \quad 0 \le x \le L, \quad t = 0 \tag{4.46}$$

4.8 Boundary Conditions

The boundary conditions can be specified by rate or pressure. The source and sink terms, q_w and q_o, are taken zero everywhere except at the inlet and outlet blocks. A no-flow boundary condition is used at the inlet face of the first block, given by

$$\frac{\partial P_w}{\partial x} = 0. \qquad x = 0, \quad t \ge 0 \tag{4.47}$$

The boundary condition at the outlet face of the block for pressure before breakthrough is given by

$$\frac{\partial P_w}{\partial x} = 0. \qquad x = L, \quad t \geq 0 \tag{4.48}$$

and after breakthrough, the pressure is specified as outlet pressure:

$$P_w = P_{specified}, \quad x = L, \quad t \geq t_{bt} \tag{4.49}$$

As shown in Fig. 4.2, by using a well type boundary condition, the inlet saturation of the core will not rise to its maximum value. When the Dirichlet type saturation boundary condition is used, the inlet saturation is assigned its maximum value, which is not correct. Instead, the inlet saturation should increase gradually. The pressure drop history depends on the inlet saturation. In a capillary dominated core flood displacement, the inlet saturation boundary condition becomes important in the early period of test interpretation.

4.9 Steady-State

The two, first order ordinary differential equations, Eq. 3.35 and 3.36, require two boundary conditions. For numerical solution purposes, the core length is divided into N equal blocks and the integration of the initial value problem is carried out backward by starting from the core outlet face. The boundary conditions are:

$$S_w = 1 - S_{gc} - \varepsilon \quad ; \quad x = 0. \tag{4.50}$$

$$P_w = P_{specified} \quad ; \quad x = 0. \tag{4.51}$$

where ε is used as a sufficiently small number, such as 0.0001 for perturbation. A subroutine solver developed by Linda, R. Petzold for ordinary differential equations is used to solve two sets of first order ordinary differential equations, Eqs. 3,35 and 3.36.

4.10 Description of Numerical Model Stability

There are two possible stability limitations in the IMPES model. Instability comes from the explicit treatment of the capillary pressure and relative permeability. The nonlinearities involved with pressure dependent properties, fluid properties, may be negligible compared to the capillary pressure and relative permeabilities in a core scale simulation.

The treatment of these nonlinearities are outlined in the literature. For an incompressible two phase flow with zero capillary pressure and gravity forces, the stability condition can be formulated from the Buckley-Leverett theory. The velocity of a constant saturation is;

$$\left(\frac{\partial x}{\partial t}\right)_{Sw=constant} = u_s = \frac{q_{inj}}{A\phi}\frac{\partial f_w}{\partial s_w} \qquad (4.52)$$

Then, the stability condition can be expressed as;

$$\Delta t \leq \frac{\Delta x}{u_s} \qquad (4.53)$$

which means that the velocity of a constant saturation, the shock velocity, can not advance a distance of one grid block per the time step. For compressible flow and with non-zero capillary pressure, the stability condition is given by Aziz and Settari.

$$\Delta t \leq \frac{\phi \Delta x^2 \left(\frac{\mu_w B_w}{k_{rw}} + \frac{\mu_g B_g}{k_{rg}}\right)_{min}}{2\left(\frac{\partial P_{cwg}}{\partial S_w}\right)_{max} k} \qquad (4.54)$$

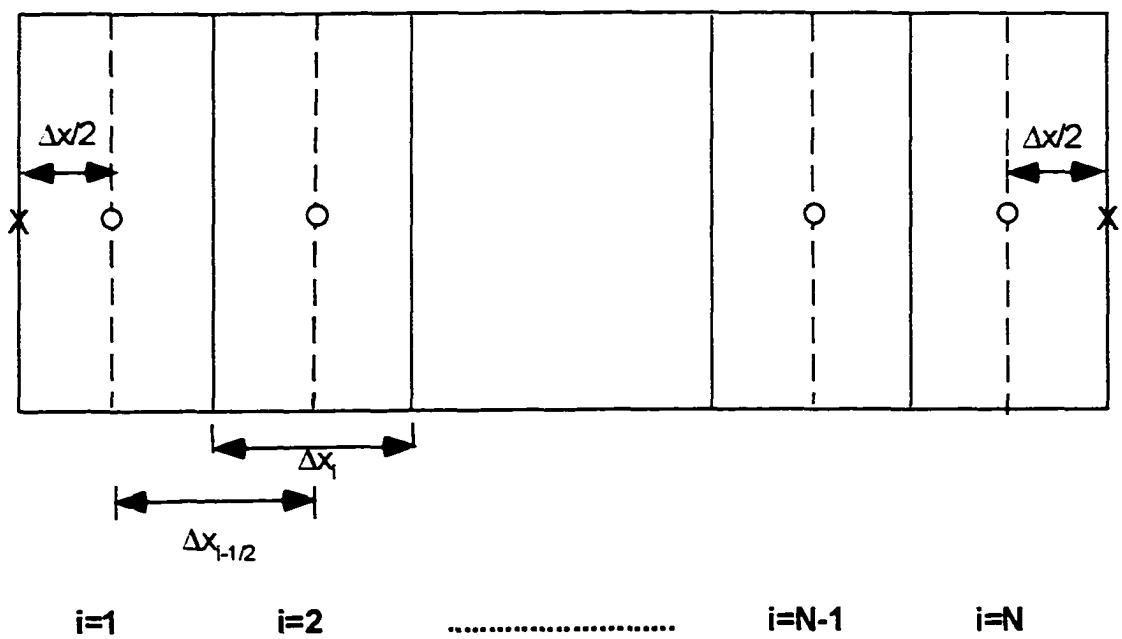


Fig. 4.1 : Grid System

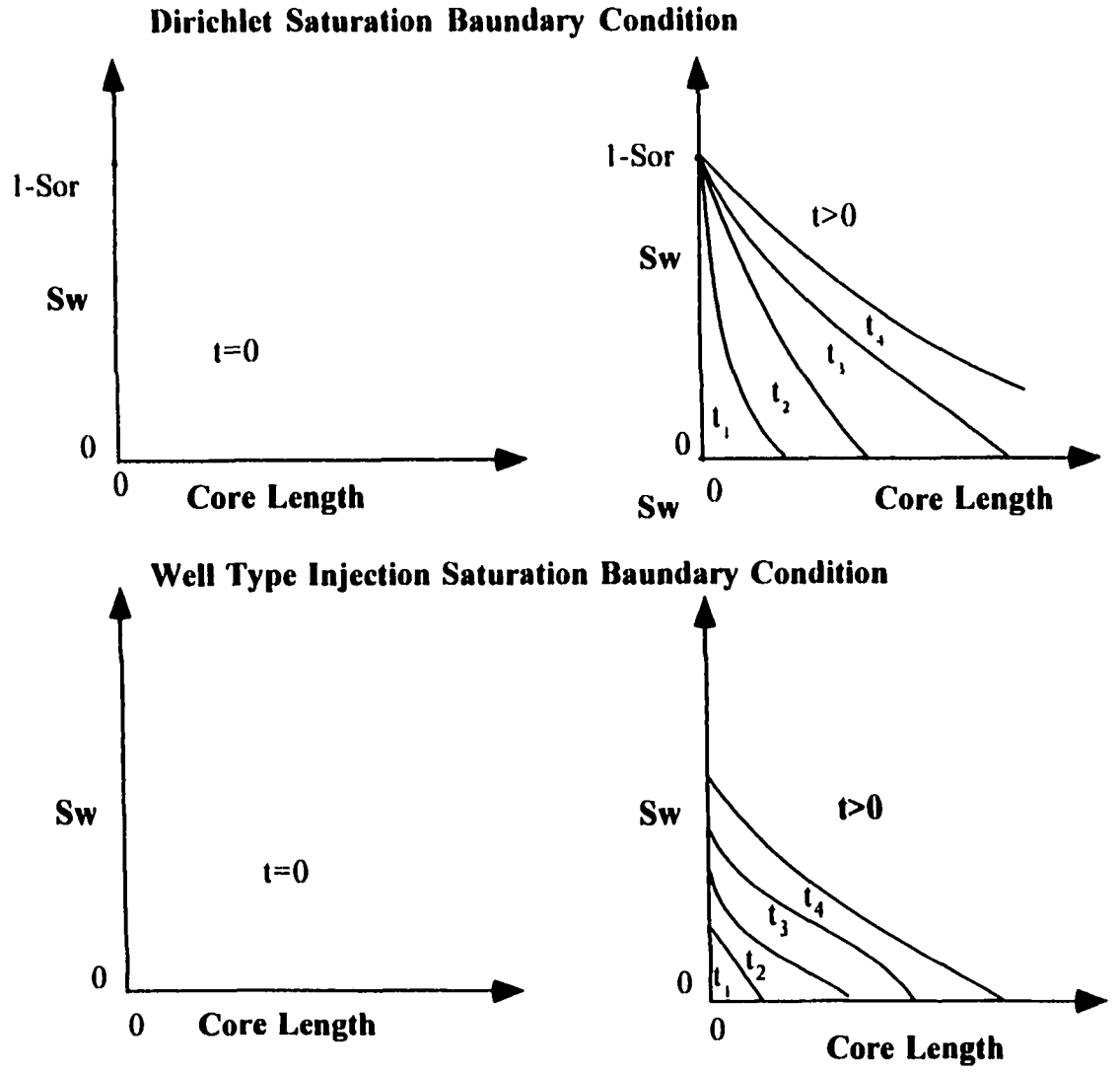


Fig. 4.2 : Dirichlet and Well Type Injection Saturation Baundary Conditions

CHAPTER V

FUNCTIONAL REPRESENTATION OF FLOW FUNCTIONS

5.1 Introduction

In industry, empirical exponential functional representation of flow functions is widely accepted and used because it is simple and implemented easily to the homogenous water wet or oil wet systems. However, when the uniqueness of the flow functions is questioned and core samples are obtained from a complex geological environment or mixed wet system, pre-assumption of the behavior of flow functions in an exponential function is not adequate and sufficient. In this study, different representations of flow functions are investigated by discrete points and local functional representation. The cubic splines as a local function for each saturation segment are used to describe the flow behavior. Finally the cubic spline representation is implemented

5.2 Discrete Points Representation

For a discrete description, the range of the initial to the residual saturations was divided into a number (N) of discrete points. Following Civan and Evans, the initial guesses for the flow functions were first assumed to be linear functions of saturation. The correct values of each flow function at discrete points were then determined by history matching.

5.3 Global Exponential Functions

The common form of the empirical expression used in the literature for a functional representation of the flow functions is the power law function of saturation. Thus, for oil and water flow, the relative permeabilities and the capillary pressure expression are given, respectively, by:

$$k_{rw} = k^{o}_{rw}(S_D)^{n_1} \tag{5.1}$$

$$k_{ro} = k^{0}_{ro}(1-S_D)^{n_2} \tag{5.2}$$

and:

$$P_c = P_{c,\max}(S_D)^{n_3} \tag{5.3}$$

where the normalized saturation is given by:

$$S_D = \frac{S_w - S_{wc}}{1 - S_{or} - S_{wc}} \qquad (5.4)$$

In this study, the n_1, n_2 and n_3 or P_{span} parameters were first determined for a global functional representation by history matching. The end-point relative permeabilities, k_{rw}° and k_{ro}°, were assumed to be known from transient well tests, and from the injection and production data. The maximum value of the capillary pressure, $P_{c,max}$ was also assumed to be known.

Eqs. 5.1-5.4 are the most frequently used forms among the various empirical functions proposed for the flow functions due to the lack of the existence of general theoretical expressions for the relative permeability and capillary pressure functions (see Honarpoor et al). These functions were proposed to fit the experimental measurements for the specific conditions.

5.4 Local Cubic Spline Functions

A single function for a single experiment can be determined usually for a data-set of limited size, monotonically increasing or decreasing with no inflection points. However, determining a single general function

for larger data sets and for strongly non-linear behavior is usually difficult and time consuming. Therefore, it is more practical to describe data locally in a piece-wise continuous manner by fitting a series of empirical functions over a series of inter-data segments. In this respect, cubic splines appear to be convenient. The relative permeability of water can be described by the following equation:

$$k_{rwi} = a_i S_D^3 + b_i S_D^2 + c_i S_D + d_i \qquad (5.5)$$

where a_i, b_i, c_i and d_i are fitting coefficients which assume different values over various segments and S_D is the dimensionless saturation defined by Eq. 5.4. For N data points, there are (N-1) intervals. Consequently, there are 4(N-1) unknown coefficients to be determined; i.e. $a_1, a_2, \ldots, a_{N-2}, a_{N-1}$; $b_1, b_2, \ldots, b_{N-2}, b_{N-1}$; $c_1, c_2, \ldots, c_{N-2}, c_{N-1}$; and $d_1, d_2, \ldots, d_{N-2}, d_{N-1}$. The continuity condition requires that the functional values at the interior points should be equal. Thus, the following set of equations can be written at various interior points:

$$k_{rw_i}^{-} = k_{rw_i}^{-} \qquad i = 1, N-2 \qquad (5.6)$$

$$a_1 S_D^3 + b_1 S_D^2 + c_1 S_D + d_1 = a_2 S_D^3 + b_2 S_D^2 + c_2 S_D + d_2$$
$$a_2 S_D^3 + b_2 S_D^2 + c_2 S_D + d_2 = a_3 S_D^3 + b_3 S_D^2 + c_3 S_D + d_3$$

....

$$a_{N-2}S_D^3 + b_{N-2}S - D^2 + c_{N-2}S_D + d_{N-2} = a_{N-1}S_D^3 + b_{N-1}S_D^2 + c_{N-1}S_D + d_{N-1} \quad (5.7)$$

On the other hand, the compatibility conditions require that the first and second derivatives at the interior points should be equal. Therefore,

$$\left(\frac{\partial k_{rw_i}}{\partial S_D}\right)^- = \left(\frac{\partial k_{rw_i}}{\partial S_D}\right)^- \qquad i = 1, N-2 \quad (5.8)$$

$$3a_1S_D^2 - 2b_1S_D + c_1 = 3a_2S_D^2 + 2b_2S_D + c_2$$
$$3a_2S_D^2 + 2b_2S_D + c_2 = 3a_3S_D^2 + 2b_3S_D + c_3$$
....
$$3a_{N-2}S_D^2 + 2b_{N-2}S_D + c_{N-2} = 3a_{N-1}S_D^2 + 2b_{N-1}S_D + c_{N-1} \quad (5.9)$$

and

$$\left(\frac{\partial^2 k_{rw_i}}{\partial S_D^2}\right)^- = \left(\frac{\partial^2 k_{rw_i}}{\partial S_D^2}\right)^- \qquad i = 1, N-2 \quad (5.10)$$

$$6a_1S_D + 2b_1 = 6a_2S_D + 2b_2$$
$$6a_2S_D + 2b_2 = 6a_3S_D + 2b_3$$
....
$$6a_{N-2}S_D + 2b_{N-2} = 6a_{N-1}S_D + 2b_{N-1} \quad (5.11)$$

In order to evaluate 4(N-1) constants, 4(N-1) conditions are required. An examination of the Eqs. 5.6, 5.8 and 5.10, indicates that there are 3N-6 conditions. However, N-1 constants, $a_1, a_2, \ldots\ldots, a_{N-2}, a_{N-1}$, can be estimated by the optimization method and three additional conditions can be obtained from the following end-point conditions:

$$k_{rw,1} = 0 \qquad S_D = 0 \quad (5.12)$$
$$k_{rw,N-1} = k_{rw}^0 \qquad S_D = 1 \quad (5.13)$$

$$\frac{\partial k_{rwI}}{\partial S_D} = C_I \qquad S_D = 0 \tag{5.14}$$

where, k_{rw}° is the end-point relative permeability which is assumed to be known and C_1 is the slope of relative permeability at the connate water and residual oil saturations, representing the degree of the wettability. This value can approximated or estimated by optimization as an additional parameter. For a strongly wet system, C_1 is very close to zero. Therefore, it is approximated to be zero. Thus, applying Eqs 5.12-5.14, Eqs 5.6, 5.8 and 5.10 leads to:

$$d_1 = 0 \tag{5.15}$$
$$b_{N-1} = k^0_{rw} - a_{N-2} - c_{N-2} - d_{N-2} \tag{5.16}$$
$$C_1 = 0 \tag{5.17}$$

Therefore, using Eqs 5.6, 5.8, and 5.10 at the first interior point, the following equations are obtained:

$$(b_1-b_2)S_D^2 + (c_1-c_2)S_D + d_1-d_2 = a_2S_D^3 - a_1S_D^3 \tag{5.18}$$
$$(2b_1-2b_2)S_D + c_1-c_2 = 3a_2S_D^2 - 3a_1S_D^2 \tag{5.19}$$
$$2b_1-2b_2 = 6a_2S_D - 6a_1S_D \tag{5.20}$$

From Eqs 5.18, 5.19 and 5.20, the following expressions can be derived:

$$d_2 = (a_1-a_2)S_D^2 + d_1 \tag{5.21}$$
$$c_2 = 3*(a_2-a_1)S_D^2 + c_1 \tag{5.22}$$

Consequently, only $a_1, a_2, \ldots\ldots, a_{N-2}, a_{N-1}$ need to be estimated initially to start the optimal search method.

Note that d_1 and c_1 are already calculated from the end point conditions (Eqs 5.15, 5.16), d_2 and c_2 can be calculated from Eqs 5.21 and 5.22. The remainder of the coefficients are determined by the recurrence relationship for the interior points, obtained from Eqs 5.21 and 5.22.:

$$d_i = (a_{i-1} - a_i) S_D + d_{i-1} \qquad i = 3, \ldots N-1 \tag{5.23}$$

$$c_i = 3(a_i - a_{i-1}) S_D + c_{i-1} \qquad i = 3, \ldots, N-1 \tag{5.24}$$

The coefficients of $b_{N-1}, \ldots, b_1$ are obtained by using Eq. 5.17 and Eq. 5.20 to obtain:

$$b_i = 3(a_{i-1} - a_i) S_D + b_{i-1} \qquad i = N-2, \ldots, 1 \tag{5.25}$$

A similar formulation is used for the non-wetting phase of relative permeability and the capillary pressure.

CHAPTER VI

HISTORY MATCHING BY THE SIMULATED ANNEALING METHOD

6.1 Introduction

The objective of this chapter is to present the general principles of the method, to highlight the important parameters that control the performance of the method, and to review its applications in reservoir engineering problems. As an application, the simultaneous estimation of relative permeability and capillary pressure curves from an unsteady-state drainage test is presented.

6.2 Introduction

The objective of any optimization method is to determine the best cases without actually testing all the possible cases by using a simple mathematical model and minimum computational effort. For this purpose, the engineering optimization problem should be formulated in such a

manner that it clearly describes the boundaries of the system under investigation, the set of operating conditions, and the independent variables that are adequate to characterize the operating conditions of the system. Before choosing any optimization method, the characteristic nature of the optimization problem should be identified. Characterization of multiphase flow properties in heterogeneous porous media is a nonlinear, multivariable, non-convex problem with multiple local minima, and nonlinear constraints. Conventional optimization methods can be classified in two simple categories: direct search methods and gradient based methods. Direct search methods such as the Simplex (S^2), Hooke-Jeeves Pattern and Powell's Conjugate Direction methods, need only an objective function evaluation but they are not well suited for global optimization problems with multiple local minimums. Similarly, gradient based methods such as Cauchy's, Newton's, Marquardt's, and the Conjugate Gradient methods require accurate values of the first and/or second derivatives of the objective functions with respect to the estimated independent variables.

It is known that if a problem is ill-posed, the solution

is not unique, or perturbation of any model parameters corresponds to arbitrary and large perturbation of solutions. Mathematicians believe that ill-posed problems do not have a physical sense, (Tarantola). However, for the reservoir engineer, an exact mathematical inversion is out of the question due to the uncertainty of data and lack of information. But ill-possedness of the problem can be alleviated by increasing the number of observable parameters, and by decreasing the number of estimated model parameters so that the maximum likelihood of predicting the performance of the reservoir can be increased.

In recent years, the number of models and their parameters to be validated by numerical simulation has been increased for integrated reservoir description and prediction of future performance of the reservoir. Due to the high number of model parameters and their broad solution domain, the characterization of the reservoir, which is formulated as an optimization problem, has a complex combinatorial nature and more than one local optimum. Generating all the possible alternatives is time consuming and not economical. For these reasons, different optimization techniques have been introduced in

the petroleum literature, (Carter, Chen, Chavent, and Dogru), of past decades. However, most of these methods used gradient based deterministic local optimization techniques, (Aarts and Eglese).

Simulated annealing (SA), (Kirkpatric), has been used as a global stochastic optimization technique as compared to deterministic local optimization techniques in order to avoid trapping in one of the local optima, to incorporate all measured data as constraints, to be able to use a hybrid approach with other heuristic methods, and to implement this in an easy and fast manner. In this method, the first or second order gradients (Hessian matrix) of the objective function, which are very expansive to calculate with respect to estimated model parameters by numerical simulation, do not need to be calculated like any gradient based method. The main disadvantage of SA is its high run times due to its stochastic nature. The efficiency of the method can improved by specially assigned computer architectures and parallelization strategies, (Panda and Ouenes).

This algorithm was first introduced by Metropolis in 1953 to simulate a collection of atoms in a solid at a given

temperature. In 1983, this algorithm was applied to optimization problems by Kirkpatric and others. Since then, the Simulated Annealing algorithm has been applied to optimization problems in such areas as computer design, image processing, molecular physics and chemistry, job scheduling and geoscience. It was first used in petroleum engineering and geology to generate the stochastic reservoir parameters (Farmer)

SA has been applied extensively to different reservoir engineering problems such as: characterization of the permeability field, fracture properties and patterns, estimation of relative permeability and capillary pressure curves, evaluation of well testing parameters, construction of reservoir simulation grids, (Farmer), and interpretation of quantitative well log evaluation, (Zhou, Szucs and Civan). Sen et al used SA to determine the 2D permeability distribution by matching the experimental variograms and tracer test responses. Ouenes et al is also used to condition the permeability field in a multi-layer actual reservoir by honoring all the measured data. Gupta et al applied SA to describe the detailed properties of fracture and distribution with a very high number of unknown parameters. Ucan et al used

SA to estimate relative permeability and capillary pressure simultaneously for unsteady-state non-Darcy displacement.

One of the main advantages of SA is to be able to incorporate diverse types of information by building a wide range of objective functions. For instance, the objective function can honor the specified variograms with the correlation length which is obtained from the analog outcrops and can simultaneously match the effective average properties obtained from well tests. At the same time, vertical distribution of the properties in the wells can also be conditioned by core and well log data. The objective function is not limited to match variograms but also production, pressure histories, saturation history profiles (core scale), and 3D images of reservoir lithofacies which are obtained from seismic and geological models.

The aim of this chapter is first, to give a brief theory of the method, to outline the general principles, and to emphasize on the important parameters that control the performance of the method. Then, one application is presented on the simultaneous estimation of relative

permeability and capillary pressure curves for the unsteady-state drainage test. By this application, it has been observed that SA is as easy to implement as a global optimization method. SA has shown great potential to obtain a unique set of relative permeability and capillary pressure curves by using the internal core data saturation history profiles along with the conventional external data, overall pressure, and effluent fluid production data.

6.3 Global Optimization

Traditional deterministic gradient-based methods for optimization are inadequate for global optimization methods. Because the gradient based-methods give a monotonicly decreasing value of the objective function, they will likely to converge to a local minimum rather than to a global minimum. As presented in Fig. 6.1, if there are several local minimum solutions, then globally minimum solutions can be found only if the gradient-based methods are started at an initial configuration, which is very near the global minimum configuration. It is generally accepted that there is no exact method for solving global optimization problems containing many

variables. Two traditional methodologies are applied to solve global optimization problems. In the first type, the problem can be divided into smaller sub-problems. Then, the sub-problems are solved and the solutions of the sub-problems are recombined to create the total solutions. This type of solution method is problem specific. The second type of method for solution is iterative improvement which accepts only the configurations which provides a decrease in the cost of the objective function. Iterative improvement methods are likely to result in local minimal solutions but this would be extremely rare. In order to find a globally optimal solution, a multi-start approach of the iterative improvement method with a different initial configuration is required. However, this method becomes very tedious and time consuming. That is why it is desirable to use a method that yields globally minimal solutions irrespective of the initial starting point.

The procedure should be conducted in such a way that the method will be different from the purely random search. Simulated Annealing is a combinatorial globally optimization method that always accepts that any solution results in an improvement in the cost of the objective

function. However, occasional solutions that increase the cost of the objective function are also accepted. The occasional up-hill moves are accepted according to the Metropolis acceptance criterion. A control parameter is introduced into the system that determines the amount of up-hill moves. The objective of these up-hill moves are to escape locally minimum solutions and to settle into globally minimum solutions.

6.4 Simulated Annealing and its Parameters

6.4.1 Physical Analogy and Theory

A heat-treated metal can be cooled by one of three processes: (1) Quenching, where the heated substance is immersed in water or oil to cool very quickly; (2) Normalizing, where the heated solid cools at room temperature; and (3) Annealing, where the solid is cooled slowly by controlling the rate of cooling. The physical properties of the final product depends on the procedure of the cooling schedule.

Simulated annealing derives its name from the physical analogy of the annealing of solids. The similarity

between a combinatorial optimization problem and statistical mechanics was first observed by Kirkpatric. Statistical Mechanics involves determining the lowest energy ground state of a physical system with many interacting atoms. The system of atoms can be characterized at any temperature (T) by the Boltzmann probability factor given by;

$$P = \exp\left(\frac{-E(r)}{k_b T}\right) \qquad (6.1)$$

Where E(r) is the energy associated with atomic position, r, T is the temperature, and k_b is the Boltzmann's constant. At a specified temperature, the process randomly perturbs the position of an atom and subsequently determines the change in the energy of the system, E(r). From the Eq. 6.1, it can be seen that when the temperature of the system is high, the probability of acceptances ,P, is close to one. On the contrary, as the temperature approaches zero, the probability of acceptances also vanishes.

Under equilibrium, the most probable states at any given temperature are those with the lowest energy states as the temperature is lowered. Low temperature is not a sufficient condition for the ground state of matter. It

is known that when crystal growth is performed without any melting or annealing of the substance, crystal structure may have many defects and ground state is metastable. Because the individual atoms are not allowed to adequately search their neighborhood space for a ground state, moving from the non-optimal state to a more stable state can be achieved by raising the temperature or melting the substance.

The analogy between the annealing of solids and the optimization problems can be summarized in the following manner. The states of a system correspond exactly to the configuration of the optimization problem. Energy is parallel to the value of the objective function or the cost function. The temperature for careful annealing is similar to a major control parameter that controls the performance of the optimization problem. The thermal equilibrium is referred to as a steady-state energy level which is obtained by a set of possible configurations at each temperature. Ground state is like the optimal solution. Quenching or suddenly lowering the temperature of a substance resembles iterative improvement.

6.4.2 SA Algorithm

In order to apply the SA method, a number of decisions have to made before its application. As shown in Table 6.1, these are divided into two groups. First, the decisions are related to the annealing schedule: 1) Initial temperature, 2) Number of iterations, 3) Temperature Reduction Schedule, and 4) Stopping criteria. Secondly, decisions related to the real problem are solved. The components of a specific problem are: 1) Representation and evaluation of the objective function, 2) Prescribing a specific number of constraints, 3) Initial solutions, and 4) Perturbation of the problem or neighbor generation.

The flow chart of the method is given in Fig. 6.2. First, the arbitrary initial model parameters have been selected, and the initial high annealing temperature has been chosen. Then, simulated annealing is implemented under two different loops. The first loop, the outer loop, updates the temperature for the cooling schedule. The second loop, the inner loop, updates the number of iterations for constant temperature. In the inner loop, the objective function (J_i) is then calculated by means

of the numerical solution of the flow model (the forward problem). The analysis of the new objective function follows according to:

1. By perturbing the estimated model parameter, the new objective function, (J_{i+1}), is calculated.

2. If the new solution poses a downhill move, $J_{i+1}<J_i$, then the new perturbed flow function is unconditionally accepted as the new configuration.

3. If the new solution poses an uphill move, $J_{i+1}>J_i$, it will still be accepted only if the Metropolis acceptance rule is satisfied. Otherwise, the nonimproved new configuration is rejected and a new configuration is generated through neighborhood search of the model parameters.

The acceptance of the uphill moves depends on the value of $\exp(-\Delta J/T)$ where $\Delta J=J_{i+1}-J_i$ and T is the temperature. Because ΔJ is always positive for an uphill move and T is also always positive, the value of $\exp(-\Delta J/T)$ will always be between (0,1). A random number, generated from a uniform (0,1) distribution, is compared with the value of $\exp(-\Delta J/T)$. The uphill move is accepted if, and only

if, the random number is less than the exponential number, $\exp(-\Delta J/T)$. Acceptance of uphill moves is based on the random number which indicates that SA has a stochastic nature. If both the left and the right neighbors search leads to higher costs, ($\Delta J>0$), the decision to accept either uphill move is based on the magnitude of the potential move that is the move with the lowest ΔJ.

In the outer loop, when the convergence of the algorithm reaches a certain number of iterations, which indicates the equilibrium state condition (i.e. steady-state condition) for assuring the convergence of the algorithm at current temperature, the temperature is then decreased to reduce the probability of the acceptance of nonimproved solutions. As the process cools, uphill moves become less likely.

6.4.3 Initial Temperature

At the beginning of the optimization processes, an initial temperature needs to be selected. If a low temperature is selected, the simulated annealing method is not likely to reach the global minimum solution

because it limits the acceptance of a non-improved solution. On the contrary, if the selected temperature is very high, unnecessarily excessive calculations will be carried out to lower the temperature. Even though the initial temperature is described theoretically by Aarts et al, experimental evaluation of the initial temperature is more commonly used. In order to test the configuration space, a certain number (n) of iterations is used. From these iterations, the mean absolute change in the objective function ($|\Delta J|$) first is first calculated:

$$|\overline{\Delta J}| = \frac{1}{n}\sum_{1}^{n}|\Delta J| \tag{6.2}$$

Then, the initial temperature is calculated from the $|\Delta J|$ by an initial acceptance probability (RN) which is defined as the ratio of the number of successful moves to the total number of attempted moves. The typical value of initial acceptance probability is very high, in the order of 0.9 and 0.95. Then the initial temperature is calculated by:

$$T_0 = -\frac{|\overline{\Delta J}|}{\ln(RN)} \tag{6.3}$$

As shown in Fig. 6.3, The effect of initial acceptance probability and average change in the objective function

on the calculation of the initial temperature is illustrated. For example, if the mean absolute change in the objective function $|\Delta J|$ is 1 and the initial acceptance probability (RN) is chosen to be 0.7, the initial temperature is approximately 2.8. In order to jump out of the local minimum and to continue searching for a better configuration, the initial temperature should be sufficiently high. Basically most of the alterations are accepted. This process is known as the heating up processes in which all particles are randomly arranged in a liquid state,(Kirkpatric et al).

6.4.4 The Number of Iterations

It is also important to find the optimal number of iterations (Length of Markov Chain) at a given temperature. Theoretical consideration is given by Aarts et al but the empirical approach has been more popular. There is no standard method for determining the proper number of iterations for the inner loop. One of the methods is the perturbation configuration (that is the flow function coefficient in the present study) until the objective function is not changing. Nevertheless, the number of iterations is usually determined by

experimentation and by the type of problem being addressed. Because the number of iterations, (L_k), depends on the cooling schedule and the neighbor search, test runs for the number of estimated parameters are first conducted to find the optimal Markov Chain Length for the given cooling schedule. The number of iterations is kept constant for each reduced temperature. The temperature is reduced after a certain number of iterations.

6.4.5 Temperature Reduction Schedule

Simulated annealing algorithms also require a cooling schedule for successful and efficient optimization. If the temperature is kept at a high value, the annealing process will not end up in a globally optimal configuration. If the temperature is decreased too quickly, it will quench and will not terminate in a globally optimal solutions. In this study, a fixed geometric cooling schedule has been used. After a certain number of iterations, L_k, (Markov chain length), the new temperature, (T), is calculated as:

$$T_i = \lambda T_{i-1} \qquad (6.4)$$

The old temperature is multiplied by a constant reduction

factor ,λ, to obtain the new temperature. The constant is less than one. Empirically λ has been chosen to be 0.8. Aarts[22] and Eglese[21] also suggested more complicated methods such as the logarithmic schedule. However, Kirkpatric et al suggest that an annealing schedule can also be developed by trial and error for a given problem. The choice of a fixed schedule depends not only on the optimization problem but also on the specific problem.

6.4.6 Stopping Criteria

To minimize computational effort and execution time, an efficient and well constructed stopping criteria is required. The stopping criteria can be defined, based on the objective function (J) or on the temperature. When the objective function attains a desired minimum value as determined by the prescribed accuracy of the matching, the search is stopped. In the second method, a final temperature is defined, based on the initial temperature. The process is said to be frozen when the procedure has gone through a certain number of consecutive passes at each flow function with no change in the objective function or this process is continued until the lowest defined temperature is attained. This

will indicate that the minimum of the objective function has been estabiished.

The advantage of simulated annealing compared to other optimization methods is the introduction of a slowly decreasing acceptance of the nonimproving solutions. Initially higher nonimproved solutions are accepted and the search ends up with a gradual, fine local search which accepts only the improved solutions. In Fig. 7.28, as the objective function is minimized with low temperatures for the displacement experiment, the number of accepted nonimproved solutions is decreasing.

6.5 Objective Function or Estimation of Flow Functions

For the simultaneous estimation of relative permeability and capillary pressure curves for the unsteady- state drainage test, the objective function is expressed in terms of saturation profiles, production, and pressure drop history, according to:

$$J(a) = W_Q \sum_k \left(Q_k^c - Q_k^m\right)^2 + W_P \sum_k (\Delta P_k^c - \Delta P_k^m)^2 + W_s \sum_k (S_{kj}^c - S_{kj}^m)^2 \quad (6.5)$$

in which W_Q, W_P and W_S are some appropriate weighting factors of production data, pressure drop, and displaced

phase saturation for scaling. If the pressure drop and saturation values are not normalized or dimensionless, then appropriate weighting factors should be used for scaling. Accuracy and importance of the pressure drop and saturation profiles may vary from experiment to experiment. By using appropriate weighting factors, accurate and important data values can be emphasized. The subscript c refers to the values computed by the numerical method and m refers to the corresponding measured data.

The flow functions are represented by quadratic or cubic splines. The monotonicity of these functions or the positive value of the flow functions can be used as constraints to determine the set of feasible solutions generated by the objective functions. In this study, cubic splines are used for piece-wise representation of the flow functions. For example, the relative permeability of water can be described by the following expression:

$$k_{rwi} = a_i S_D^3 + b_i S_D^2 + c_i S_D + d_i \qquad (6.6)$$

where a_i, b_i, c_i and d_i are some fitting coefficients which assume different values over various segments and S_D is dimensionless saturation. For N data points, there

are (N-1) intervals. Consequently, there are 4(N-1) unknown coefficients to be determined. On the other hand, the continuity and compatibility conditions require that the function values and the first and second derivatives at the interior knots should be equal. As a result, the total number of unknown coefficients to be estimated by simulated annealing is reduced to N-1. This search process is repeated at the same temperature until all the flow function properties are tested at each discrete saturation value selected to determine the discrete values of the relative permeability and capillary pressure.

The saturation range was divided into five equal segments from the initial to the residual saturations and a piece-wise functional representation was used. The saturation history profiles and the production and pressure drop histories were used as constraints to generate the flow functions. As shown in Fig. 7.18, the initial experimental flow functions for the forward simulation were retrieved successfully within a reasonable level of accuracy. The coefficients of the cubic spline and the first and second order derivatives at the interior knots are presented in Table 6.2.

6.6 Final Remarks

Simulated Annealing (SA) has been implemented as a global stochastic optimization technique to avoid trapping in one of the local optimum. All the measured data could be easily incorporated as constraints. SA has shown great potential to obtain a unique set of relative permeability and capillary pressure curves by using the internal core data saturation history profiles along with the conventional external data, overall pressure, and effluent fluid production data. An undesirable feature of this method is that it can be computationally high intensive and time consuming if it is not fine tuned for a specific problem.

Table 6.1. Simulated Annealing Parameters
Annealing Schedule
T_0 Initial Temperature L_k Number of Iterations (Length of Markow Chains) T_0 Temperature Reduction Function T_{min} Stopping Criteria
Problem Dependent
i_0 Initial Solution j Neighbour Generation ΔJ_{ij} Construction and Evaluation of Objective Function

Table 6.2. Coefficients of relative permeability and first and second derivatives at different knots

$(K_{rw,i} = a_i S_D^3 + b_i S_D^2 + c_i S_D + d_i)$

i		S_D	a	b	c	d
2		0.7838	0.0756	0.2742	0.8297	0.1533
3		0.5676	0.1790	0.5174	0.6391	0.1035
4		0.3514	0.5806	1.2181	0.2414	0.0282
i	$K_{ro,i}$	$K_{ro,i+1}$	$K'_{ro,i}$	$K'_{ro,i+1}$	$K''_{ro,i}$	$K''_{ro,i+1}$
1	0.6291	0.6291	1.1202	1.1202	0.1928	0.1928
2	0.3932	0.3932	1.0534	1.0534	0.4241	0.4241
3	0.1813	0.1813	0.8787	0.8787	1.1912	1.1912

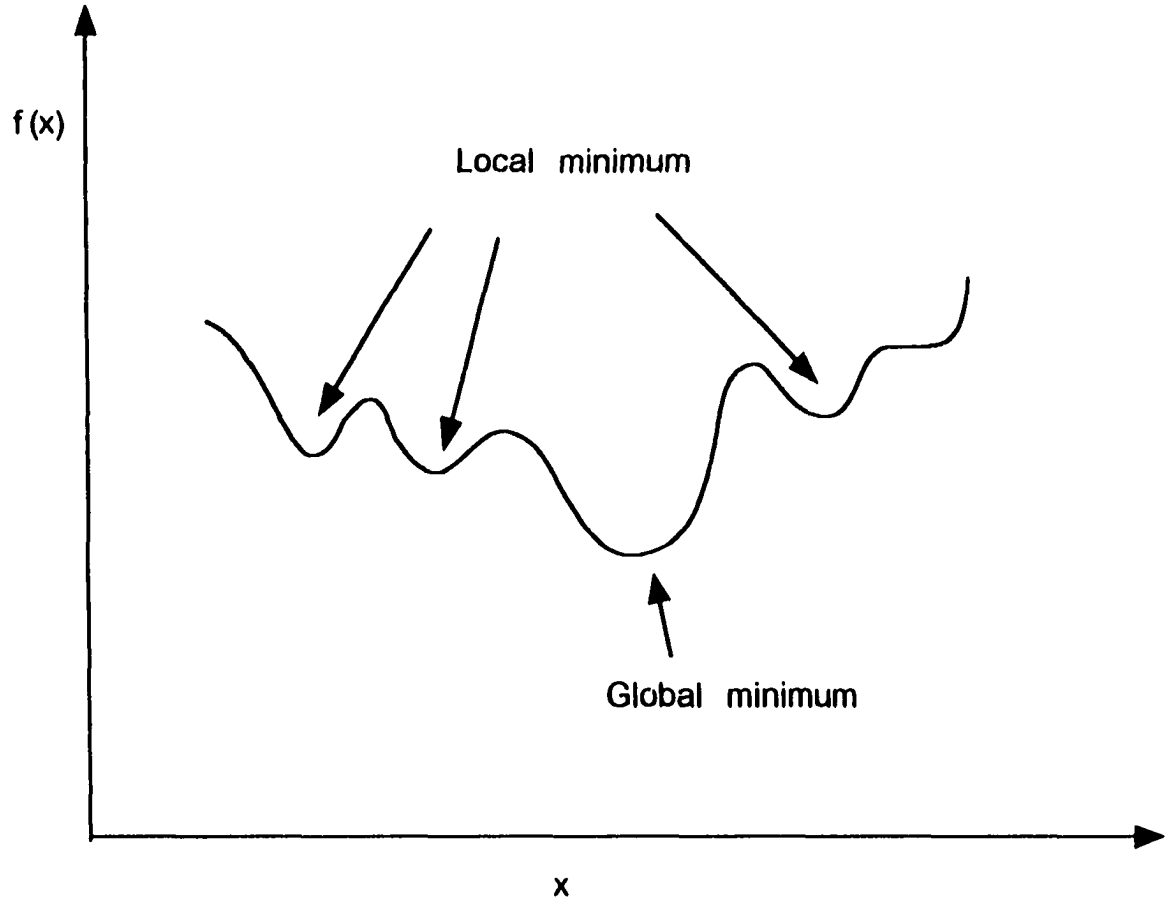


Fig. 6.1: Global and local minima

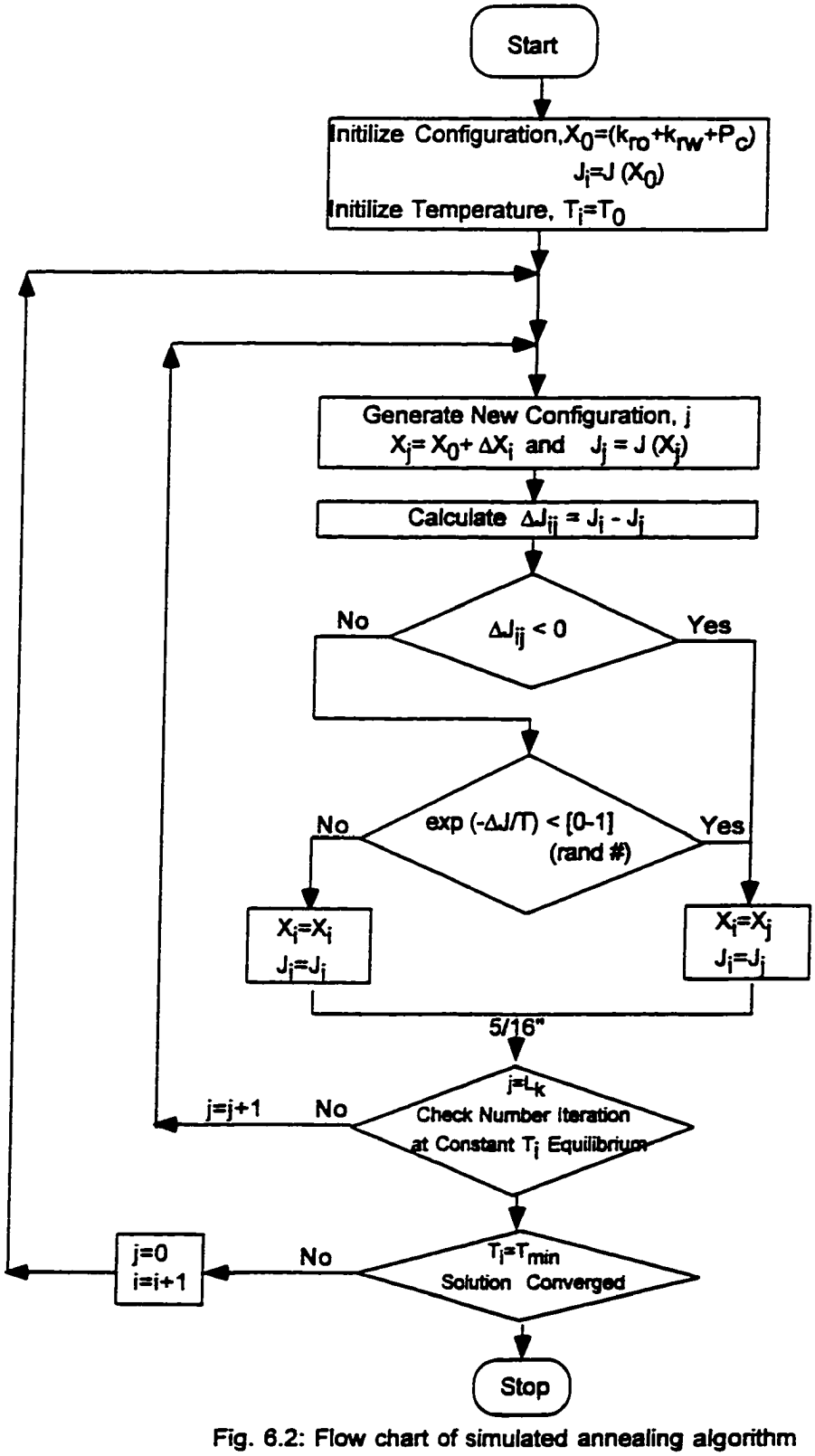


Fig. 6.2: Flow chart of simulated annealing algorithm

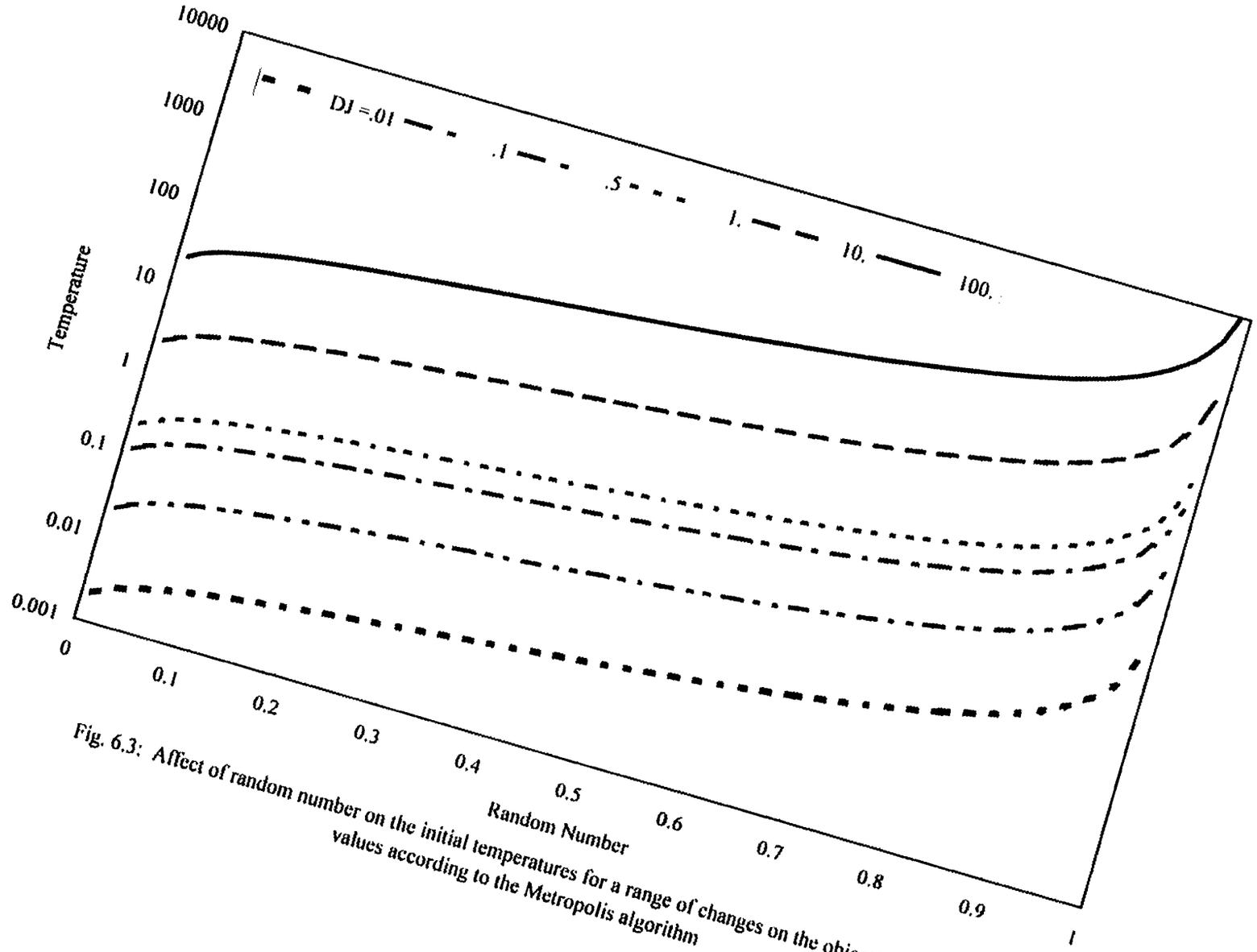


Fig. 6.3: Affect of random number on the initial temperatures for a range of changes on the objective function values according to the Metropolis algorithm

CHAPTER VII

MODEL VALIDATION AND DATA ANALYSES

Introduction

In this chapter, in order to investigate the uniqueness and the simultaneous predictability of the flow functions, five different experimental data sets are used to demonstrate and test the methodology for simultaneous determination of the relative permeability and capillary pressure curves. Drainage and imbibition displacement processes, oil/water and gas/liquid, are analyzed for different functional representation of flow functions. Effect of capillary pressure and flow regimes on the estimation of flow functions are addressed for steady-state and unsteady-state tests.

7.1 Unsteady-State Systems

7.1.1 Drainage Displacement I, oil/water system

In this case, displacement of oil by water in an oil-wet core, using the saturation history profiles and

pressure differential data for global functional and piece-wise local functional representation of flow functions, is considered.

First, the computer code was tested for the forward problem by using experimental data obtained from Richmond and Watson. The rock properties and operating conditions are given in Table 7.1. The relative permeability and capillary pressure curves, Fig. 7.1, are representative of an oil-wet system. The core flood simulator was also checked to determine whether it could handle the end effect properly for drainage experiments and the results were compared with Richmond and Watson's data in a previous study by Ucan et al., where pressure drop history and cumulative production history were matched successfully. This also indicates that an appropriate grid size and time step were chosen for minimum numerical dispersion. The breakthrough time is not retarded because the capillary pressure values are at the minimum value before the injected phase arrive at the end of the core.

As a second exercise, the uniqueness and the predictability of the flow functions were investigated.

For this purpose, the global empirical functions were first attempted for a history match. As the initial estimate, flow function exponents were assumed to be n_1=2, n_2=2 and n_3=2 for the drainage experiment. As shown in Fig. 7.2 and Fig. 7.3, the history matching with the assumed exponents was unsuccessful. The assumed curvature of the relative permeability of water is substantially different than that of the experimental curve (Fig. 7.1). Applying simulated annealing, the global optimal values of the exponents were determined to be n_1=5.1444, n_2=2.8326 and n_3=2.4857. A comparison of the experimental and the newly estimated flow functions is given in Fig. 7.4. The relative permeability of water at high saturations is not as good as it is at low saturations. The pressure drop history, was matched well but the cumulative production history, Fig. 7.5, is still not satisfactory and flow functions are not retrieved accurately. This confirms the limitation of using an empirical global functional representation of the flow functions.

The inverse numerical code, first, the newly estimated flow functions were used as the forward problem; then, the new observable parameters were generated. By using

the generated observable parameters, the flow functions were recalculated. As shown in Fig. 7.6, the global functional representations of the flow functions were recovered exactly by the simulated annealing method.

In order to improve the history matching and retrieve the initial experimental flow functions data, the saturation range was divided into five segments from the initial to the residual saturation and a piece-wise functional representation was used. Saturation history profiles and the pressure drop history were used as constraints to generate the flow functions. Fig. 7.7 shows that the initial flow functions were retrieved successfully within a reasonable range of accuracy. With these two constraints, the pressure drop history, the cumulative production history (Fig. 7.8) and the saturation history profiles (Fig. 7.11) were also matched well. Saturation front can be seen from the pressure history profiles before breakthrough, Fig.7.9. The pressure difference between the non-wetting and wetting phases is the capillary pressure. As shown in the Figs 7.9-7.10, the capillary pressure has high value in the core inlet face and it is diminishing towards to the saturation front. From these two different runs, it

can be concluded that a local piece-wise continuous functional representation is a better approach to determine the shape of the flow functions.

7.1.2 Imbibition Displacement, Oil-Water System

In the imbibition case, displacement of oil by water in a water-wet core, using (1) the recovery curves and pressure differential data, (2) the saturation history profiles and pressure differential data for discrete and piece-wise local functional representations of the flow functions was considered. To test the numerical code, the simulated experimental data obtained from Richmond and Watson were used. The rock properties and operating conditions are given in the Table 7.2. The relative permeability and capillary pressure curves, Fig. 7.12, are representative of a strongly water-wet system. Results are compared with Richmond and Watson. The pressure drop history and the cumulative production histories were matched successfully in a previous study by Ucan et al. Due to the end-effect, the breakthrough time was retarded. For imbibition processes, the capillary pressure should reach zero when the wetting phase pressure equals the non-wetting phase pressure and

then the production of the injected phase should begin. After the computer code was tested for a simulated imbibition experiment, the relative permeability and capillary pressure curves were estimated under two different constraints by using the same core properties and operating conditions.

First, the flow functions by discrete representation, Fig. 7.12, were estimated by using only the recovery curves and pressure differential data. Second, the pressure drop and cumulative production of oil and water were recalculated by using the estimated relative permeability and capillary pressure. Finally, the pressure drop history, the cumulative production history (Fig. 7.13) and saturation history profiles (Fig. 7.14) calculated from the estimated flow properties were compared with the initial history performance. As shown in Fig. 7.13, a good history match was obtained for the pressure drop and cumulative production history with the estimated flow function properties. However, the saturation history profiles, Fig. 7.14, did not match well. This indicates that matching saturation history profiles guarantees matching of the cumulative production history but the reverse is not true. A

similar procedure was applied for a piece-wise functional representation by using only the external data. As seen from Fig. 7.15, the relative permeability of oil does not match the initial curve, but the recovery of water relative permeability and capillary pressure curves are within an acceptable range. The history matchings of the pressure drop, the cumulative production and the saturation profiles are given in Figs. 16, and 17, respectively. By using the piece-wise functional representation, the history matching of the saturation history profiles (Fig. 7.17) was improved as compared to the discrete representation (Fig. 7.12).

Next, the saturation history profiles and pressure drop history were used as constraints to generate the flow functions by a piece-wise functional representation (Fig. 7.18). The initial flow functions were retrieved successfully. With these two constraints, the pressure drop history, the cumulative production history (Fig. 7.19) and the saturation history profiles (Fig 22) were matched well. Saturation front can be also seen from the pressure history profiles before breakthrough, Fig.7.20. As shown in the Figs 7.20 and Fig. 7.21, the capillary pressure value before breakthrough is higher than the

capillary pressure value after breakthrough for the imbibition test.

As the last exercise, only the before breakthrough information was used to generate the flow functions because conventional unsteady-state methods only provide information after breakthrough. The average water saturation prior to break through is 0.63 . The flow functions obtained from the unsteady-state method will be limited to the saturation range (0.63-0.7625). By using saturation history profiles and pressure drop information prior to breakthrough, similar flow functions (Fig.18) were obtained. From these three different runs, it can be concluded that using the recovery curves with the pressure drop history is not sufficient to determine the shape of the flow functions accurately. The estimated flow and the calculated saturation history profiles based on the discrete representation are not smooth monotonic functions like the saturation profiles and the flow functions obtained from the piece-wise functional representation. By using the saturation history profiles, the pressure history drop along with a piece-wise functional representation, the flow functions can be retrieved accurately. Removing

the saturation history profiles as a constraint on the problem leads to non-unique flow functions. Results of drainage and imbibition applications are summarized in the Table 3.

7.1.3 Non-Darcy Flow Regime

In order to study the effect of viscous inertial forces, the previous drainage experiment was simulated assuming non-Darcy flow conditions for a range of different beta coefficient values. The magnitude of non-Darcy flow coefficient, β, is calculated by the following correlation, (Liu at al.);

$$\beta = \frac{8.91x10^{8}\tau}{\phi k} \qquad (7.1)$$

where, k is the permeability expressed in md, ϕ is porosity, (fraction), τ is the tortuosity of the porous medium, and β is expressed as in ft^{-1}. For the drainage experiment, β is approximated to be 1.6 10^{7}, cm^{-1} and tortuosity is assumed to be 1.4 for cubic packing.

As seen from Fig. 7.23 and Fig. 7.24, the pressure drop and cumulative production rate increased for increasing values of the b coefficient. But the saturation history profiles did not change as much under the non-Darcy flow conditions, Fig. 7.25. The non-Darcy flow number for multiphase flow is greater than the non-Darcy flow number for single phase flow. In other words, the non-Darcy multiphase flow properties are closer to the Darcy multiphase flow properties than to the non-Darcy single phase flow properties. The pressure history profiles of the wetting and non-wetting phases for non-Darcy flow before and after breakthrough are presented in Figs. 7.26 and 7.27, respectively. The non-Darcy pressure values, (7.26 and 7.27), are higher than the Darcy flow pressure values,(7.9 and 7.10) but they have a similar trend.

The initial control parameter and the reduction factor for the control parameter was obtained from the Metropolis algorithm and average change (DJ) of the objective function. The minimization of the objective function, the number of accepted improved and non improved configurations and the rate of convergence of the algorithm at each control parameter are given in Fig. 7.28. In order to increase the rate of convergence,

the terms defined in the objective function, such as the cumulative production rate and the pressure drop, had to be scaled to the same order of magnitude by appropriate weighting coefficients or by using dimensionless forms of the immiscible displacement flow equations. The effect of core heterogeneity on the relative permeability and capillary pressure curves can be considered by using a permeability and porosity distribution along the core.

7.1.4 Drainage Displacement II, Gas Water System.

The gas/water data for this case were obtained from Ouenes and Fasanino. The core properties and operating conditions are presented in Table 7.4. The history matching was not successful with their estimated relative permeability and capillary pressure curves, although in their paper a near perfect history match was reported. The estimated capillary pressure curve reported by Ouenes and Fasanino[5] is a typical imbibition capillary pressure curve rather than a primary drainage capillary pressure curve. The results obtained by the simulated annealing method in the present study indicate a successful match of pressure drop history and cumulative production

histories, as shown in Fig. 7.29 and Fig. 7.30. The estimated capillary pressure and relative permeability curves are presented in Fig. 7.31. As can be seen, the present capillary pressure curve is representative of a primary drainage capillary pressure curve. The pressure drop before breakthrough did not match well compared to after breakthrough data because the cumulative injection rather than the injection rate information was available before breakthrough. The saturation and pressure history profiles are given in Fig. 7.32 and Fig. 7.33, respectively. Before breakthrough, there is not much difference between the two phase pressure profiles because the capillary pressure values are very small for average gas saturation values before breakthrough. When the water saturation approaches the residual water saturation, the two phase pressure profiles separate significantly (Fig. 7.34). The minimization of the objective function and the rate of convergence of the algorithm at each temperature for the number of simulations are given in Fig. 7.35. The same experimental data were rerun for non-Darcy flow conditions but there was not any difference between them using the non-Darcy flow coefficient estimated from the Katz et al and Liu et

al correlation for single phase flow. β was found to be 3.4×10^5 (1/cm) for this experimental data, (Ucan at al.).

7.2 Stead-State Gas-Liquid Systems

Two different data sets involving gas/brine and nitrogen/water were used to demonstrate and test the methodology for simultaneous determination of the relative permeability and capillary pressure from steady-state test data.

7.2.1 Stead-State Gas-Brine System

In the first case, the computer code was tested for the forward problem using a simulated experimental data given by Christiansen and Howarth. Global functional representations are used to express the saturation dependent properties. Corey-type exponential relative permeability curves and logarithmic capillary pressure curve according to Bentsen and Anli are used. They have the following forms:

$$k_{rw} = \left(\frac{S_w - S_{wi}}{1 - S_{wi}} \right)^{n_w}, \qquad (7.2)$$

$$k_{rg} = k_{rg,max}\left(\frac{1-S_w-S_{gc}}{1-S_{wi}-S_{gc}}\right)^{n_g} \qquad (7.3)$$

and

$$P_c = P_{ct} - P_{span} \ln\left(\frac{S_w-S_{wi}}{1-S_{wi}}\right) \qquad (7.4)$$

S_{wi} is the irreducible water saturation, S_{gc} is the critical gas saturation, P_{ct} is the threshold capillary pressure, $k_{rg,max}$ is the maximum gas relative permeability and n_w , n_g and P_{span} are some parameters that need to be determined by a global optimization technique.

The rock properties and operating conditions are given in Table 7.5. The relative permeability and capillary pressure curves, Fig. 7.36, are used with parameters, n_w is 1.7 , n_g is 1.5 and P_{span} is 3.4 to represent a water-wet system. With three different total flow rates and fractional flow rates of 20% brine and 80% gas, the saturation and pressure profiles are generated. As shown in the Fig. 7.37, by increasing the flow rate, flat saturation profiles are achieved and the size of region at the end of core affected by the capillary force is decreasing. The pressure drop, Fig. 7.38, is

also increasing and pressure profiles are being stabilized along the core as the flow rate increases.

For the inverse problem, initial saturation and pressure profiles determined above using assumed parameter values are used as constraints and arbitrary values are assigned to the parameters, such as n_w is 2.0, n_g is 2.0 and P_{span} is 2.0. By using the simulated annealing as a global optimization technique, the initial parameters are retrieved successfully, as n_w is 1.691, n_g is 1.496 and P_{span} is 3.409. It has been observed that the number of iterations in optimization of the saturation and pressure profiles by using the two low flow rates is less than that of the number of iterations by using the two high flow rates saturation. Because non flat saturation profiles and non linear pressure profiles preserve the characteristic information about the capillary pressure and relative permeability curves, it is easier to estimate the flow functions by this inverse interpretation method when the capillary force, or the end effect is dominant.

Having tested the inverse model, the affect of non-Darcy flow on saturation and pressure profiles and relative

permeability and capillary pressure curves are examined. For this purpose, the saturation and pressure profiles are generated using different non-Darcy flow numbers (F_{nd}). As shown in Fig. 7.39, as the non-Darcy flow becomes more dominant for the gas, higher pressure drop is observed for the gas phase. On the other hand, for water phase, pressure drop is very low compared to the gas phase because Darcy flow was assumed for water. As more pressure dissipation occurs due to the non-Darcy flow, the gas saturation profiles for non-Darcy flow develop faster than the Darcy flow saturation profiles. As illustrated in Fig. 7.40, higher the non-Darcy flow for gas, lower the water saturation profiles for the same flow rate.

In order to determine the affect of the non-Darcy flow on the flow functions, calculated non-Darcy flow saturation and pressure profiles are used as Darcy flow saturation and pressure profiles in the inverse model to generate the relative permeability and capillary pressure curves. The following results are obtained. For the non-Darcy flow number, F_{ndg} , 0.8 and 0.6, the flow functions parameters are: n_w is 1.716, n_g is 1.594 and P_{span} is 3.339, and n_w is 1.749 , n_g is

1.723 and P_{span} is 3.334. As shown in Fig. 7.41, the curvature of the gas relative permeability is increasing with the degree of the non-Darcy flow regime. However, the relative permeability of the water and capillary pressure curves do not change significantly due to Darcy flow assumption for brine.

7.2.2 Stead-State Nitrogen-Water System

In the second application, nitrogen-water data by Satik et al concerning the saturation distribution, obtained by an X-ray computer tomography (CT) is used. The rock properties and operating conditions are given in Table 7.6. As shown in Fig. 7.42, for the fractional flow rate of 16% water, saturation profiles do not show flat saturation regions. As the fractional flow rate of water is increased to 84% then flat saturation is achieved with some noise in data. The noisy nature and non flat saturation distribution may be due to core heterogeneity, nitrogen-water segregation, strong inlet effect due to improper mixing at the injection core face. Smoothing is not applied to the saturation distribution data for estimation of flow functions. By using the similar global functional representation for

the flow functions given by Eq. 16-18, and simulated annealing as global optimization technique, the initial parameters are found to be: n_w is 6.411 , n_g is 2.90 and P_{span} is 1.12. As shown in Fig. 7.43, the relative permeability curves calculated by the inverse model is comparable to those obtained with the conventional steady-state tests. It should be noted that by inverse interpretation model, the flow functions are described in the full saturation range. However, conventional steady-state tests give data for only a small saturation range. In order to enlarge the description of the flow functions to full saturation range, the number of fractional flow rates, and the total flow rates should be increased. Consequently, the time frame required to conduct tests increases proportionally. By inverse model, time requirement for conducting the test can be decreased by specifically assigning certain number of fractional flow rates and total flow rates.

7.3 Discussion

Flow functions estimated by history matching can be influenced by different sources of errors. These are modeling, numerical and measurement errors. In many

applications, it is very hard to get porosity and permeability distribution along the core. Assuming a core homogeneous core is unrealistic. In most case, the clean Brea sandstone has some heterogeneity. By cutting the core, we introduce some fractures at the inlet and outlet of the core. For this reason, it is difficult to match the real experimental saturation distribution at the inlet and outlet of the core. Test parameters and conditions such as conditioning the wettability, establishing initial water saturations and measuring the end-point relative permeabilities at residual oil saturations and initial water saturations have a great impact on the estimation of the relative permeability curves.

Moreover, there are numerical errors introduced by the truncation errors and numerical dispersion. This problem can be alleviated by using appropriate time step and number of grids

Finally, the measurement errors can be classified in two categories, First, measured rock and fluid properties that are used in the forward problem, such as viscosity, compressibility, and constant values of the initial

water and residual oil could have some errors. Usually initial water and residual oil distributions are not constant and they are variable along the core. Therefore, matching real experimental saturation distributions can not be exact. Second, measured experimental data that are used in the inverse problem such as pressure drop, flow rates and saturation distributions would have some noise. Because the optimization technique using simulated annealing is not requiring any first or/and second derivatives and are based on random generation number (stochastic), the noise in the experimental data would not alter the results and effect the efficiency of the optimization techniques.

Table 7.1. Core Properties and Operating Conditions, Simulated Imbibition Water Flood (Richmond and Watson)	
Core Properties	
k, md	1,270
ϕ	0.249
L, cm	7.62
A, cm^2	5.06
S_{rw}	0.2882
S_m	0.2373
Operating Conditions	
Q, cm^3/min	0.36
μ_w, cp	1
μ_n, cp	10
Total fluid injected, PV	14.8

Table 7.2. Core Properties and Operating Conditions, Drainage Water Flood Experiment (Richmond and Watson)	
Core Properties	
k, md	9.6
ϕ	0.262
L, cm	7.13
A, cm^2	11.3
Swi	0.10
Operating Conditions	
Q, cm^3/min	2.0
μ_w, cp	0.262
μ_o, cp	0.725
Total fluid injected, PV	17.8

Table 7.3. Summary of Application

Case	Constraints on Objective Function	Functional Representation	Figures	Comment
Drainage	None	Experimental[4]	-	Forward problem is validated
"	None	Global functional representation (n_1=2., n_2=2., n_3=2.)	1-3	History matching with the assumed exponents was unsuccessful
	Saturation history profiles and pressure drop histories	Global functional representation (n_1=5.144, n_2=2.8326, n_3=2.4857)	4-5	Cumulative production history is still not satisfactory and flow functions are not retrieved accurately
"	"	Global functional representation (n_1=5.14, n_2=2.83, n_3=2.48)	6	Inverse problem is validated
"	"	Local piece-wise continuous functional representation	7-11	History matching was improved and initial experimental flow functions are retrieved successfully

Table 7.3. Summary of Application (Continued)

Case	Constraints on Objective Function	Functional Representation	Figures	Comment
Imbibition	None	Experimental[4]	-	Forward problem is validated
"	Cumulative production and pressure drop histories	Discrete representation	12-14	Saturation history profiles did not match but cumulative and pressure drop histories were matched
"	"	Local piece-wise continuous functional representation	15-17	initial experimental flow functions are not still retrieved
"	" Saturation history profiles and pressure drop histories	Local piece-wise continuous functional representation	18-22	History matching was good and initial experimental flow functions are retrieved successfully

Table 7.4. Core Properties and Operating Conditions, Actual Gas/Water Draining (Ouenes et al.)	
Core Properties	
Core length L	37.8 cm
Core cross section A	11.7 cm^2
Permeability k	311 md
Porosity ϕ	30.1
Initial gas saturation S_{1in1}	0.0%
Residual water saturation S_{2res}	63.3%
Operating Conditions	
Injection flow rate Q	150.0 cm^3/hr
Gas density ρ_1	0.875 g/cm^3
Brine density ρ_2	1.003 g/cm^3
Gas viscosity μ_1	0.018 cp
Brine viscosity μ_2	1.02 cp

Table 7.5. Core Properties and Operating Conditions, Simulated Gas/Water flow (Christiansen and Howarth)	
Core Properties	
k, Darcy	15 E-09
ϕ	0.10
L, cm	20.0
A, cm^2	50.27
S_{wi}	0.2
S_{gc}	0.1
Operating Conditions	
Q, cm^3/hr	0.0001
μ_w cp	1.
μ_g, cp	0.01
P_{outlet} , atm	1.0

Table 7.6 Core Properties and Operating Conditions, Nitrogen and Water flow (Satik and Horne)	
Core Properties	
k, md	601
ϕ	0.184
L, cm	25.4
A, cm^2	20.26
Swi	0.20
Operating Conditions	
Q, cm^3/min	12.0
μ_w, cp	1.0
μ_g, cp	0.018
P_{outlet} , atm	1.0

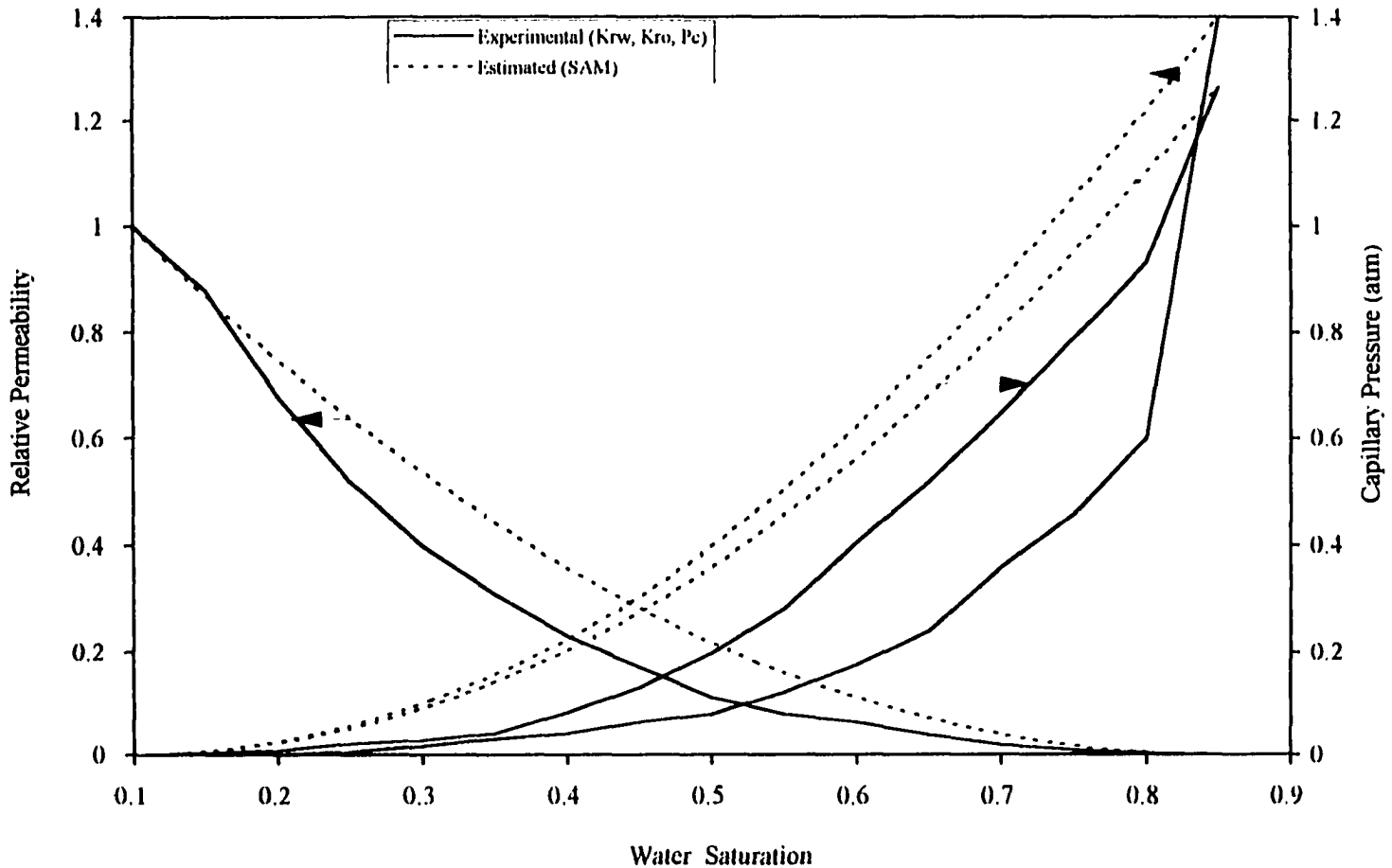


Fig. 7.1: Comparison of experimental (forward) and assumed global functional representation of flow function (n_1=2., n_2=2., n_3=2.)

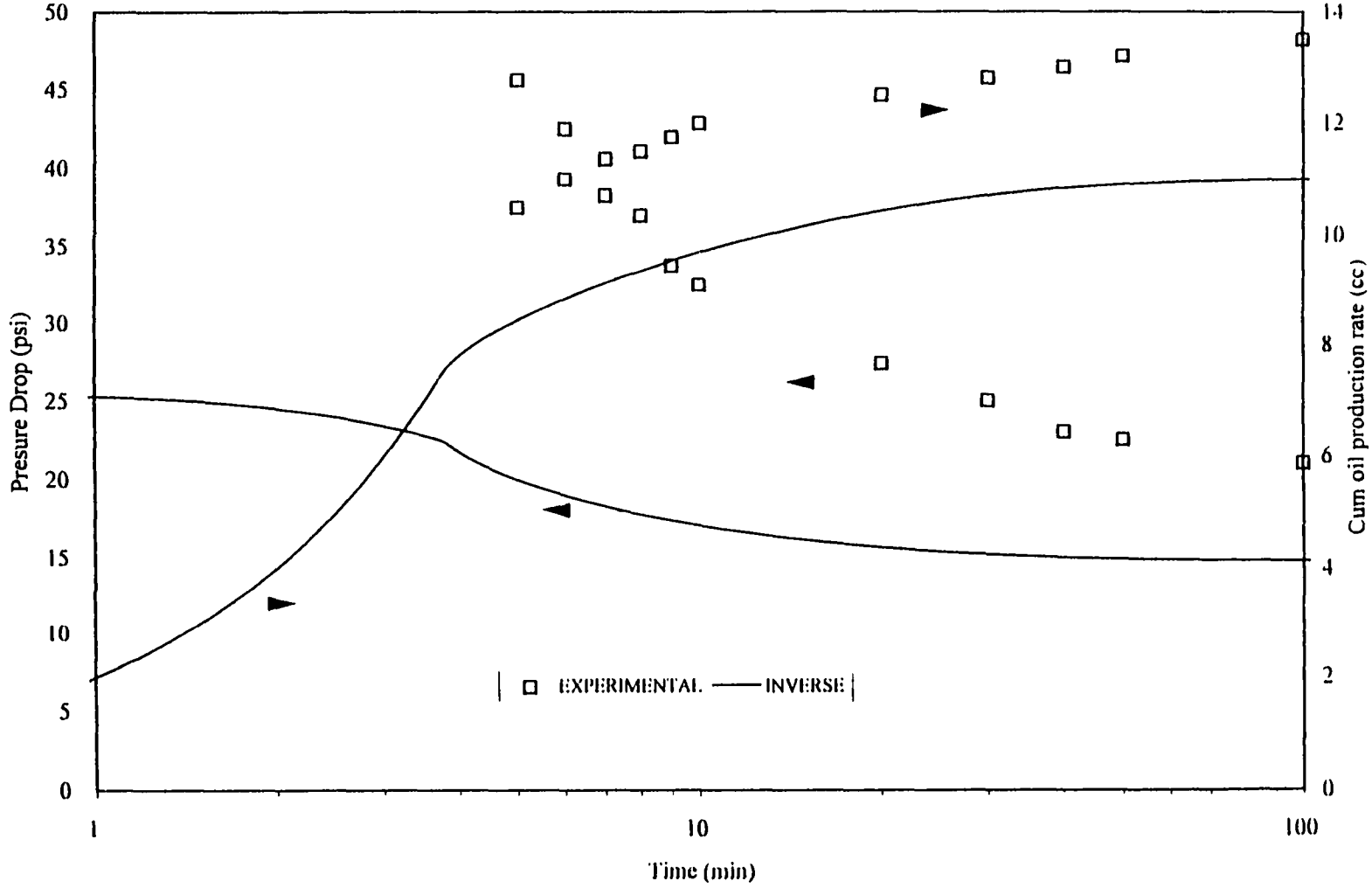


Fig. 7.2: Pressure drop and cumulative production history for the drainage experiment by using global functional representation (n_1=2., n_2=2., n_3=2.)

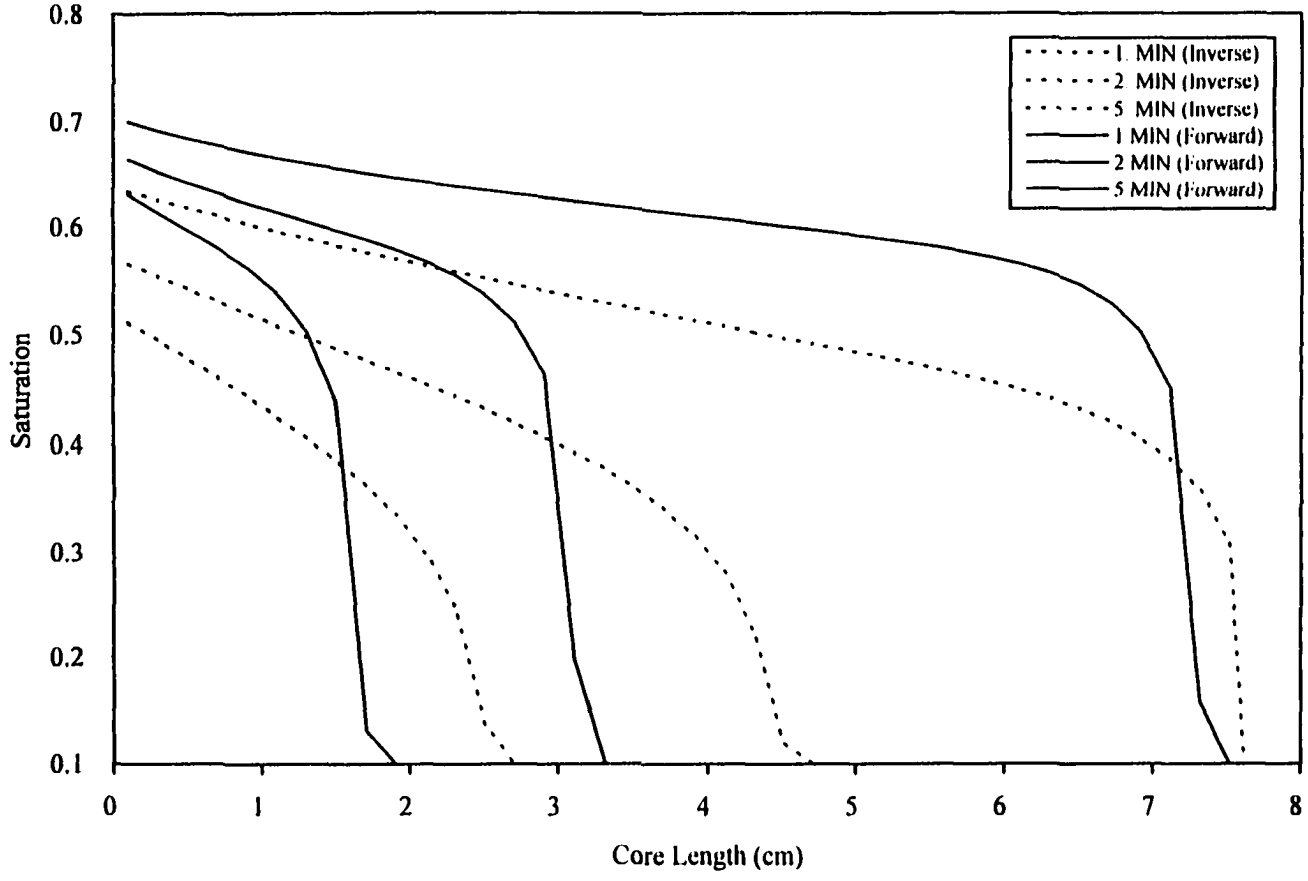


Fig. 7.3: Saturation history profiles for the drainage experiment by using global functional representation (n_1=2., n_2=2., n_3=2.)

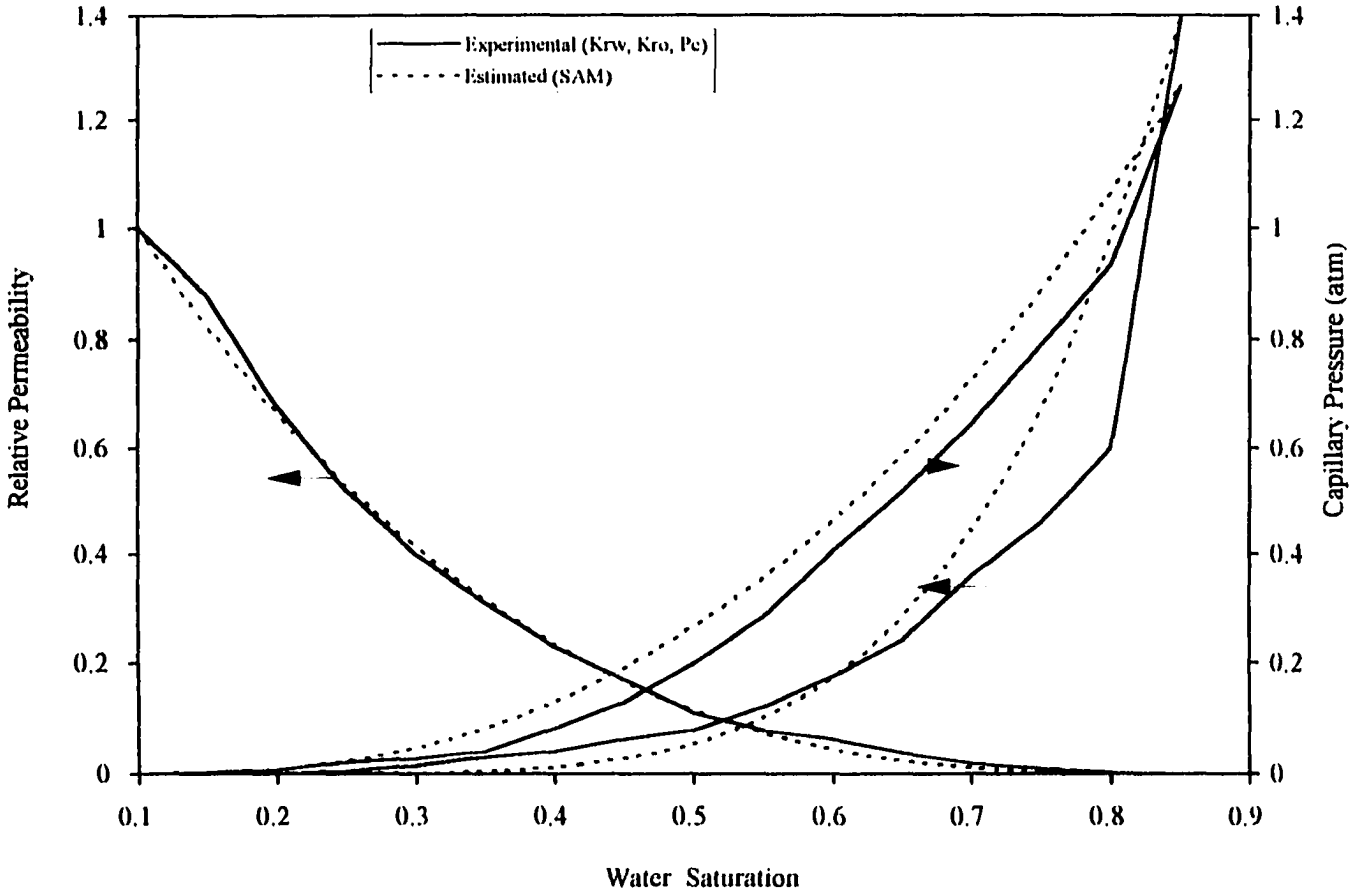


Fig. 7.4: Comparison of experimental (forward) and estimated (inverse) representation of flow function by simulated annealing method (n_1=5.1444, n_2=2.8326, n_3=2.4857)

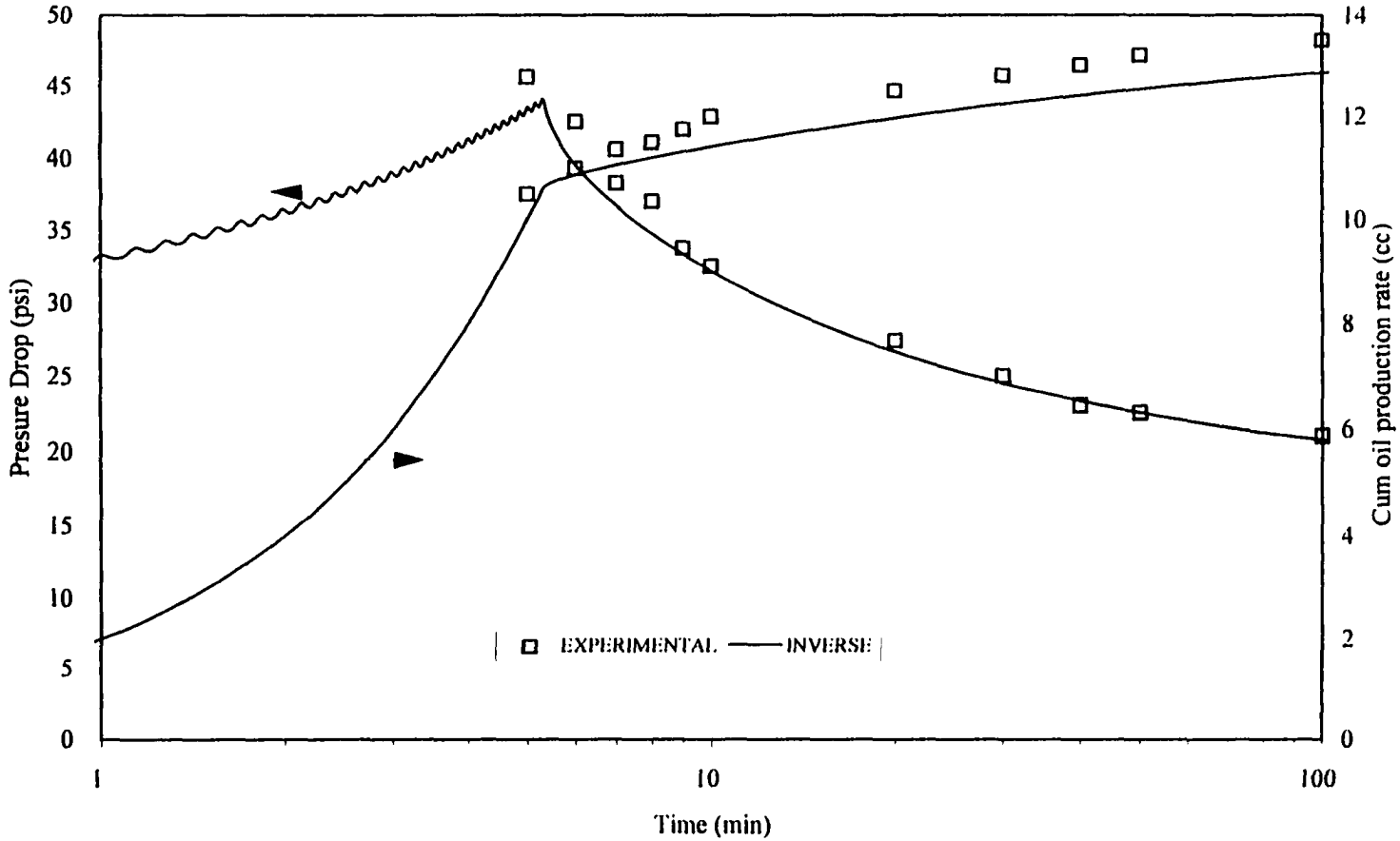


Fig. 7.5: Pressure drop and cumulative production history for the drainage experiment by using global functional representation (n_1=5.1444, n_2=2.8326, n_3=2.4857)

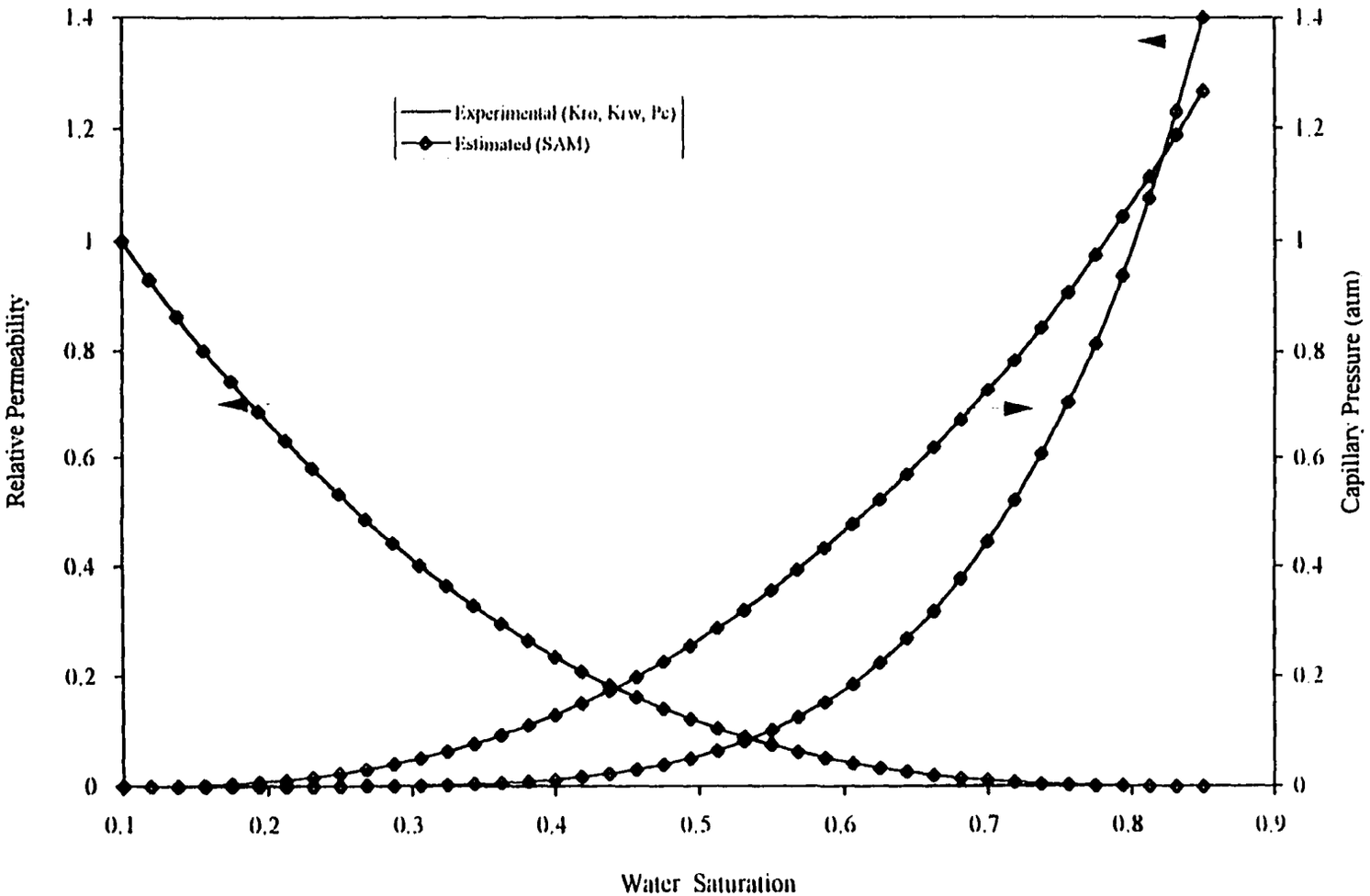


Fig. 7.6: Comparison of experimental (forward) and estimated (inverse) global functional representation of flow function

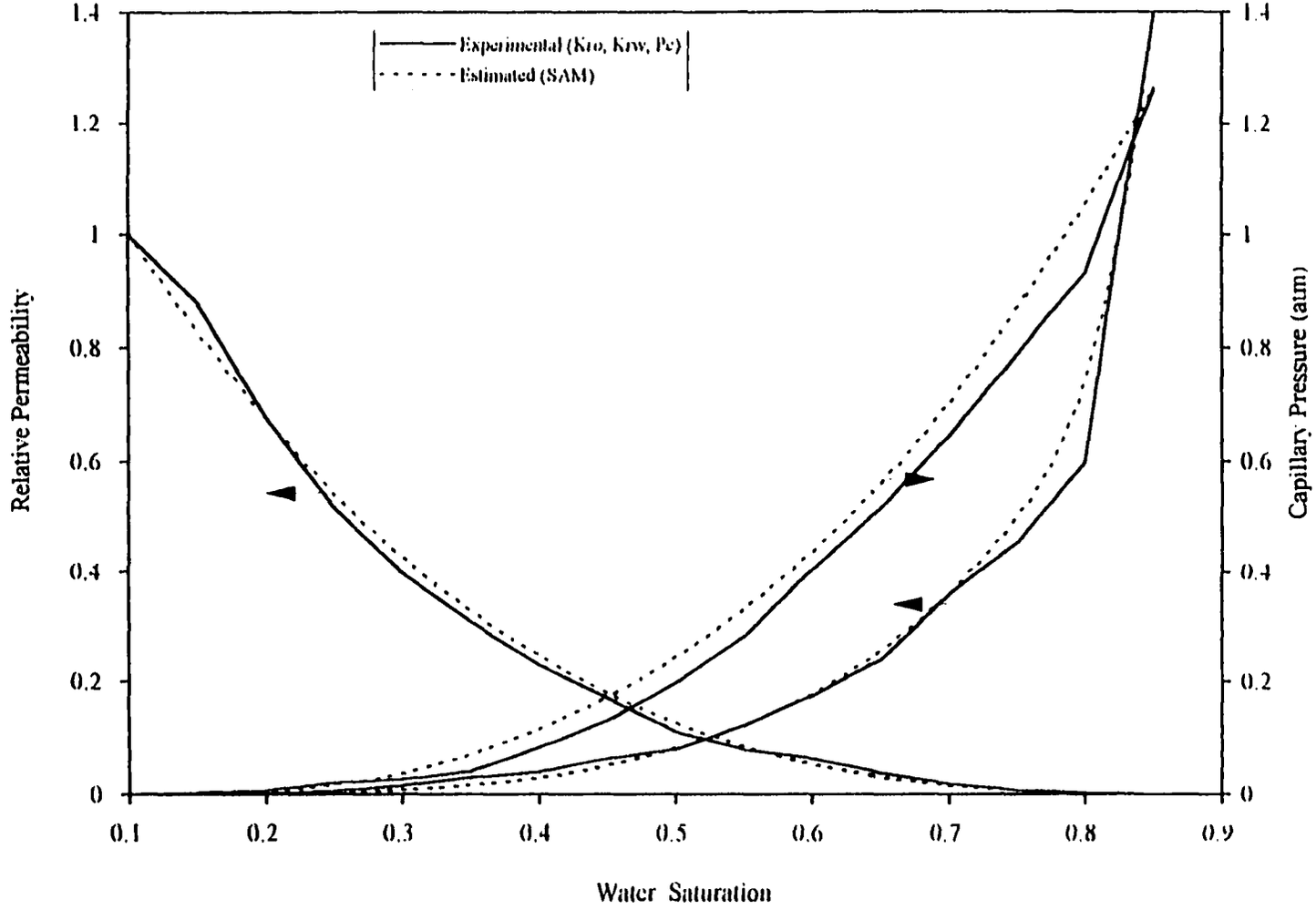


Fig. 7.7: Comparison of experimental (forward) and estimated (inverse) local functional representation of flow function by simulated annealing method

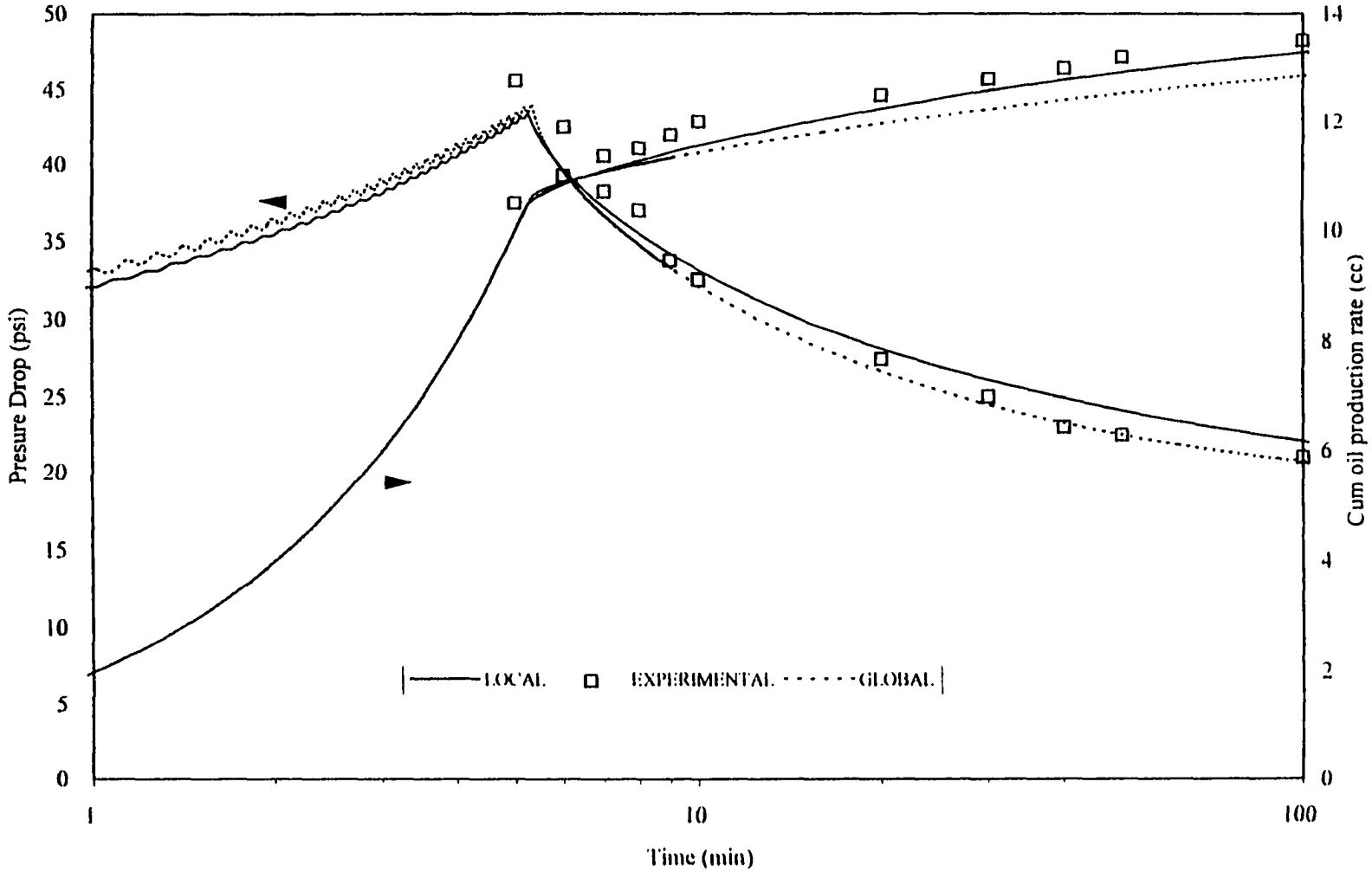


Fig. 7.8: Pressure drop and cumulative production history for the drainage experiment by using global and local functional representation

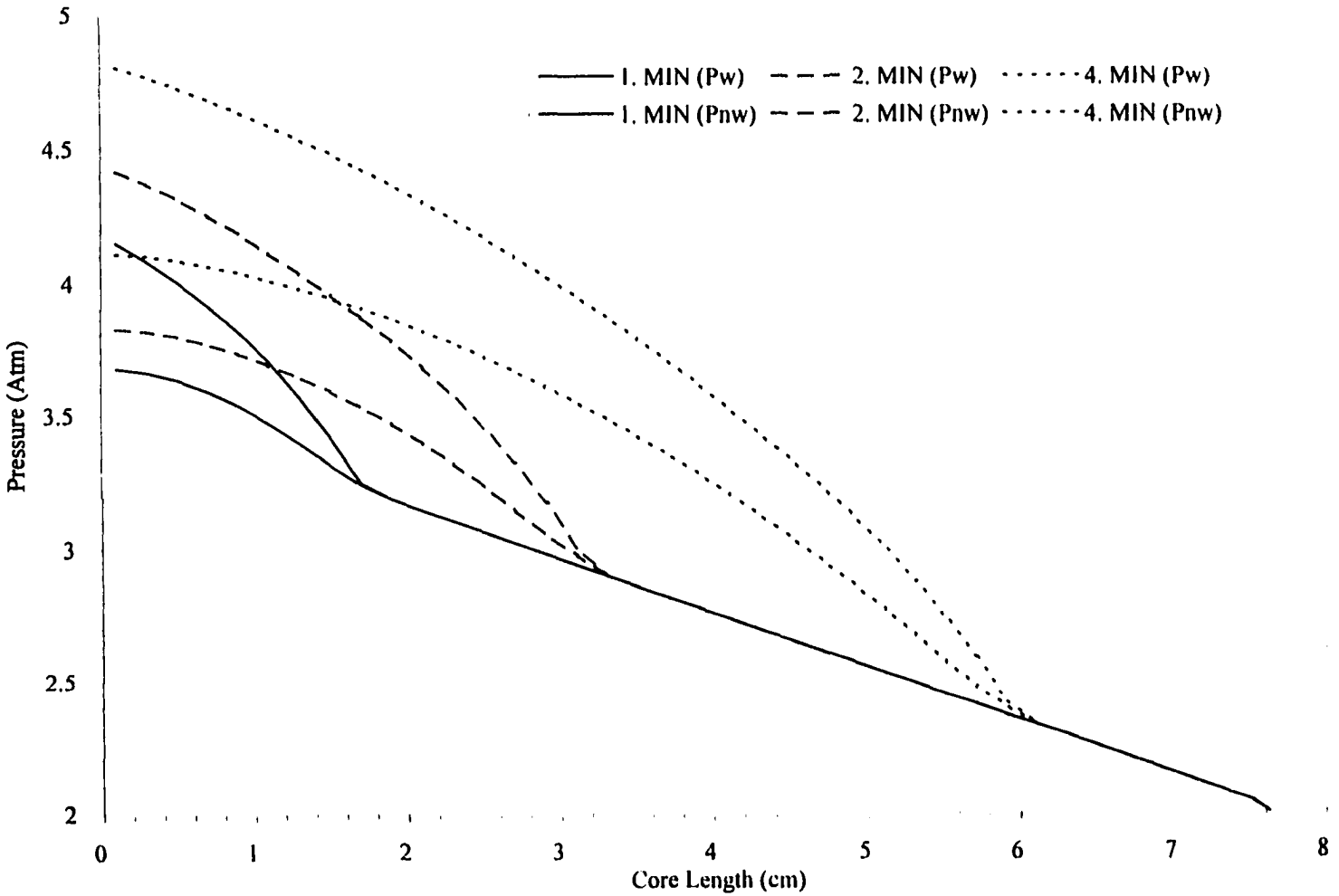


Fig. 7.9: Pressure history profiles before the breakthrough for the drainage experiment

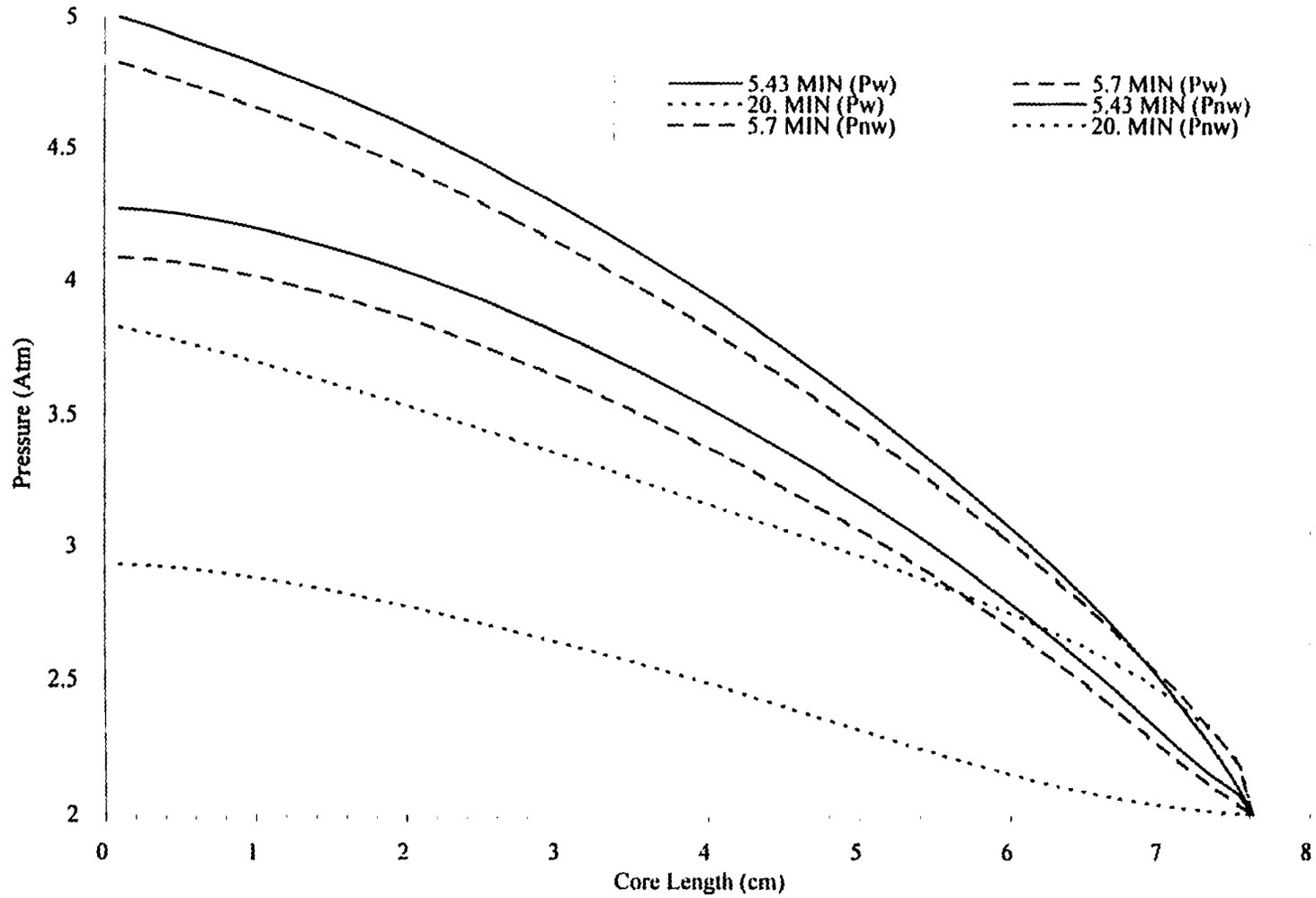


Fig. 7.10: Pressure history profiles after the breakthrough for the drainage experiment

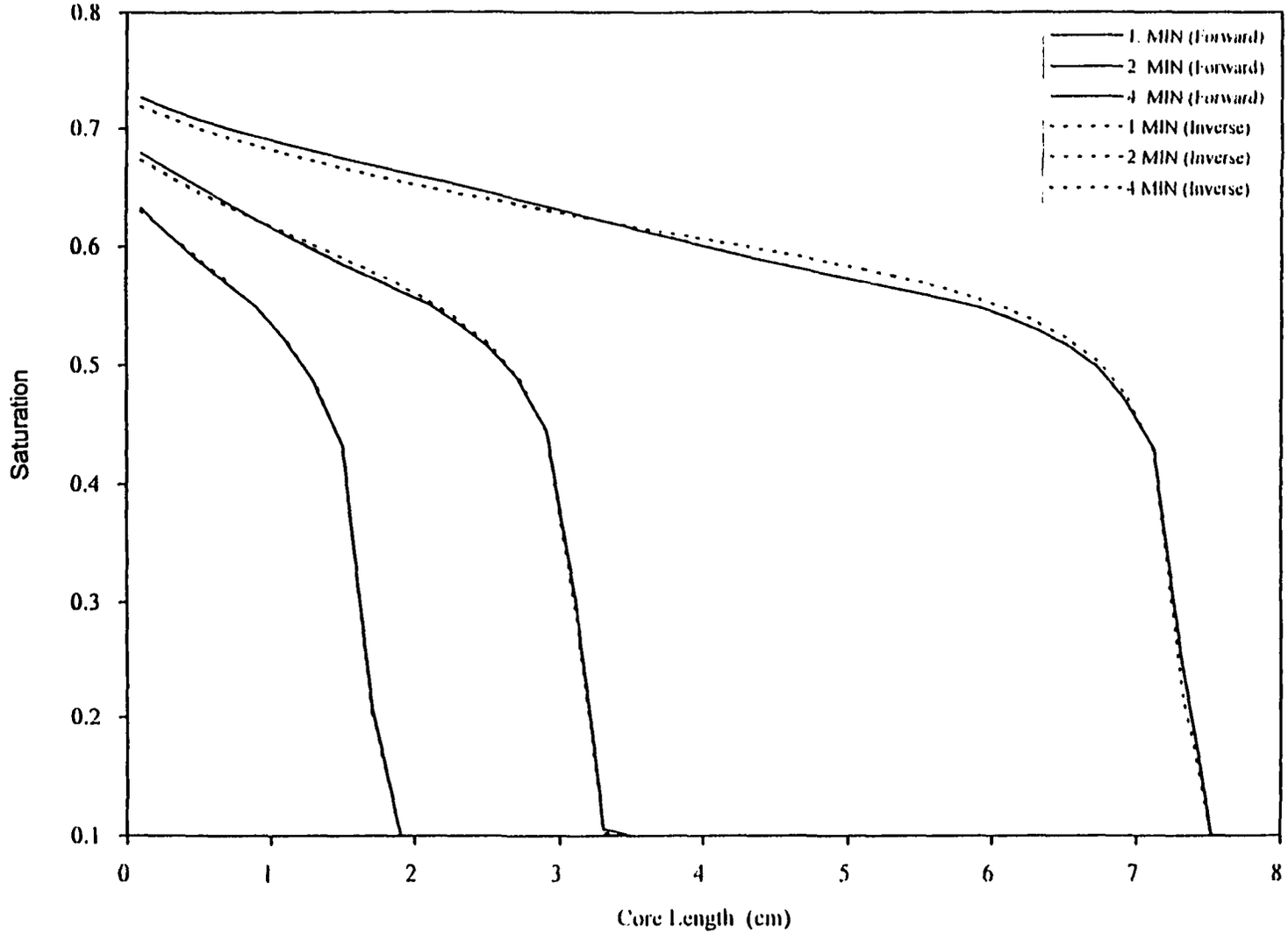


Fig. 7.11: Comparison of saturation history profiles using the estimated and initial flow functions

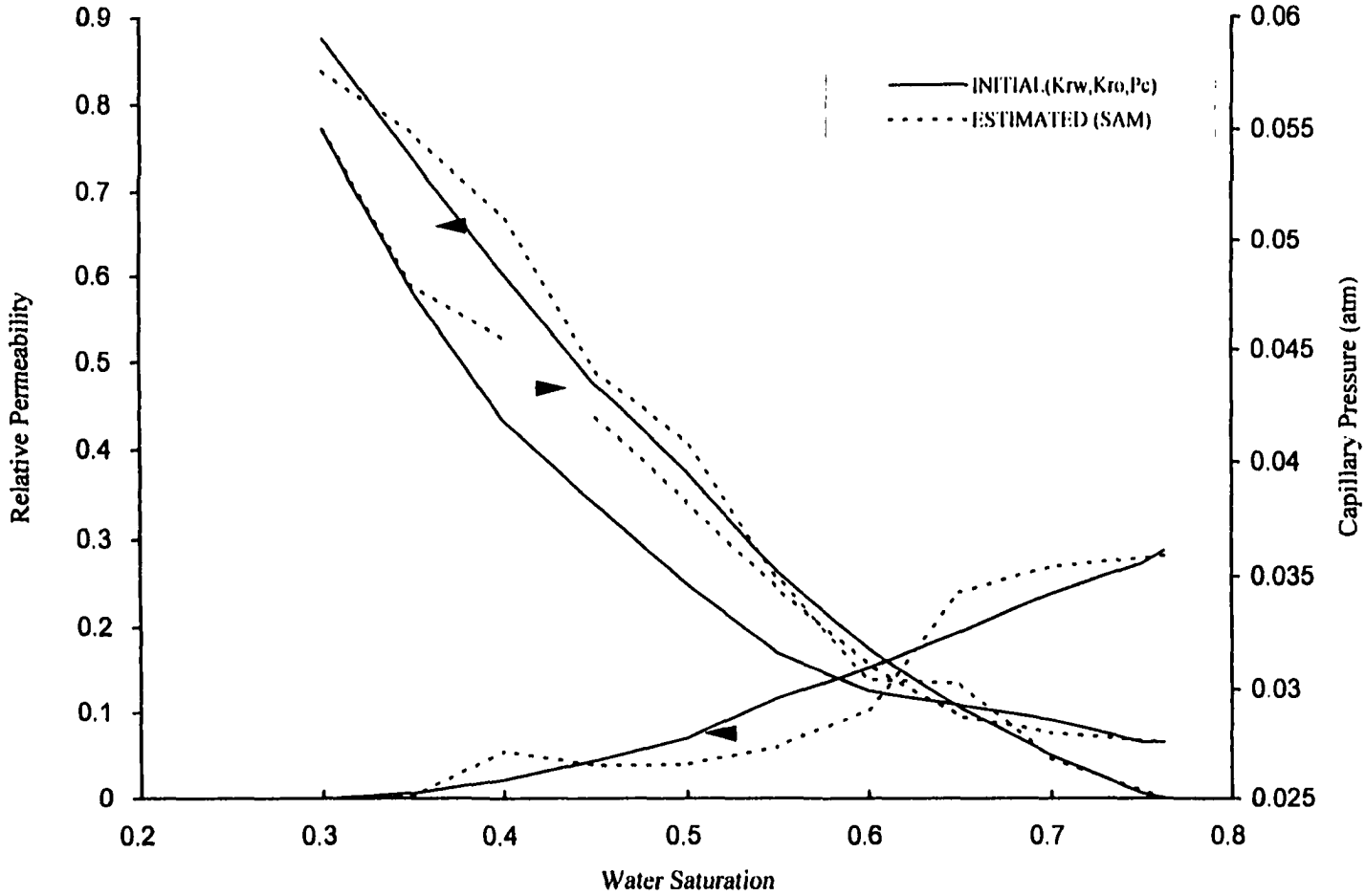


Fig. 7. 12: Comparison of initial and estimated discrete representation of flow function by simulated annealing Method (Ucan et al.)

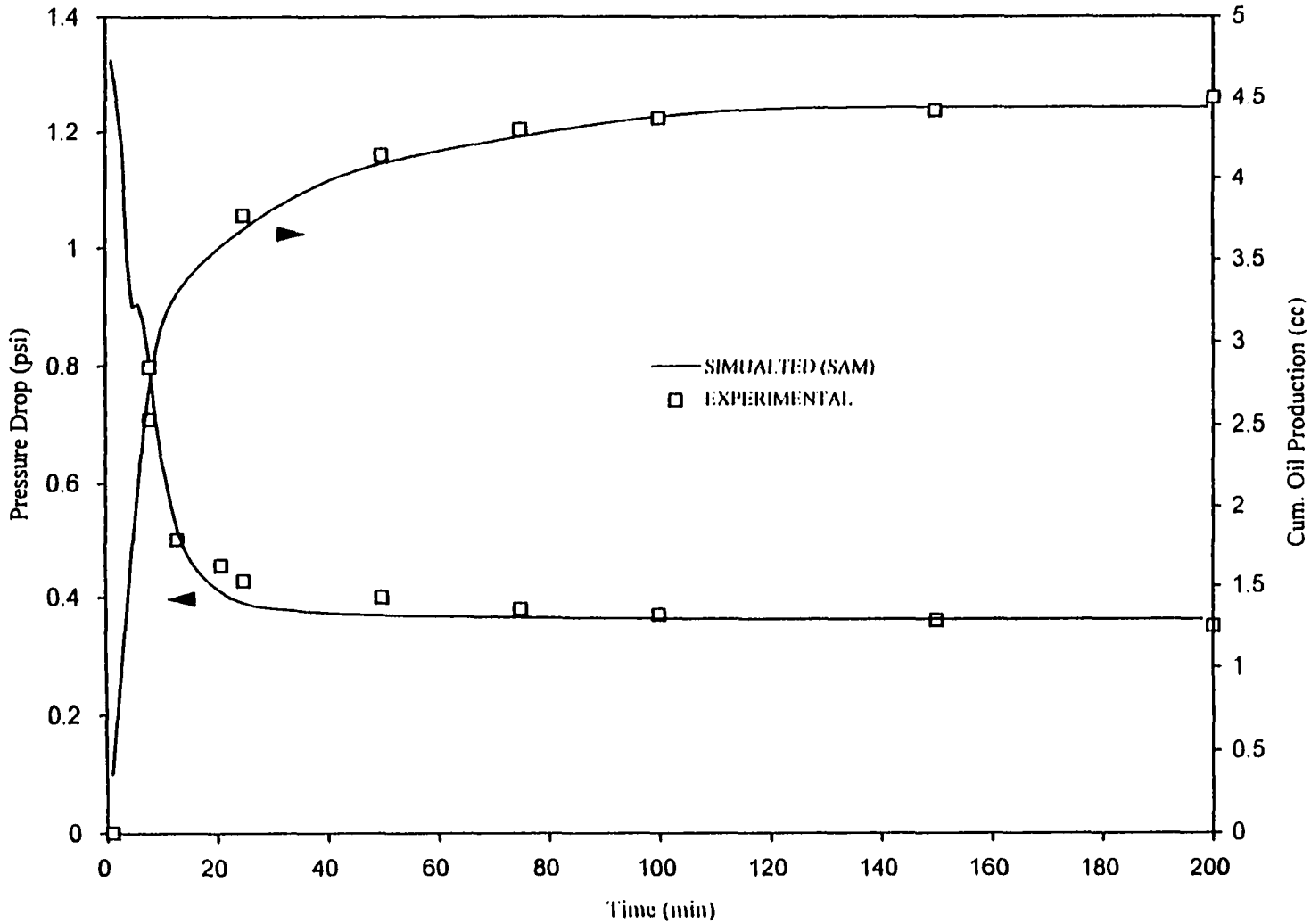


Fig. 7.13: Pressure drop and cumulative production history for the imbibition experiment by using discrete representation of flow functions

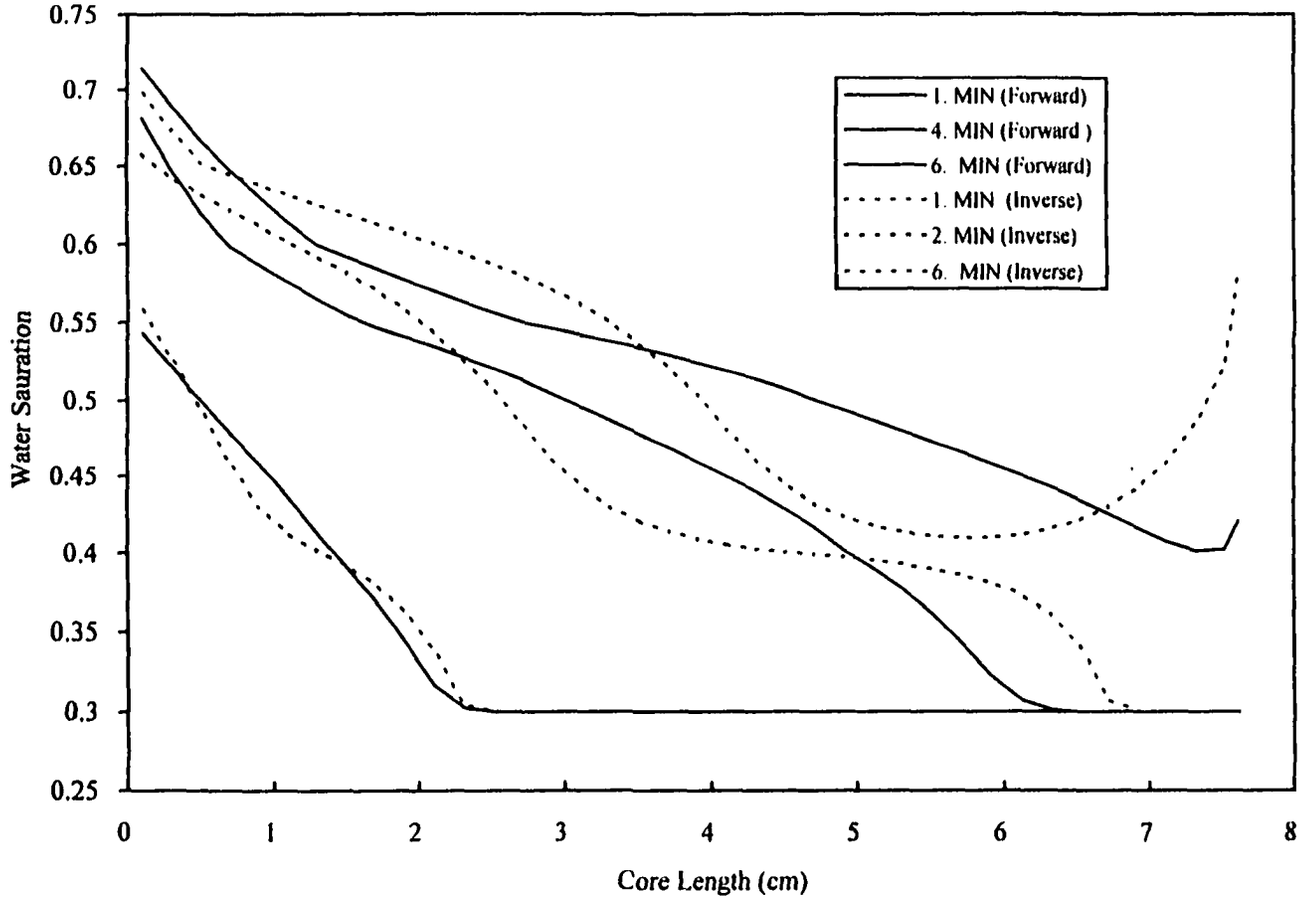


Fig. 7.14: Comparison of saturation history profiles for the imbibition experiment by using experimental and discrete representation of flow functions (Ucan et al.)

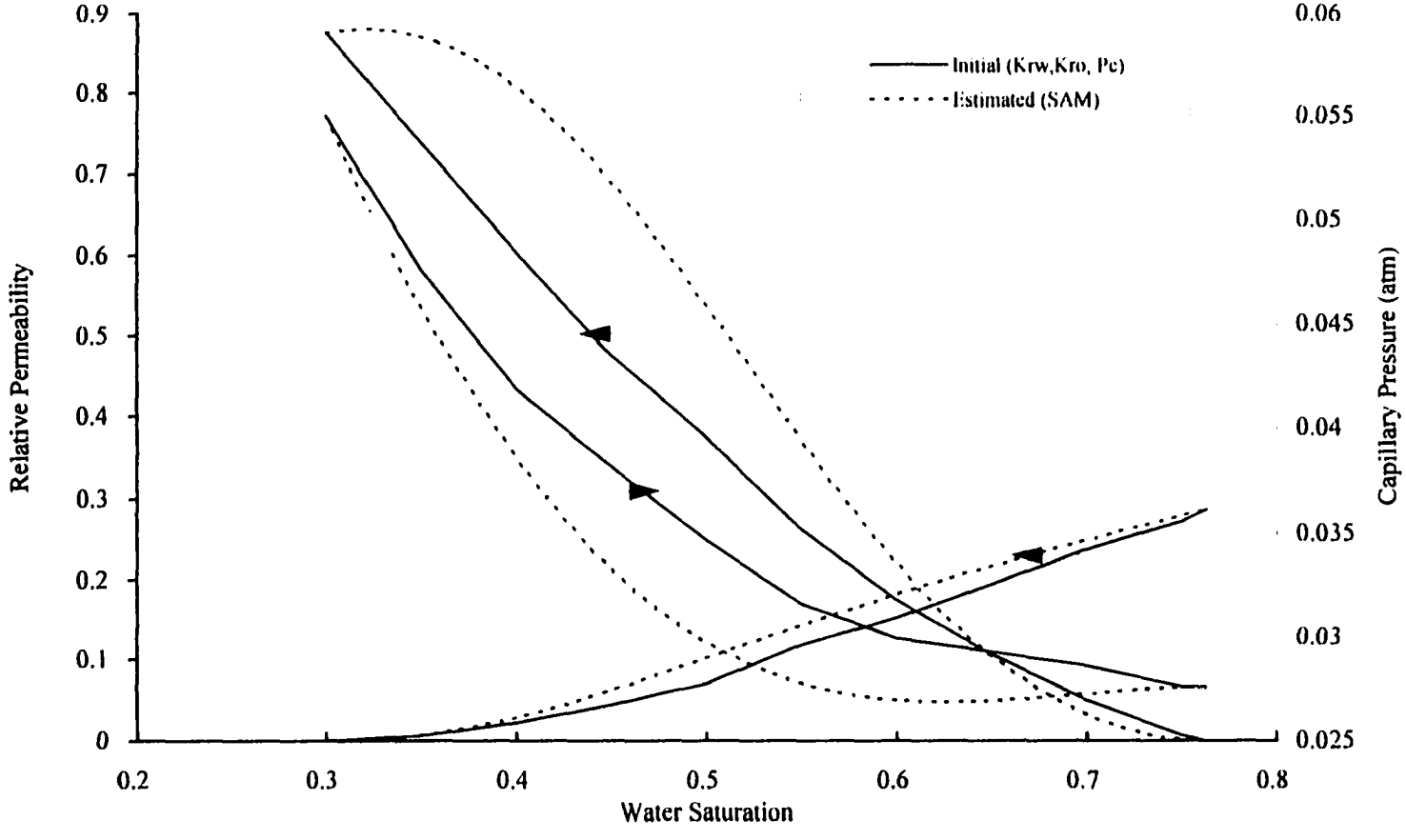


Fig. 7.15: Comparison of initial and estimated local functional representation of flow functions by using external core data

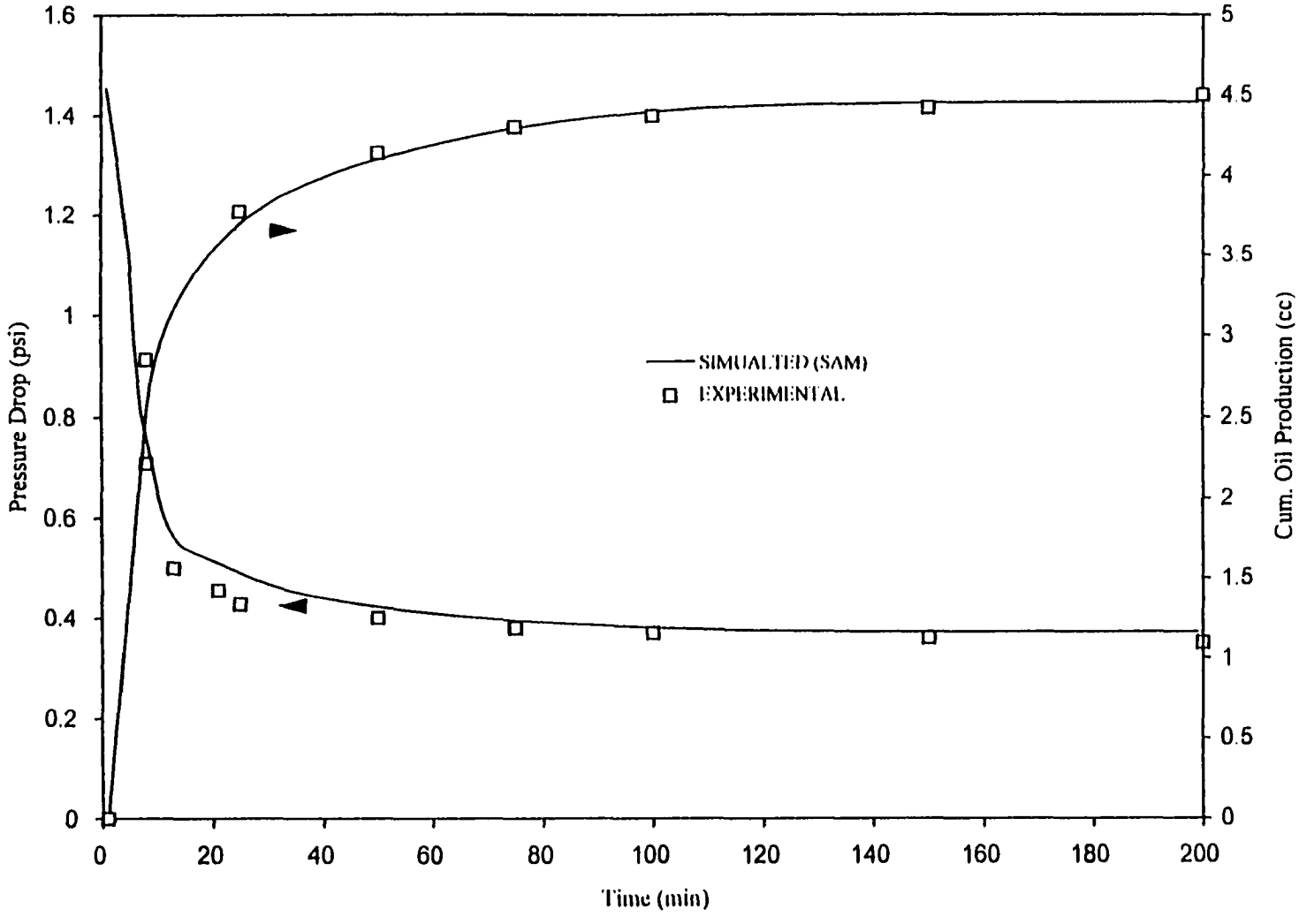


Fig. 7.16: Pressure drop and cumulative production history for the imbibition experiment by using local functional representation

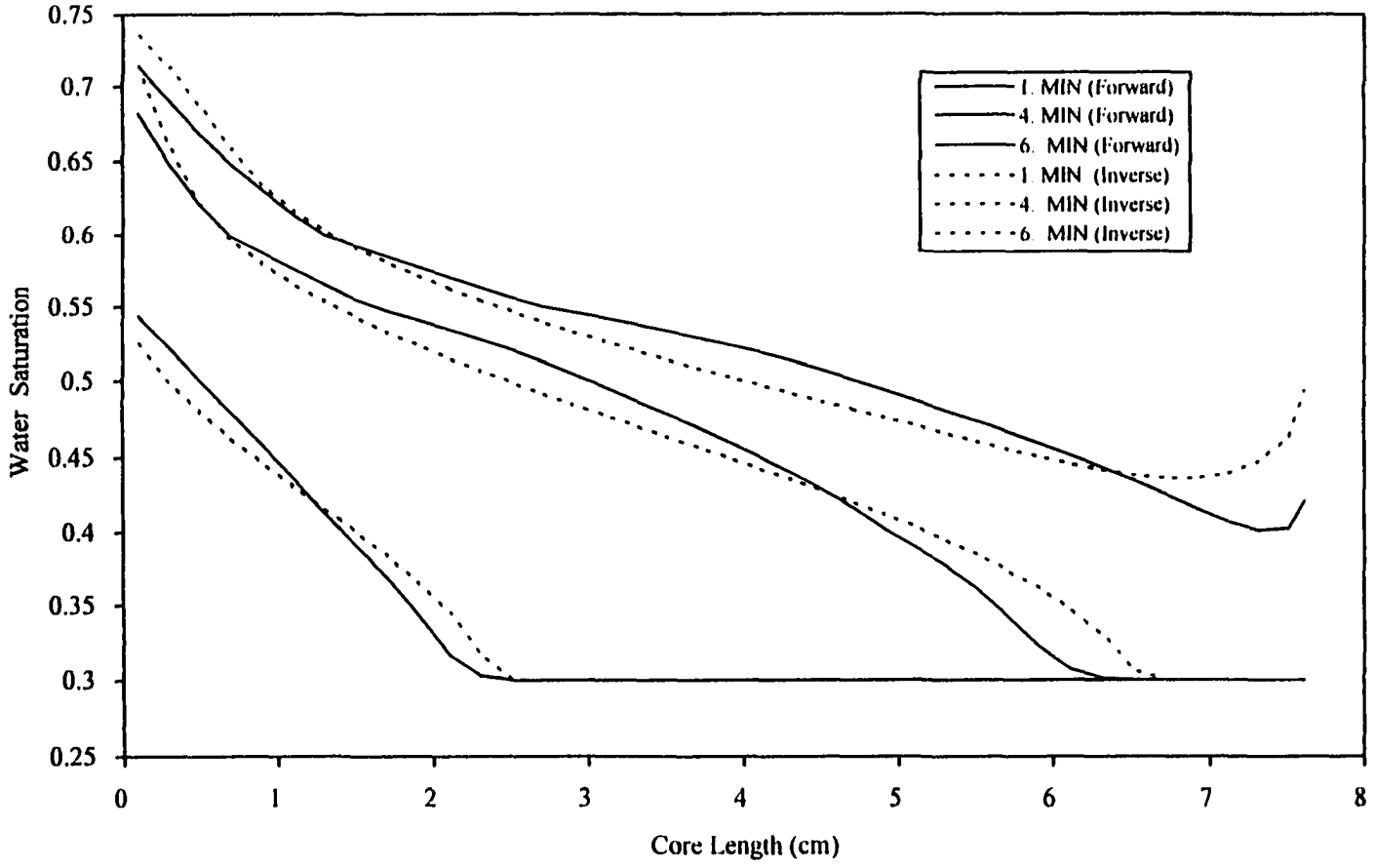


Fig. 7.17: Comparison of saturation history profiles using the estimated and initial flow functions

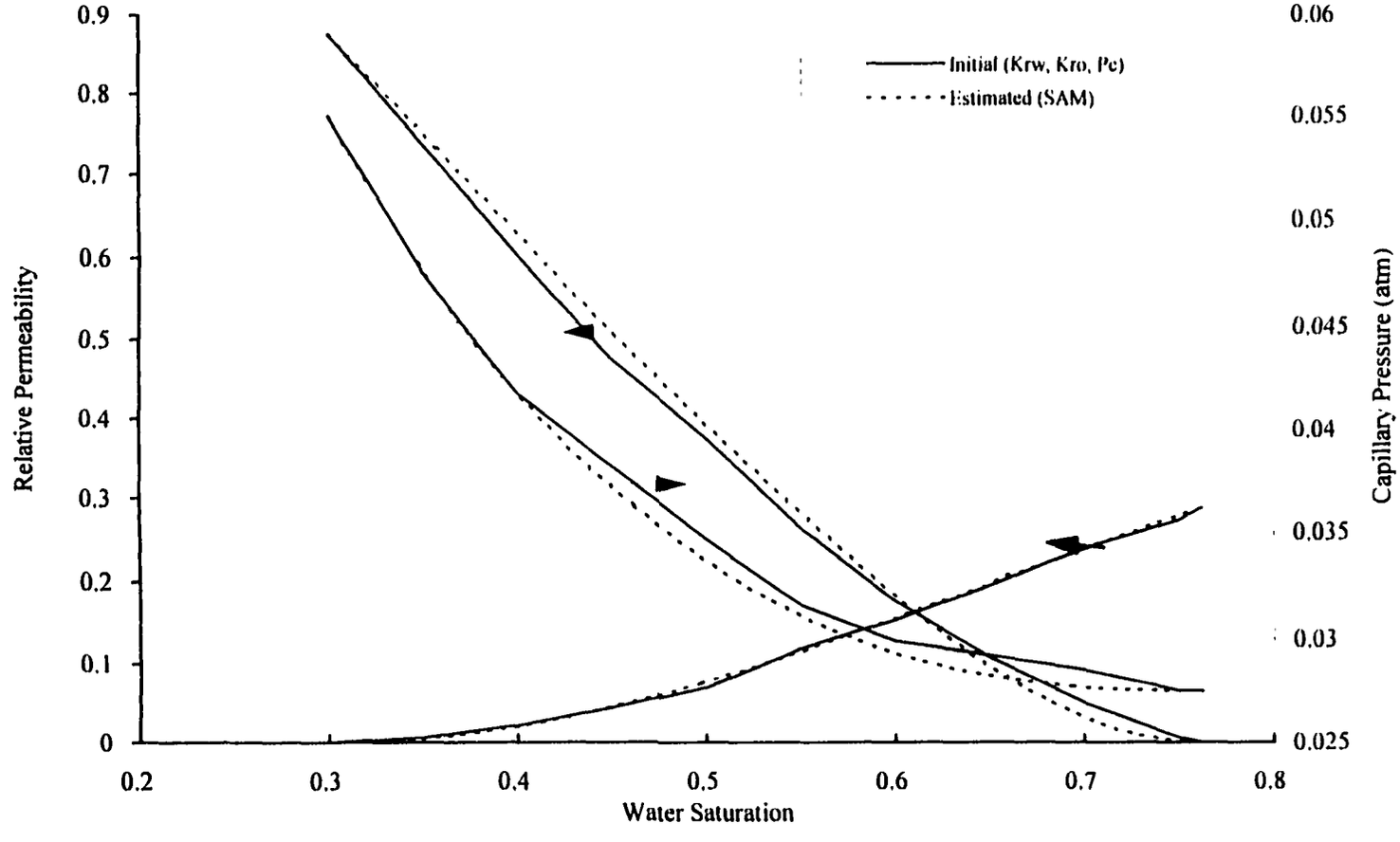


Fig. 7.18: Comparison of initial and estimated local functional representation of flow functions by using internal and external core data

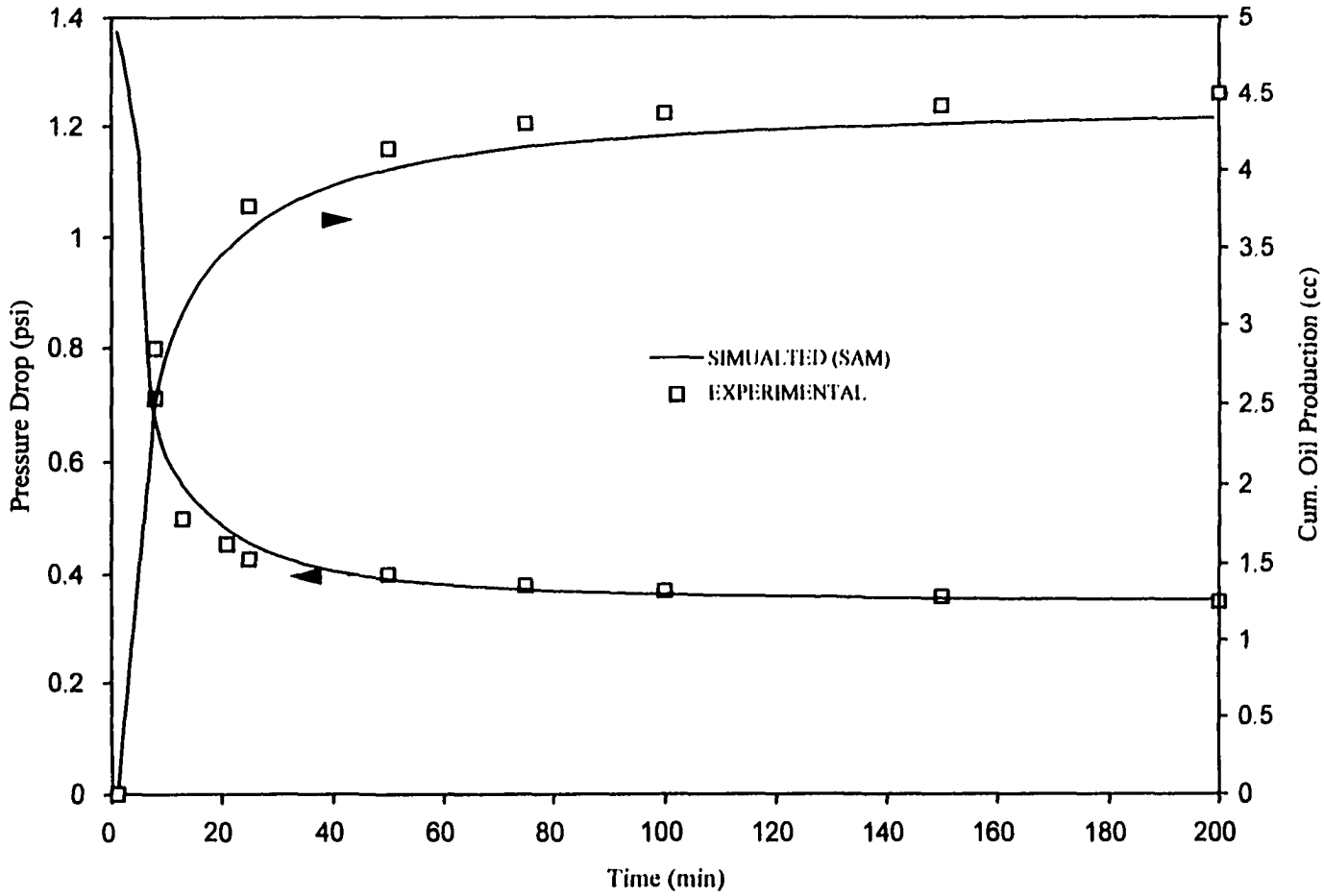


Fig. 7.19: Pressure drop and cumulative production history for the imbibition experiment by using local functional representation

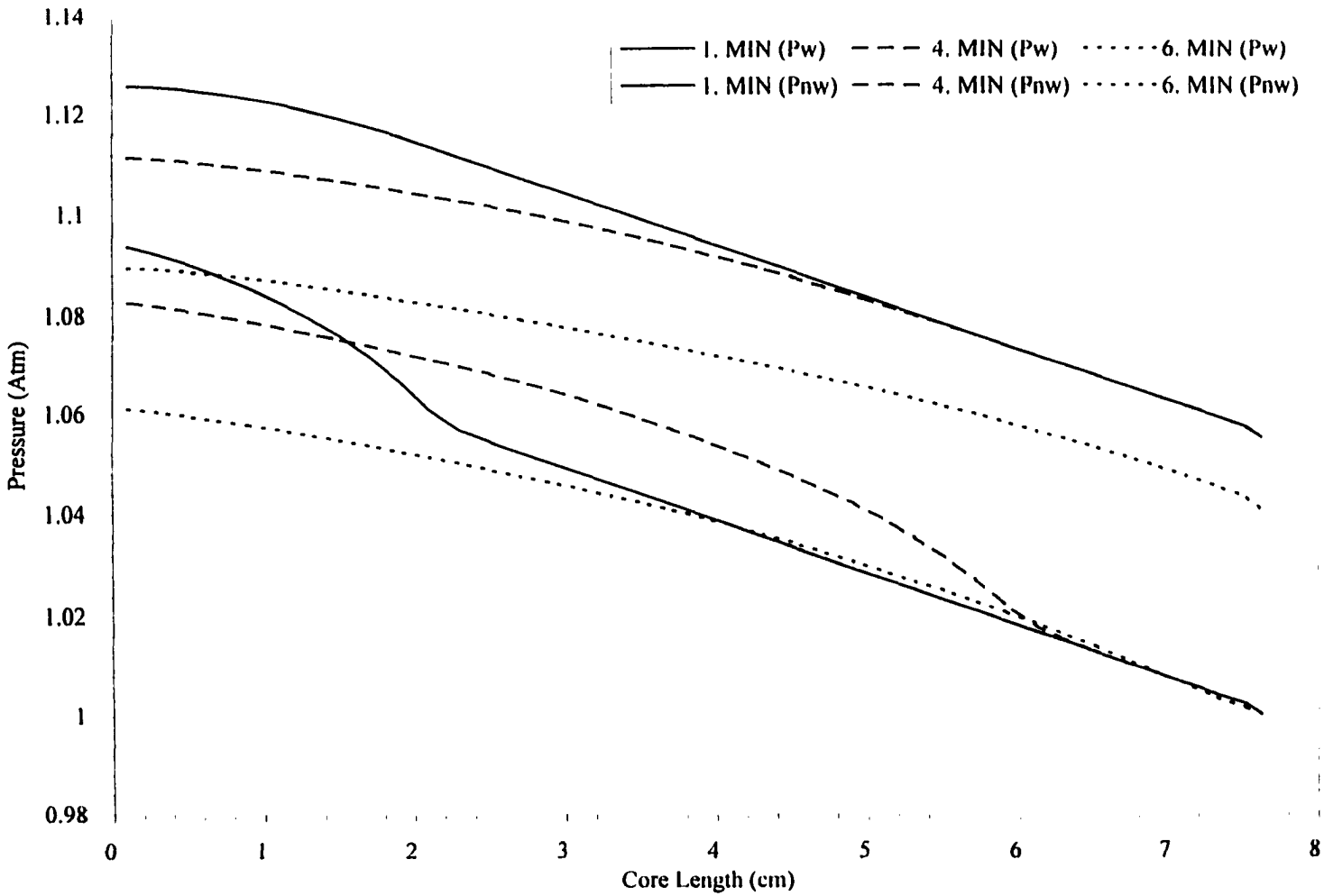


Fig. 7.20: Pressure history profiles before the breakthrough for the imbibition experiment

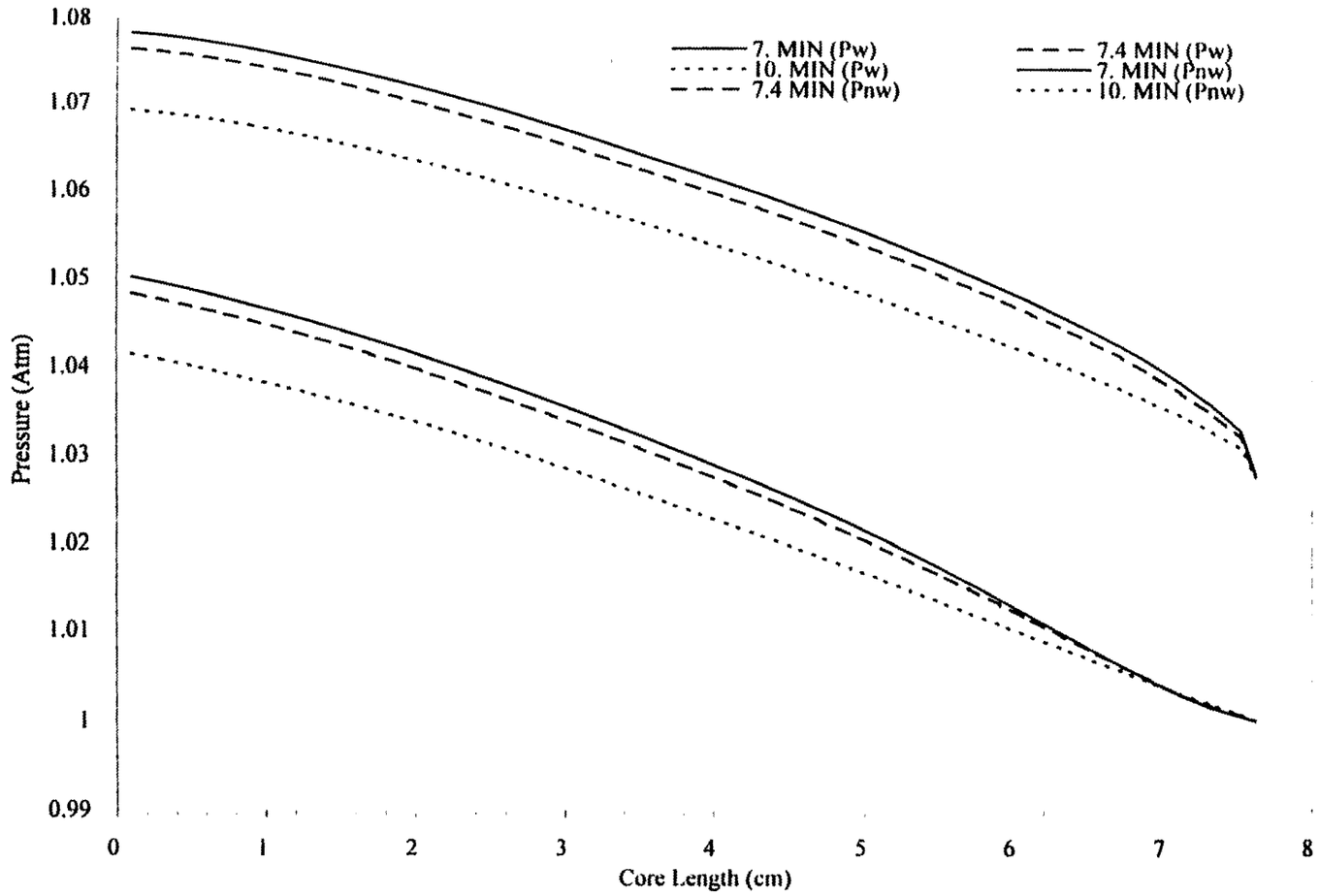


Fig. 7.21: Pressure history profiles after the breakthrough for the imbibition experiment

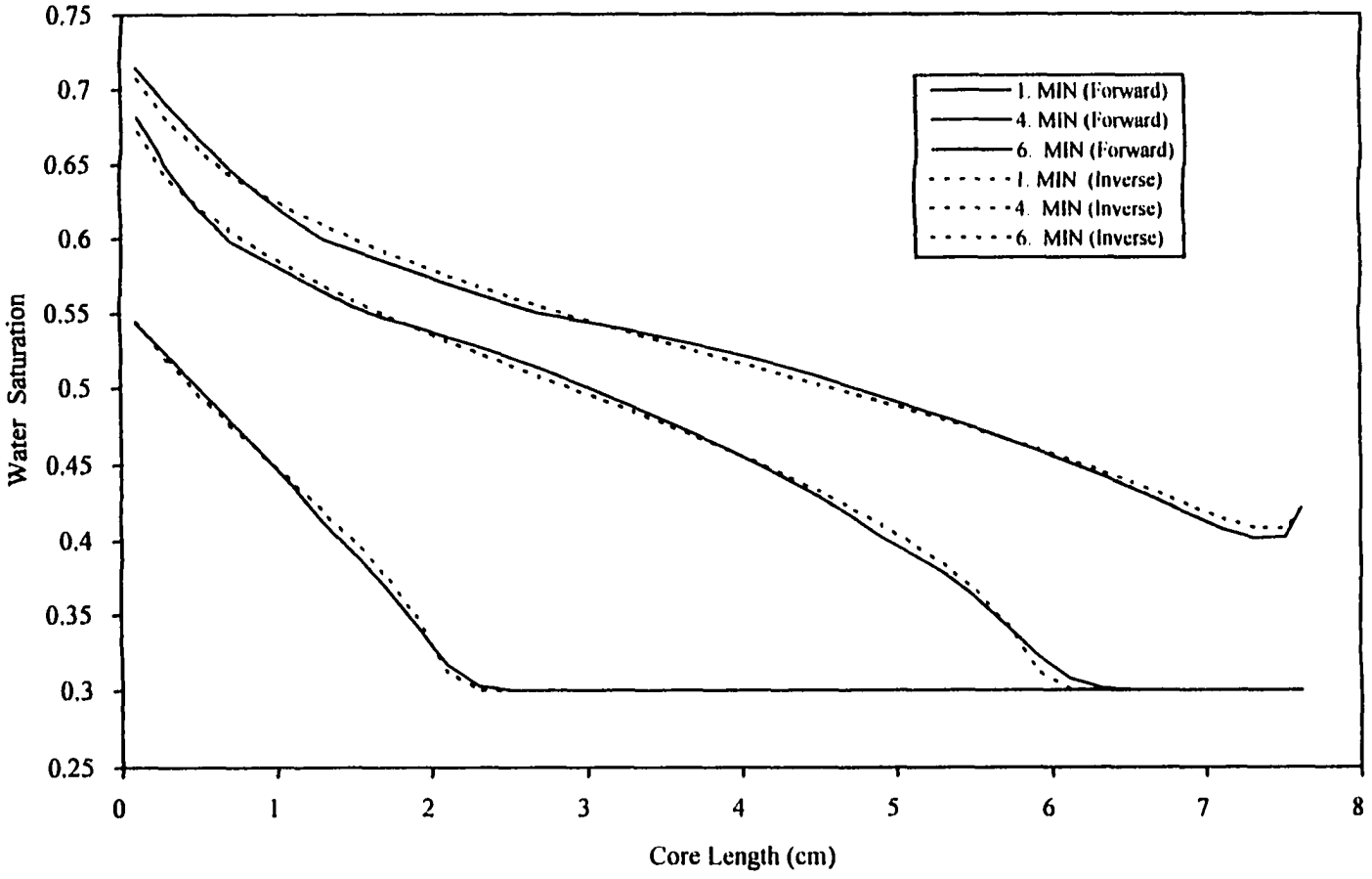


Fig.7.22: Comparison of saturation history profiles using estimated and initial flow functions

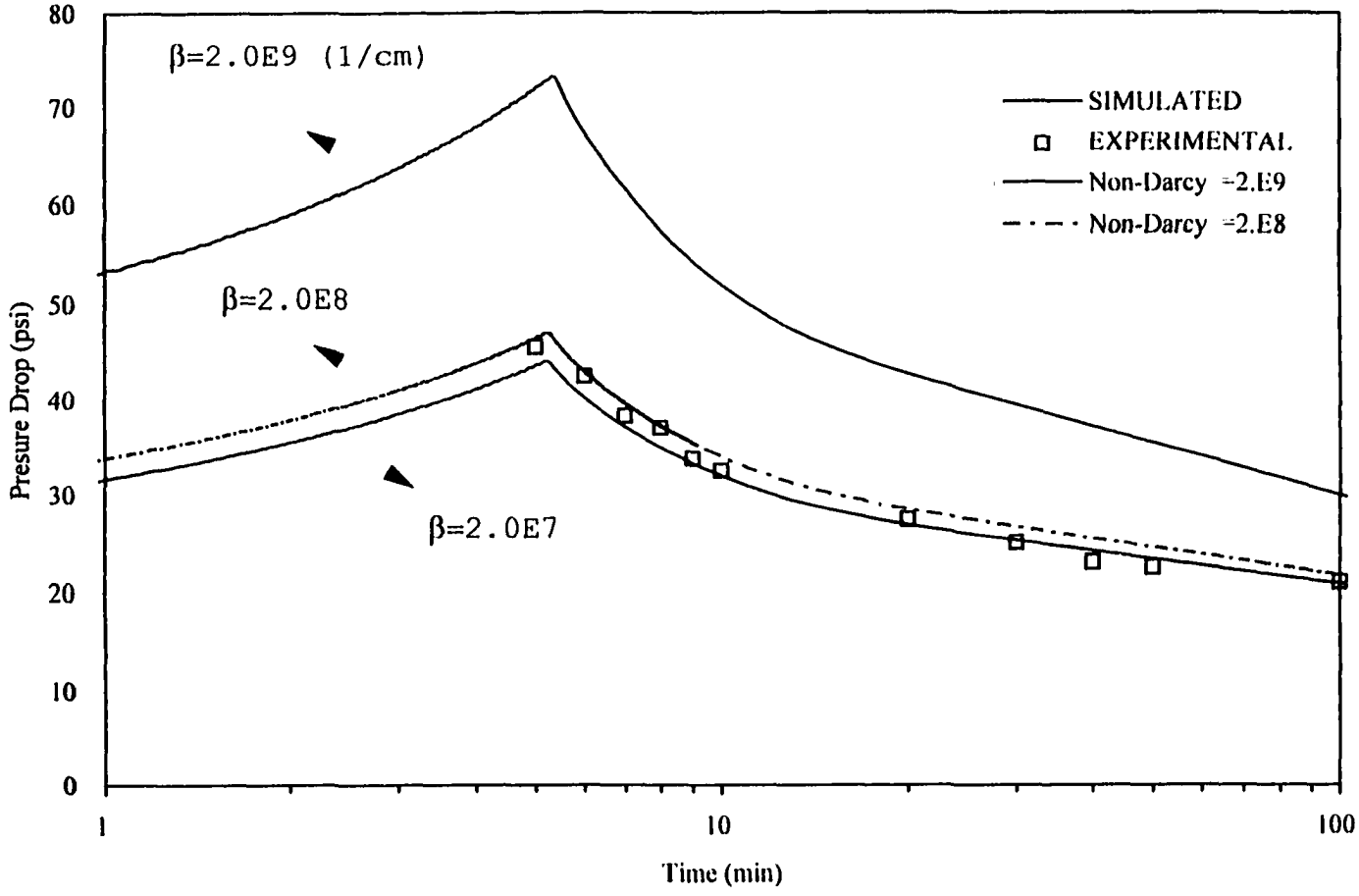


Fig. 7.23: Effect of the inertial flow coefficient on the pressure drop

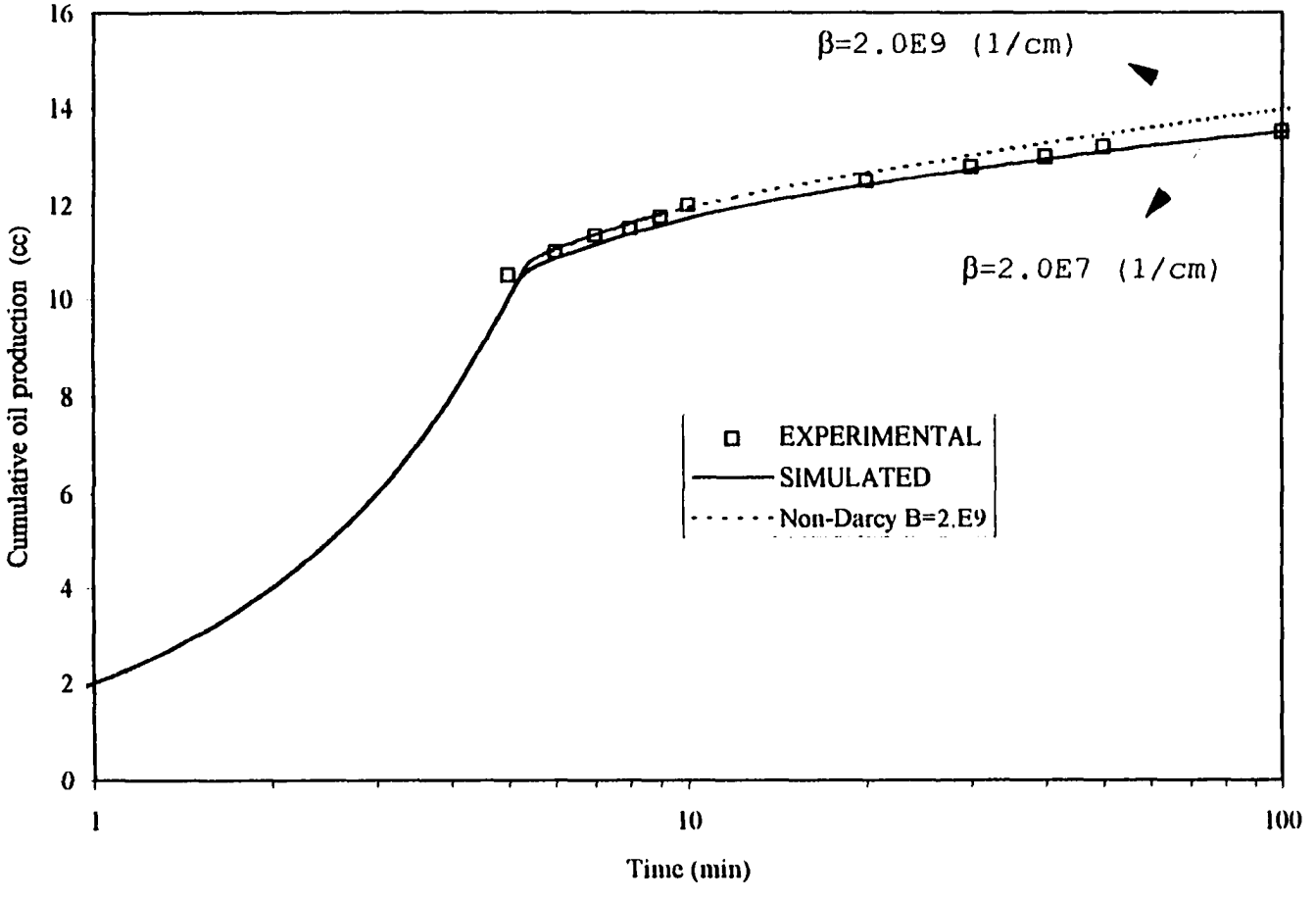


Fig. 7.24: Effect of the inertial flow coefficient on the cumulative production rate

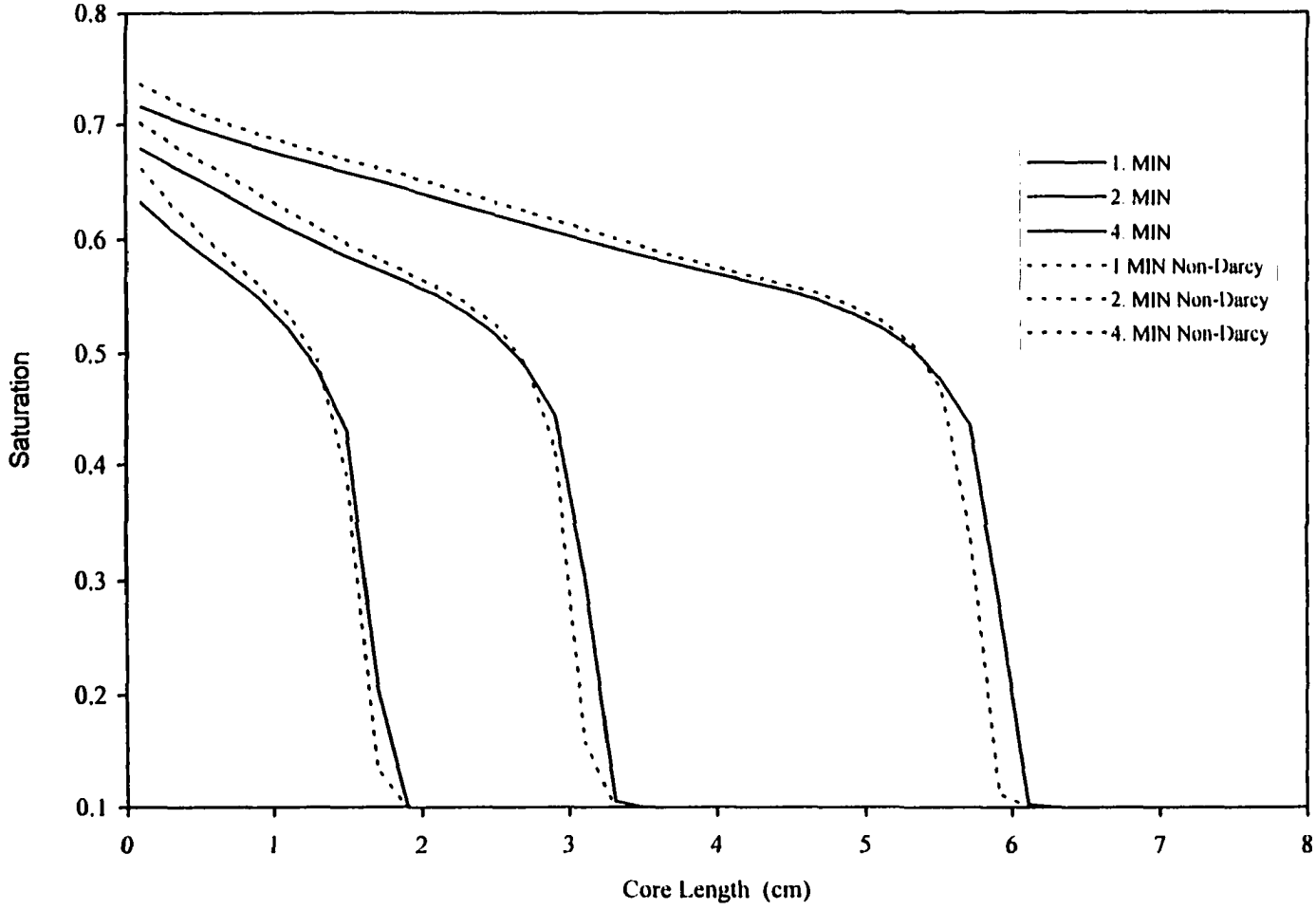


Fig. 7.25: Effect of the inertial flow coefficient of saturation history profiles for Darcy and non-Darcy flows

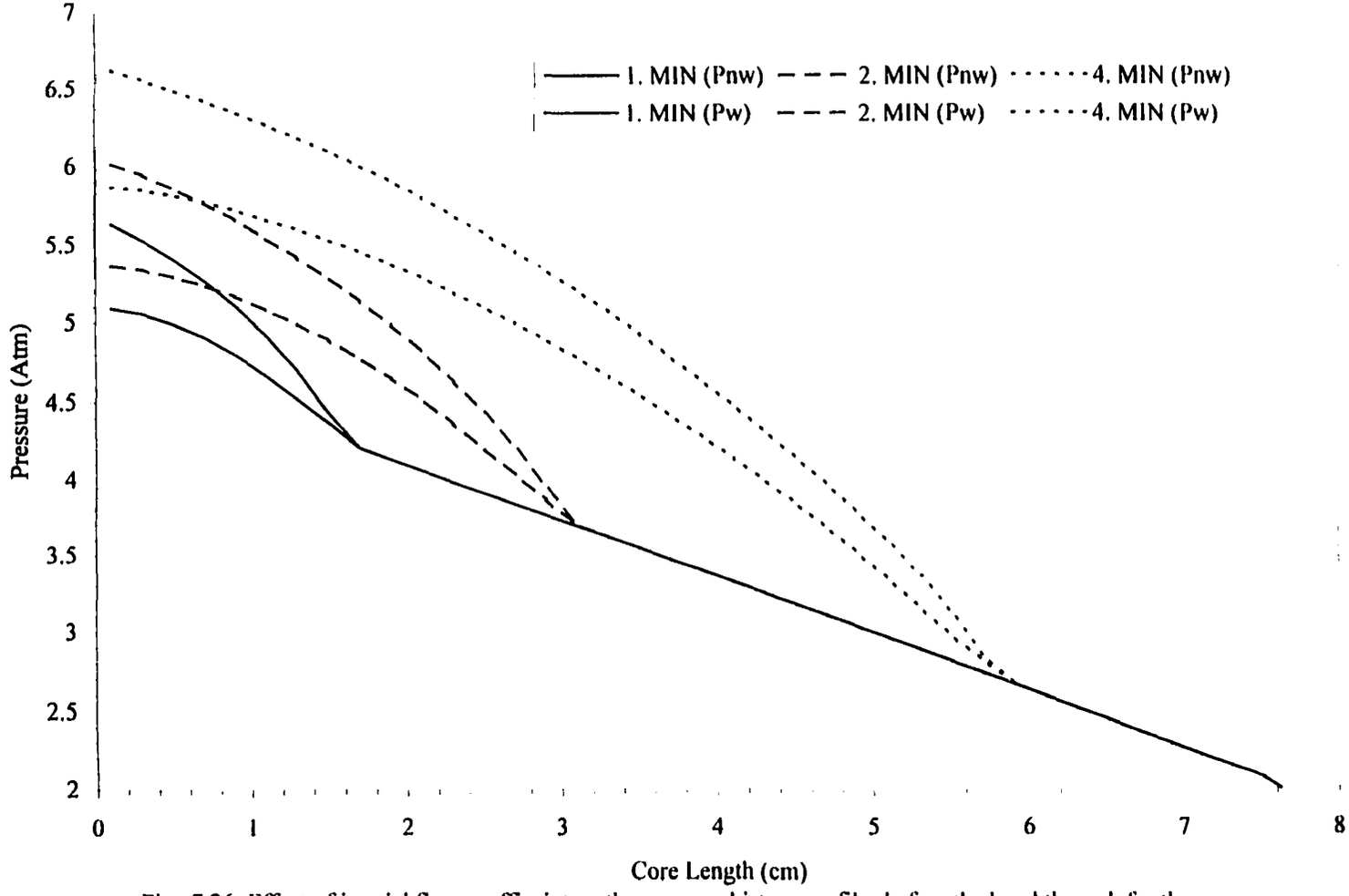


Fig. 7.26: Effect of inertial flow coefficeint on the pressure history profiles before the breakthrough for the drainage experiment

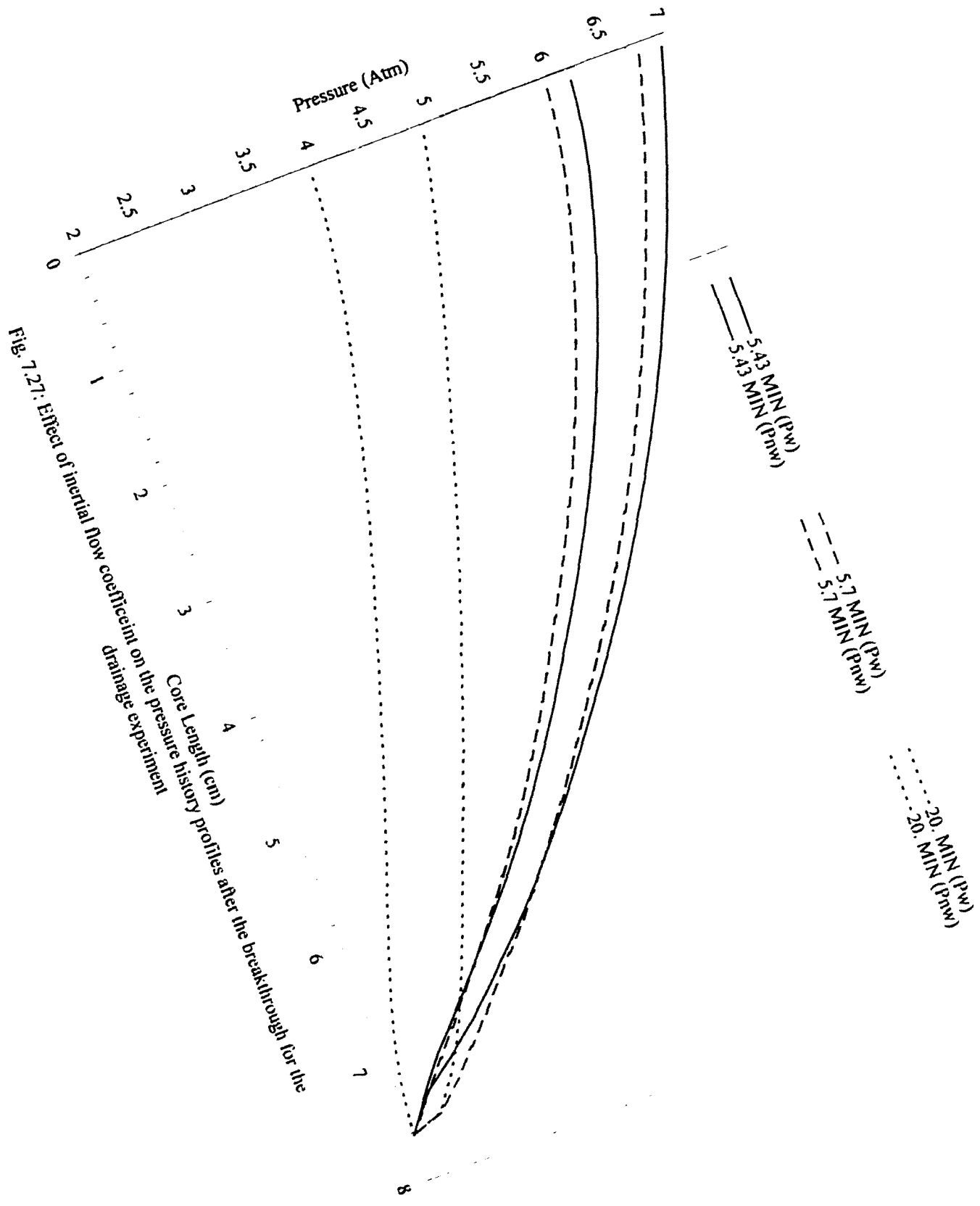


Fig. 7.27: Effect of inertial flow coefficeint on the pressure history profiles after the breakthrough for the drainage experiment

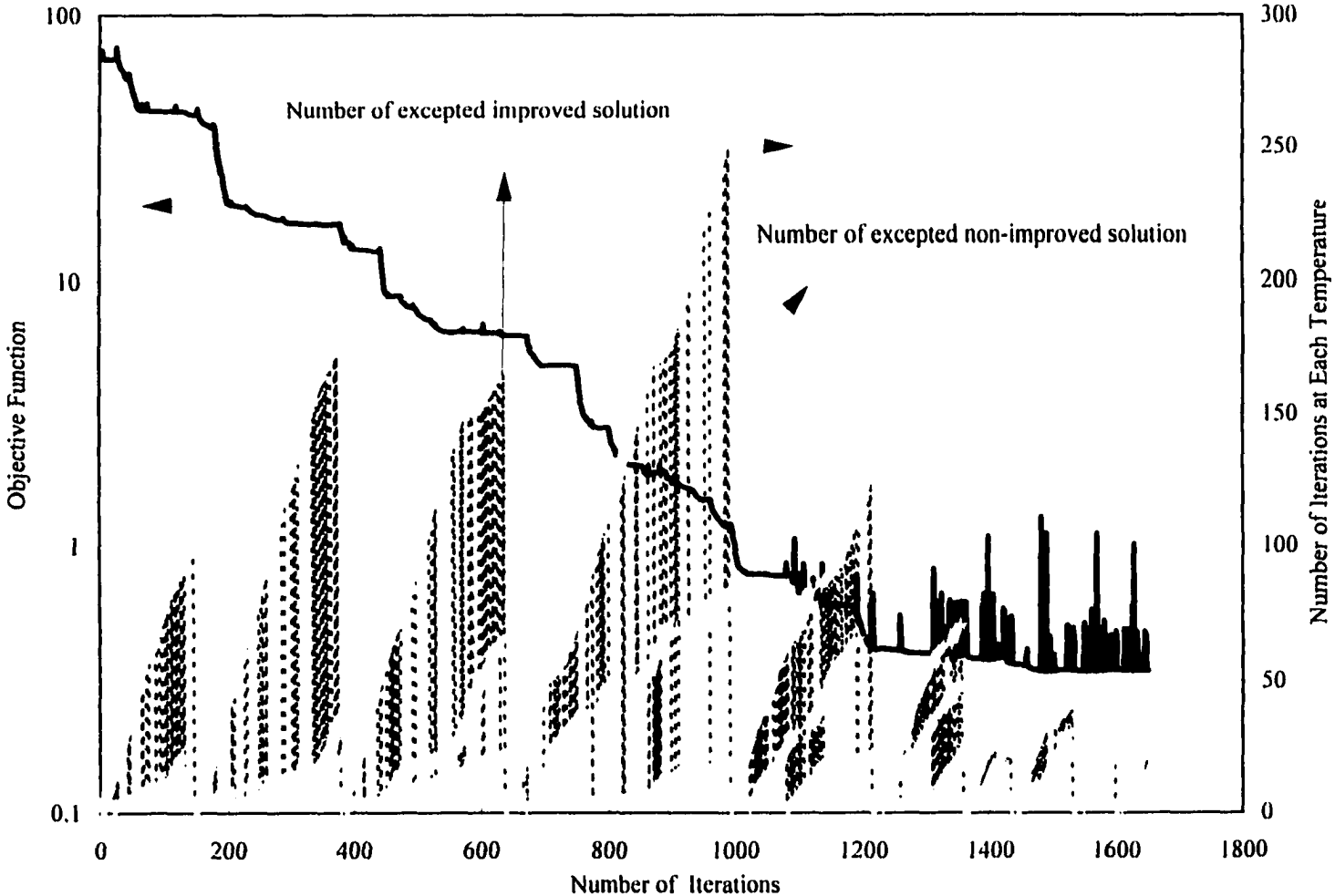


Fig. 7.28: Minimization of the objective function at the reduced temperature for the imbibition experiment

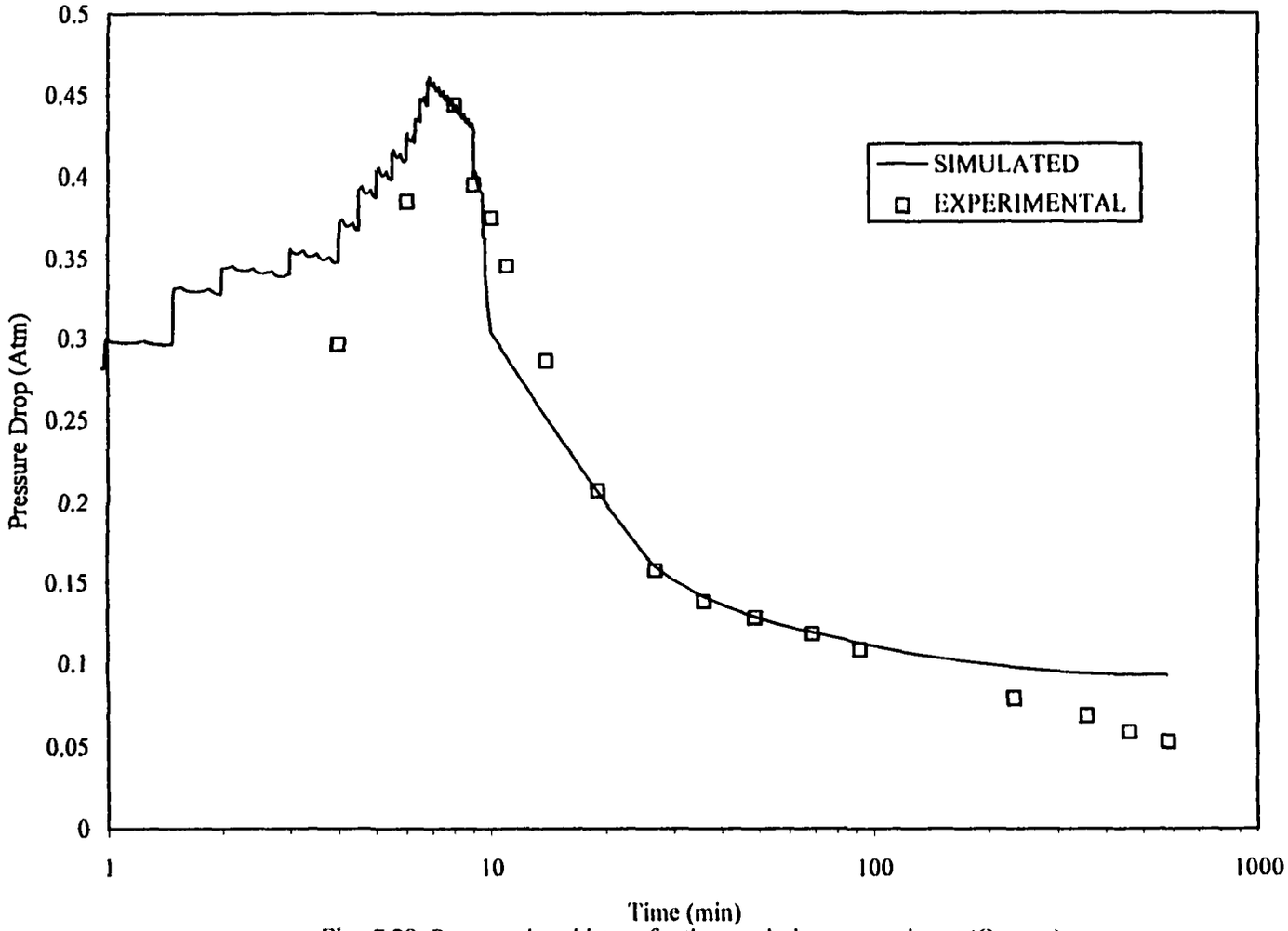


Fig. 7.29: Pressure drop history for the gas drainage experiment (Ouenes)

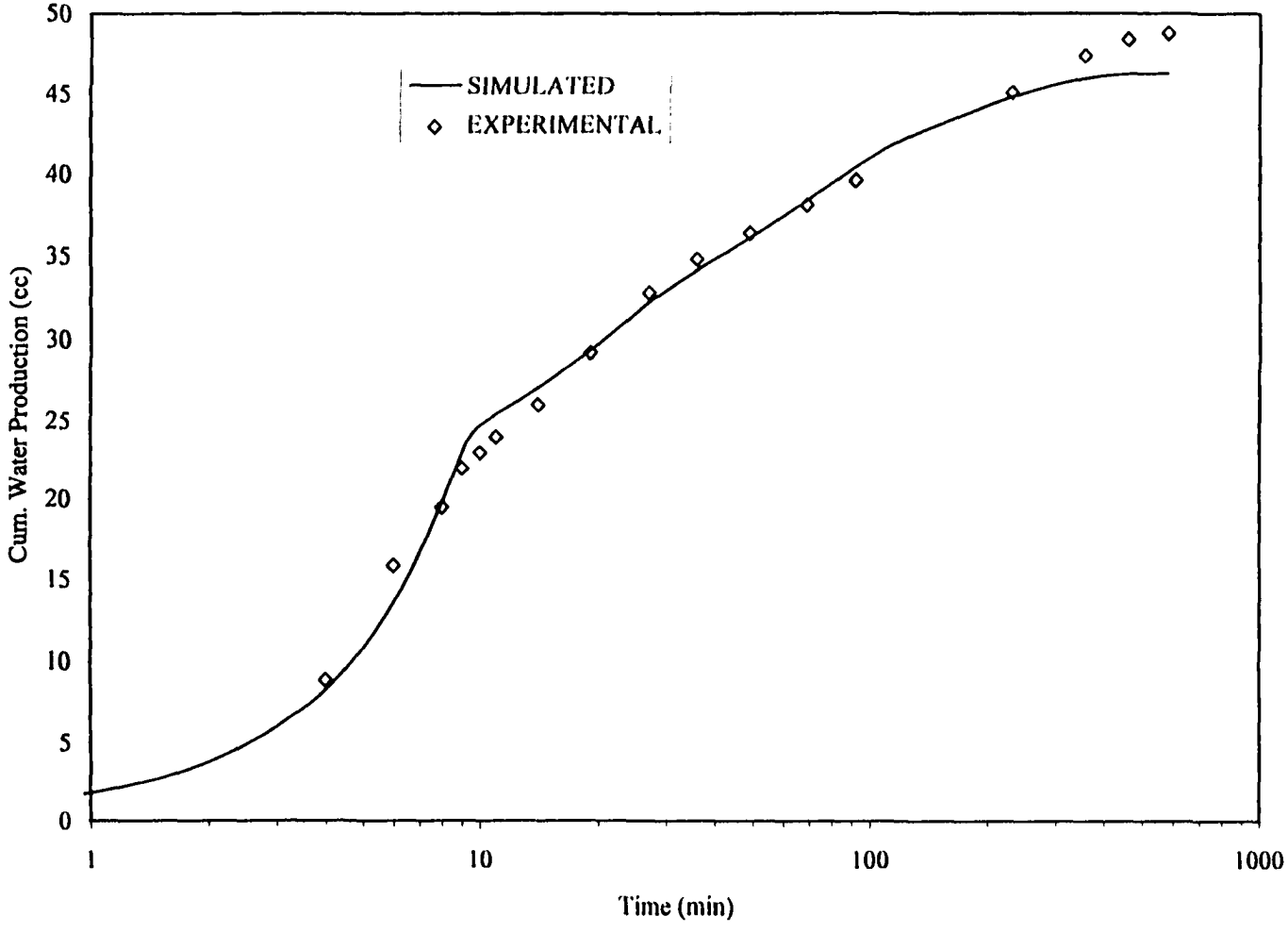


Fig. 7.30: Cumulative production rate for the gas drainage II experiment (Ouenes)

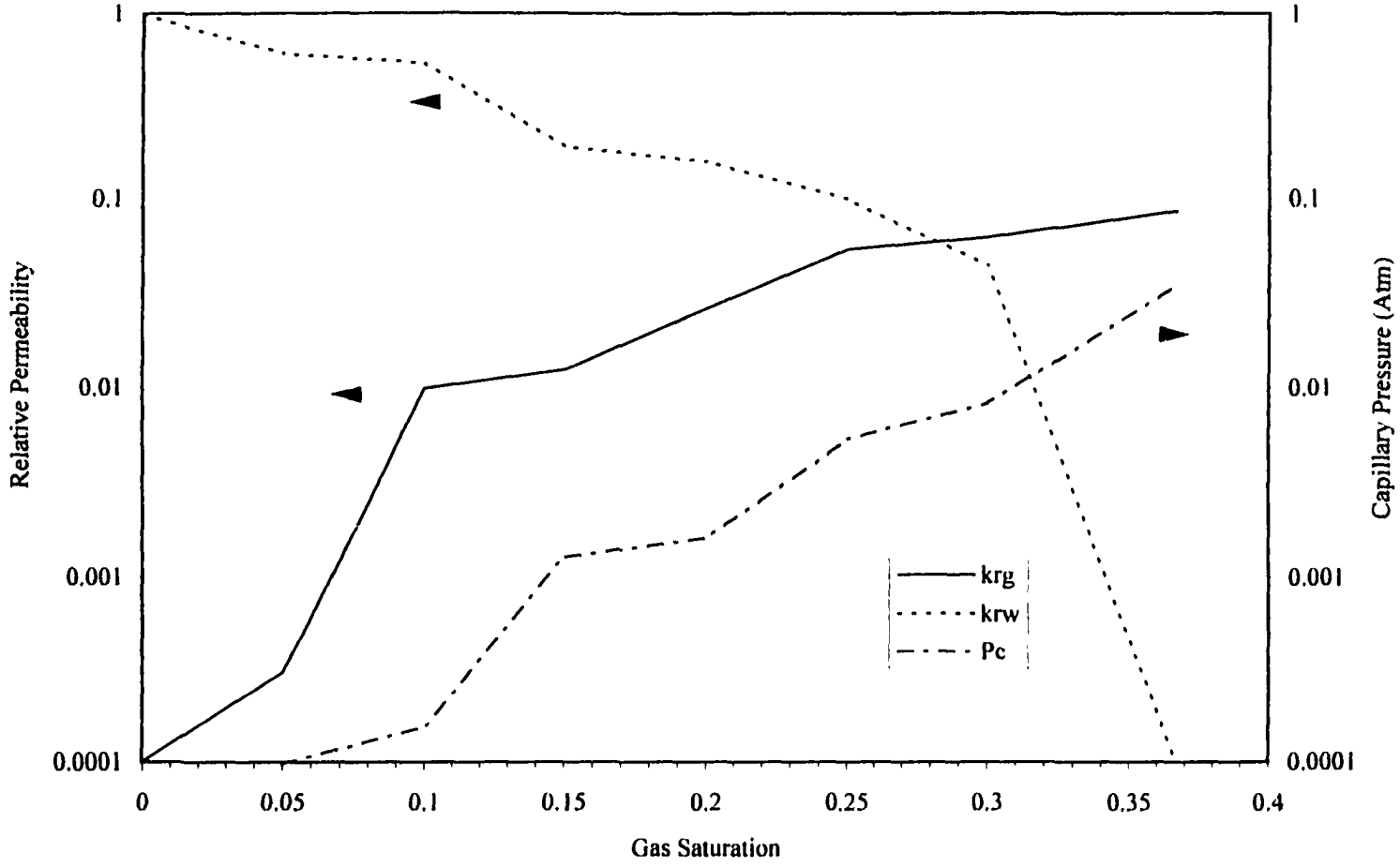


Fig.7.31: Estimated relative permeability and capillary pressure curves obtained for the gas drainage II experiment

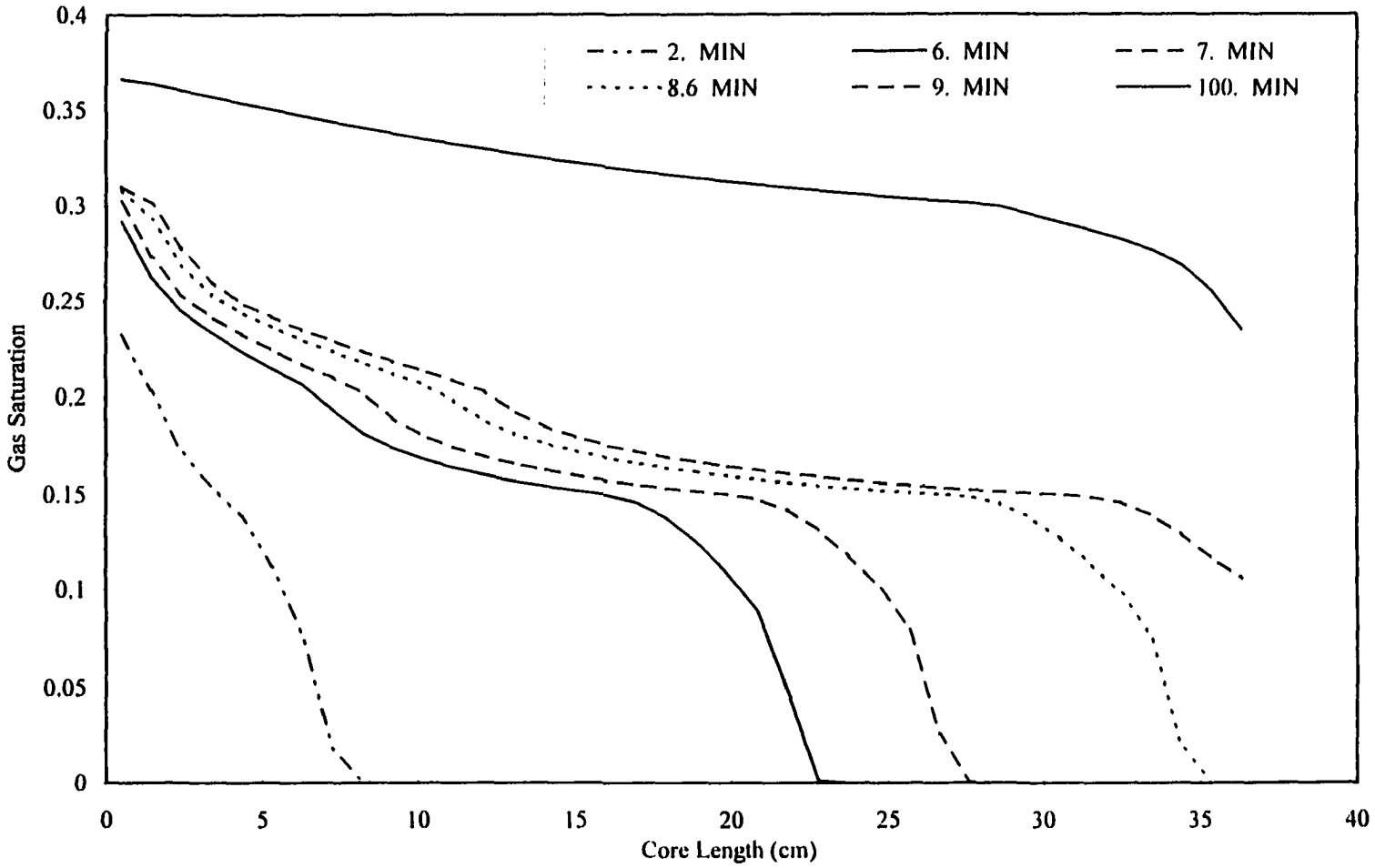


Fig.7.32: Saturation history profiles obtained for gas drainage II experiment

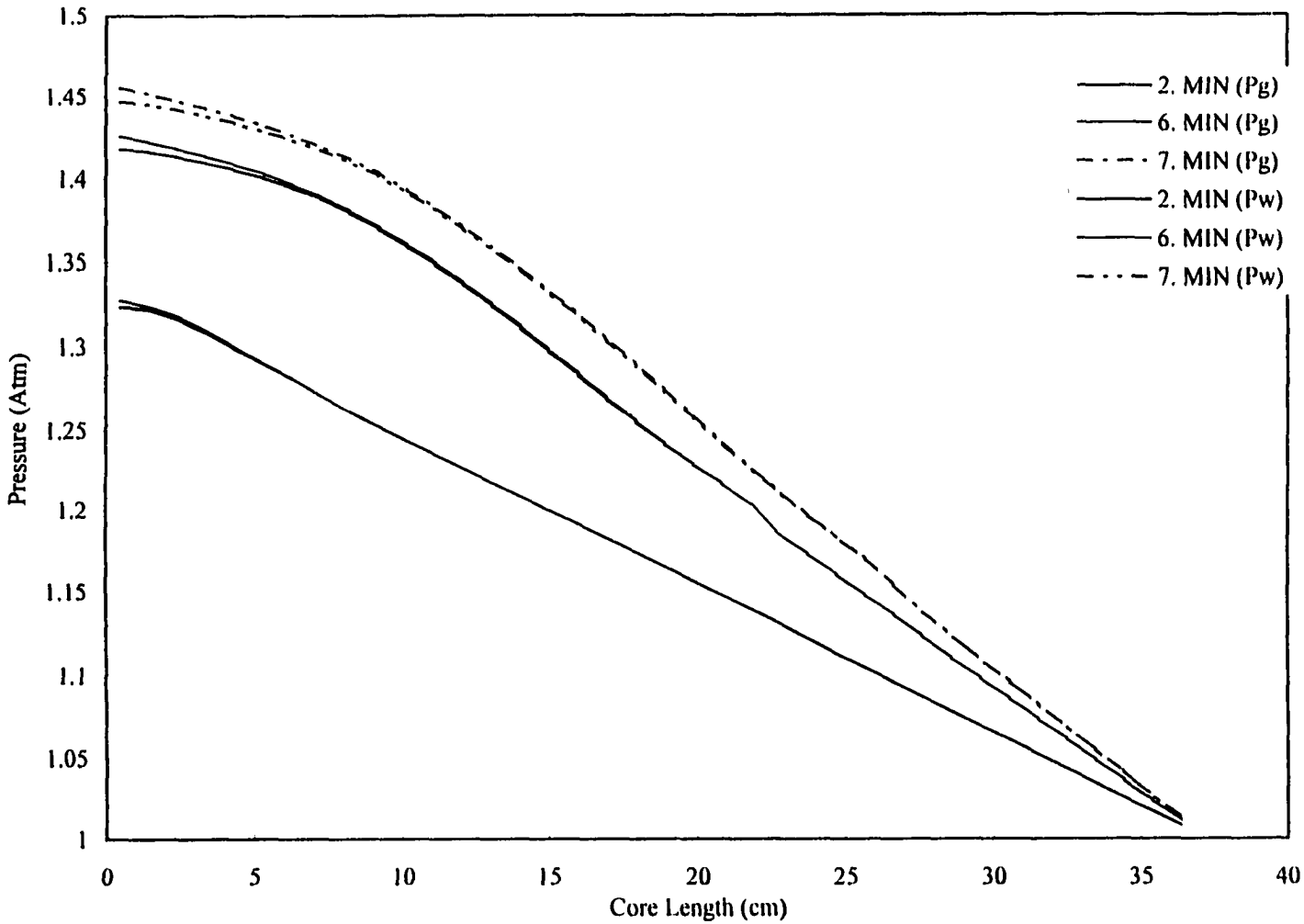


Fig. 7.33: Pressure history profiles before the breakthrough for the gas drainage II experiment

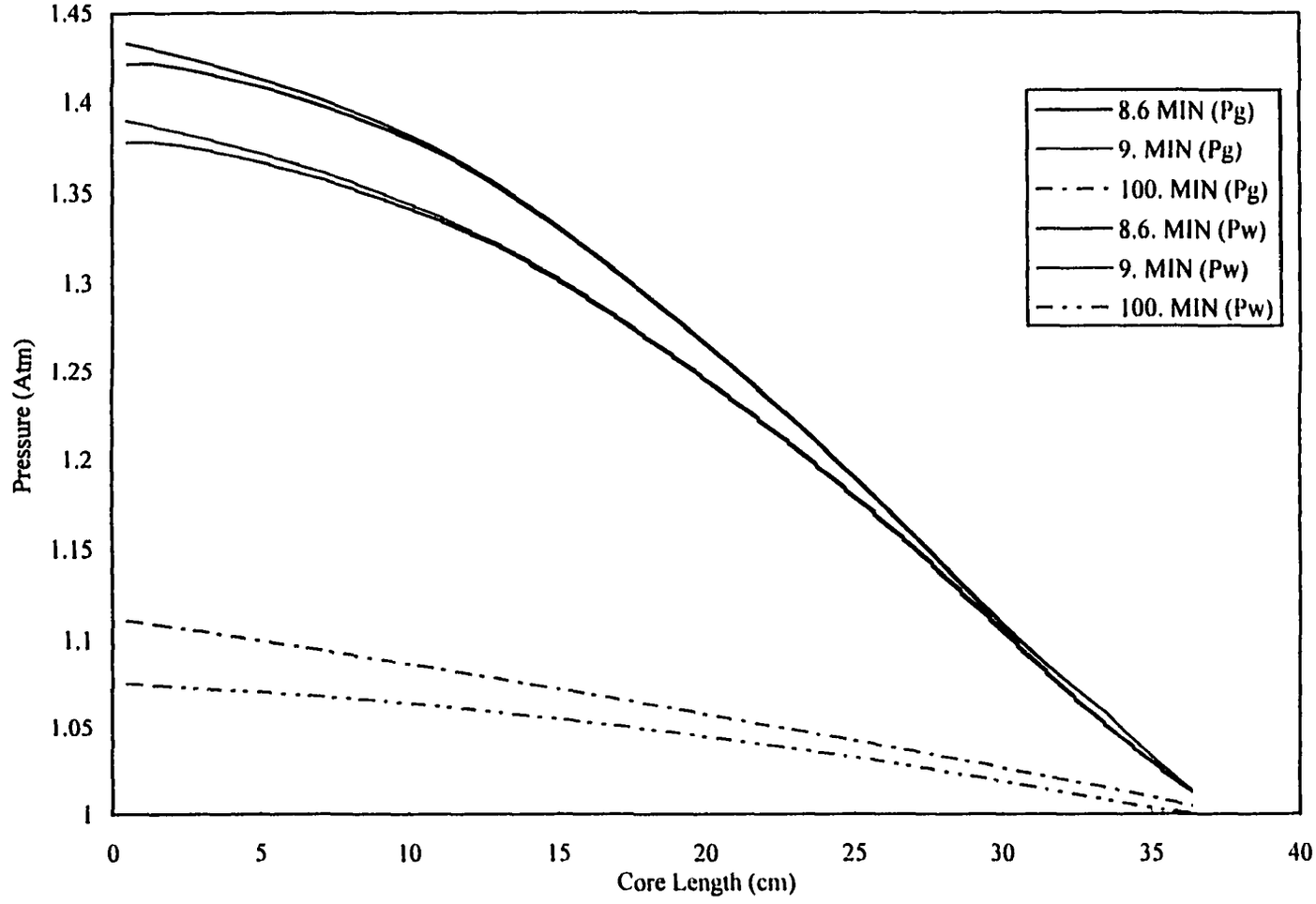


Fig. 7.34: Pressure history profiles after the breakthrough for the gas drainage II experiment

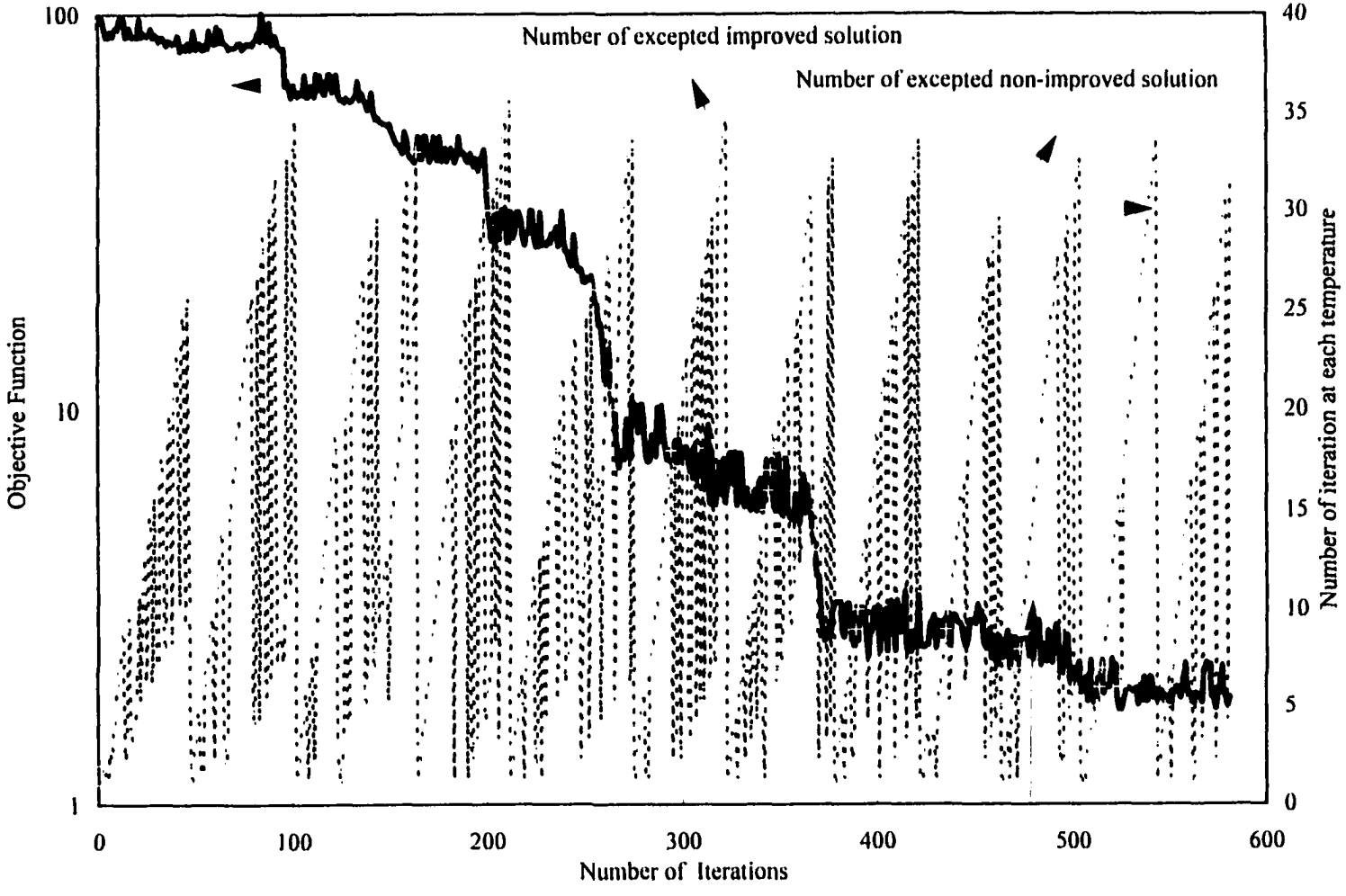


Fig. 7.35: Minimization of the objective function at the reduced temperature for the gas drainage II experiment

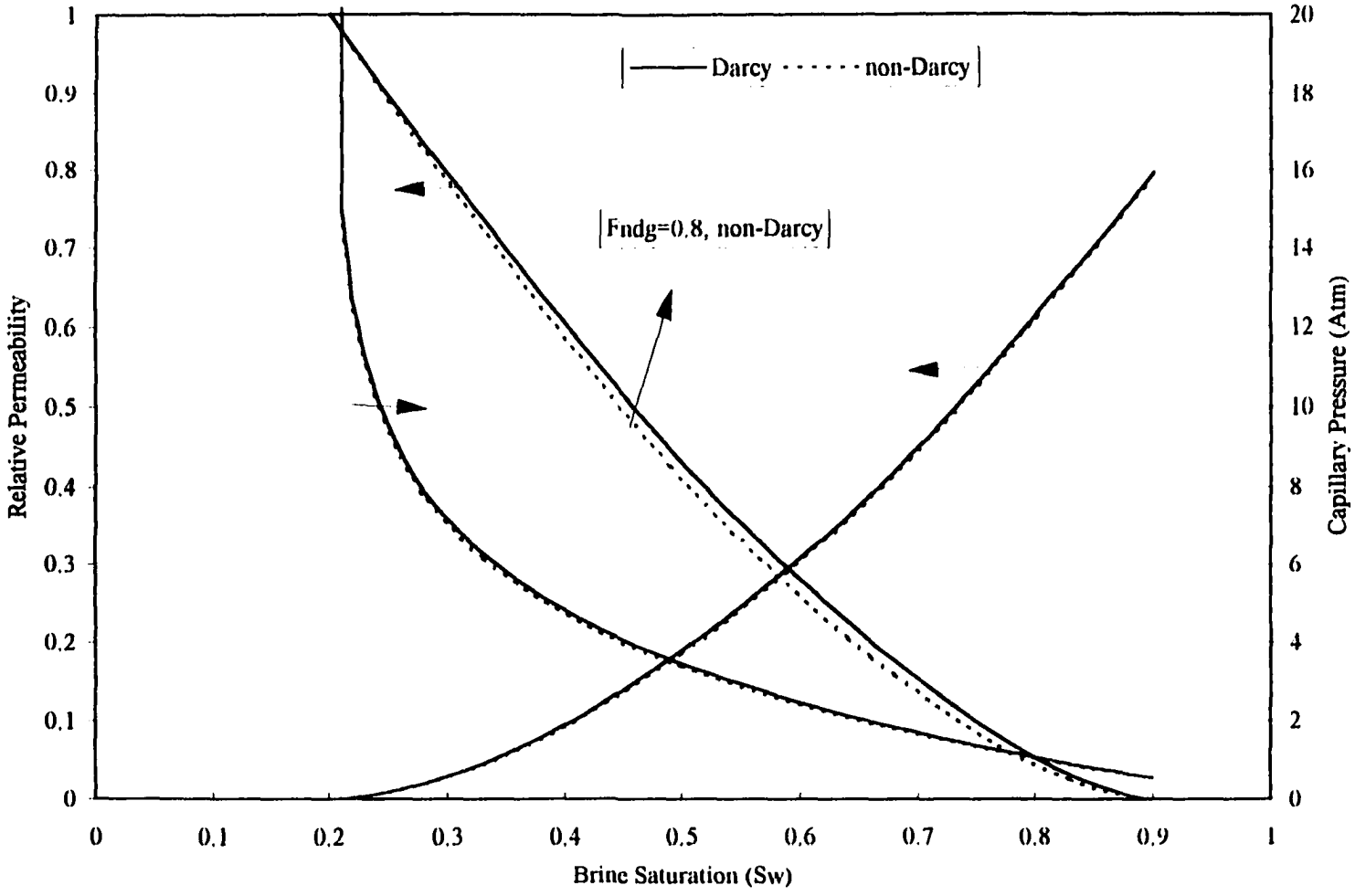


Fig. 7.36: Relative pereability and capillary pressure curves for the simulated Darcy and non-Darcy flow.

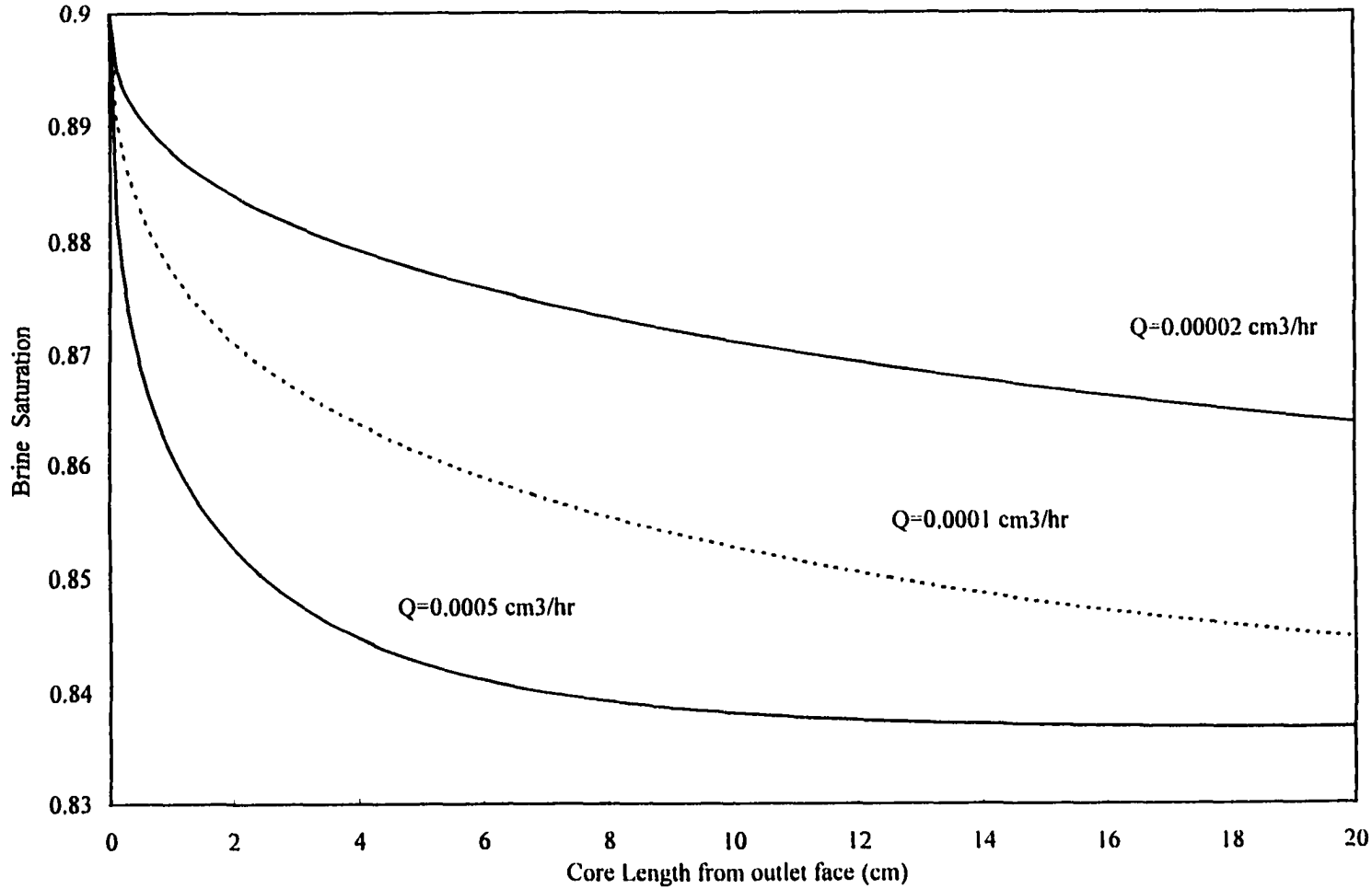


Fig. 7.37: Saturation profiles for different total flow rate.

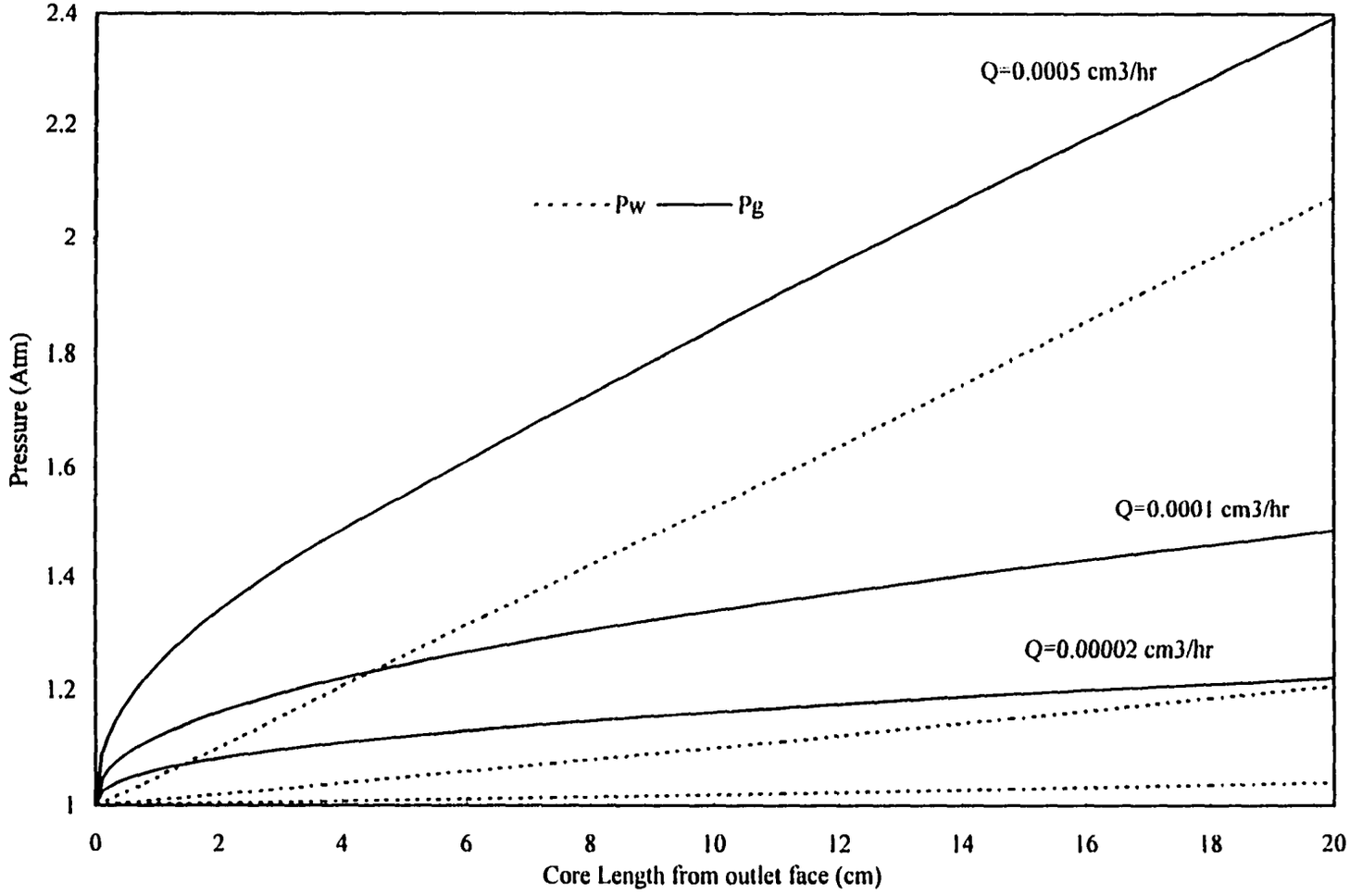


Fig. 7.38: Two phase pressure profiles for wetting and non wetting phase at the different flow rate.

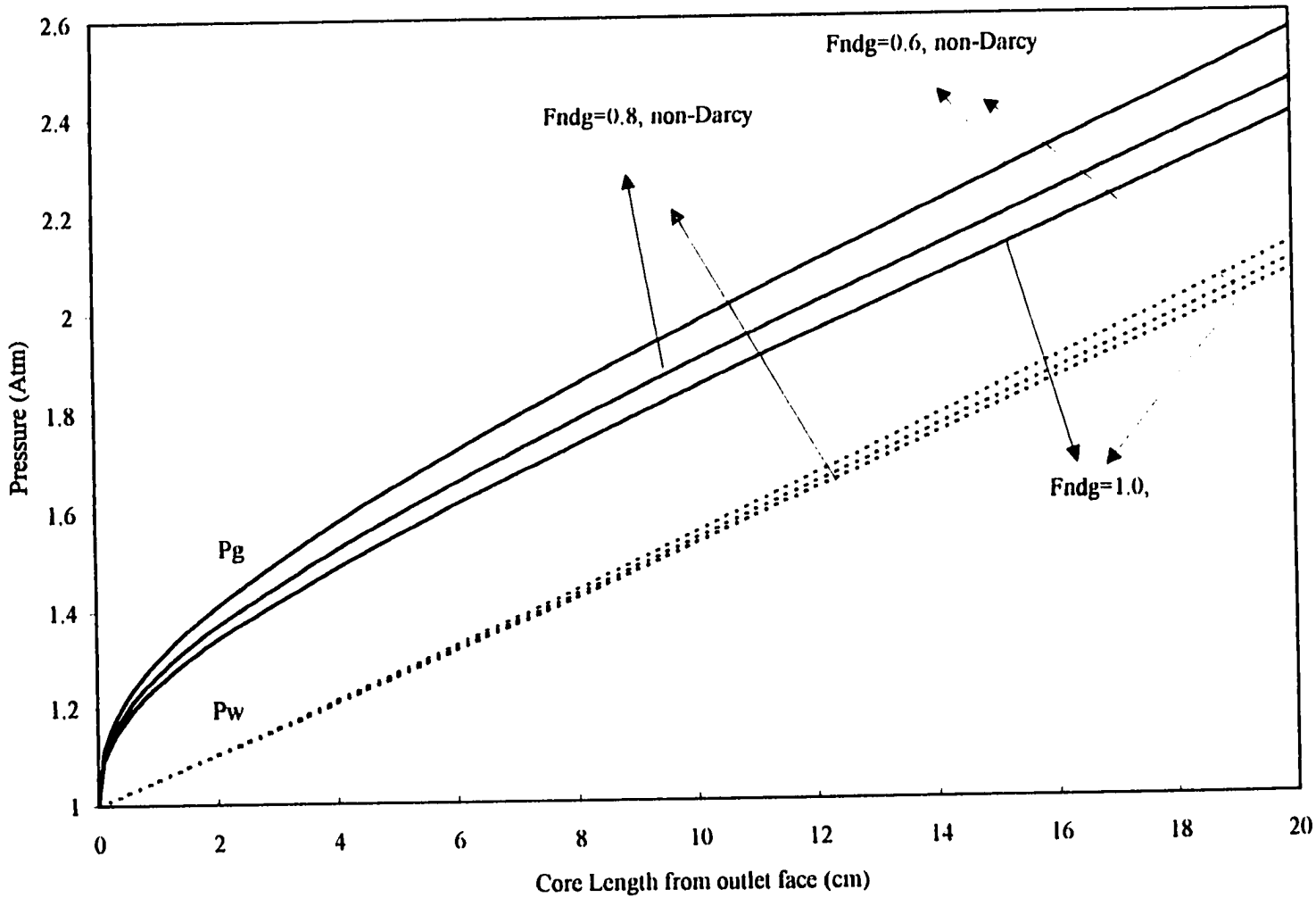


Fig. 7.39: Affect of non-Darcy flow on the two phase pressure profiles.

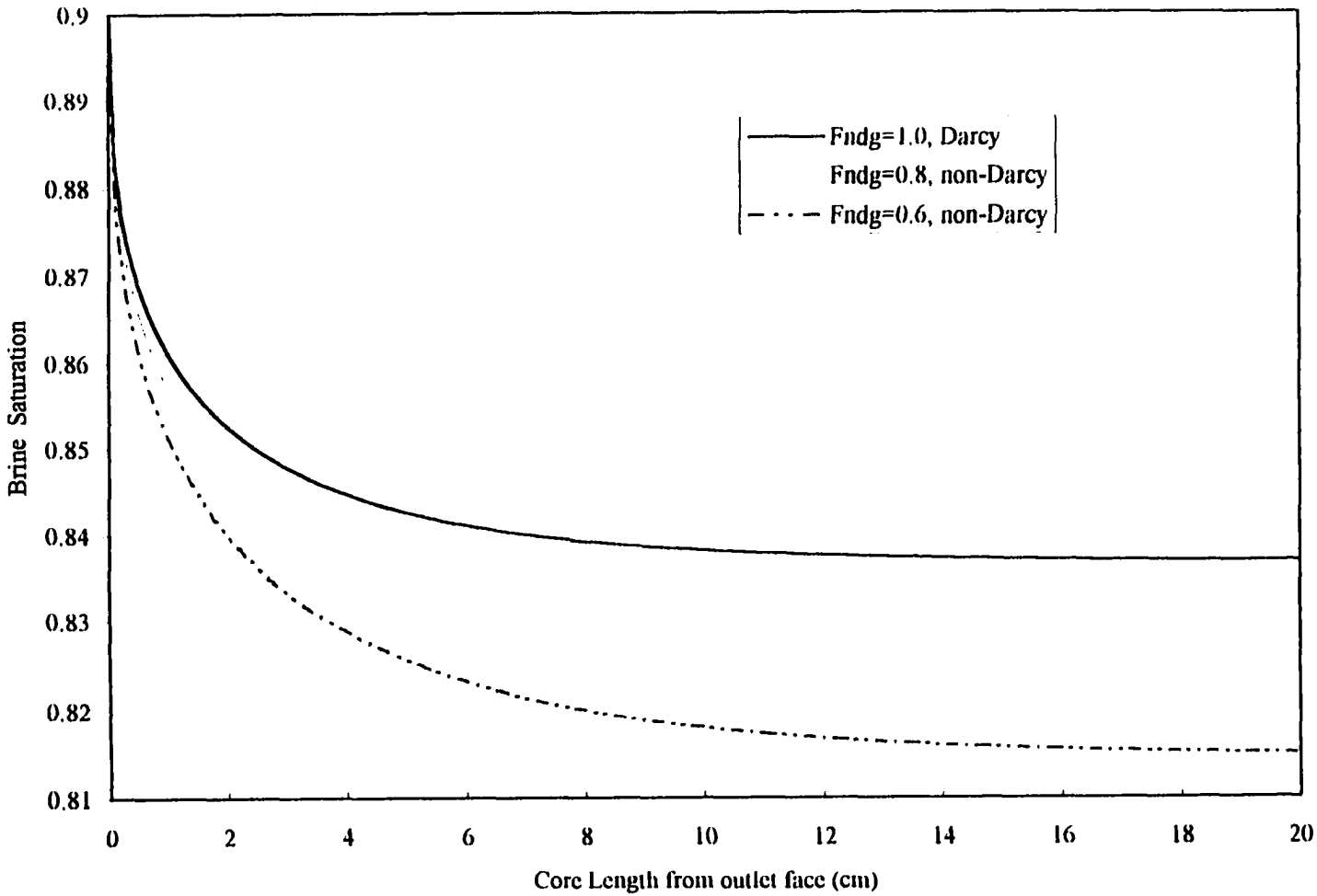


Fig. 7.40: Affect of non-Darcy on the saturation profiles .

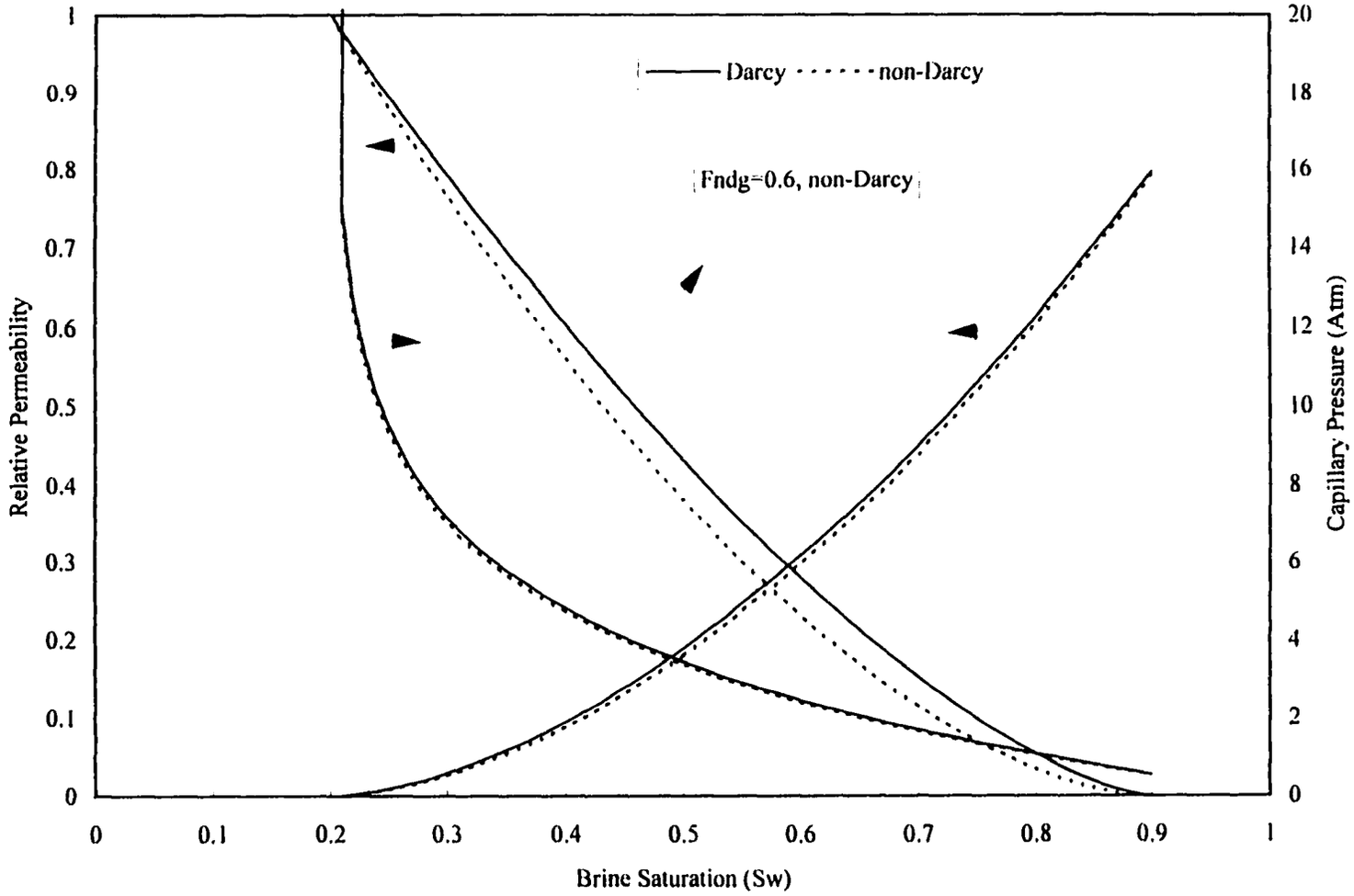


Fig. 7.41: Affect of non-Darcy flow on the relative pereability and capillary pressure curves.

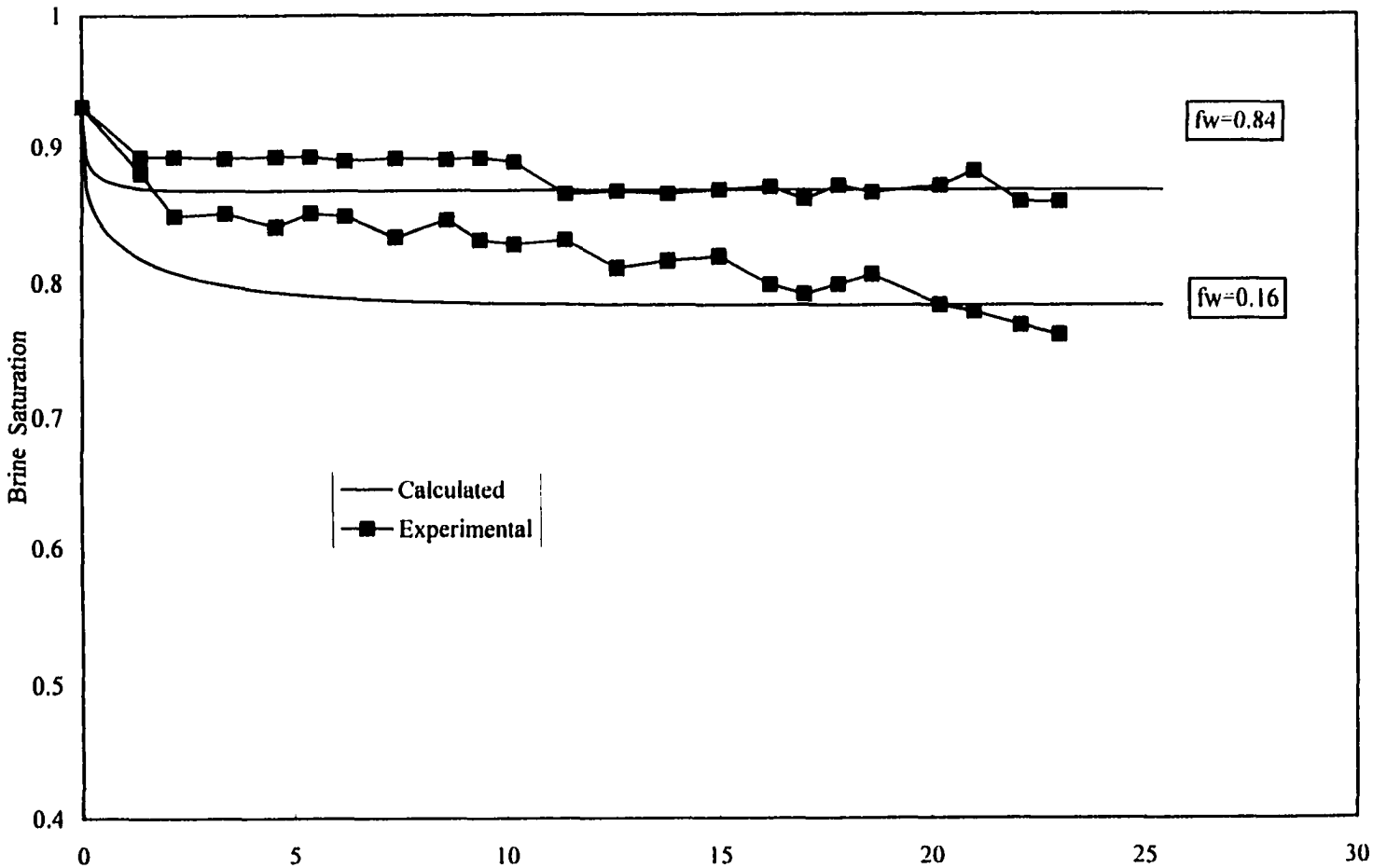


Fig. 7.42: Affect of non-Darcy on the saturation profiles .

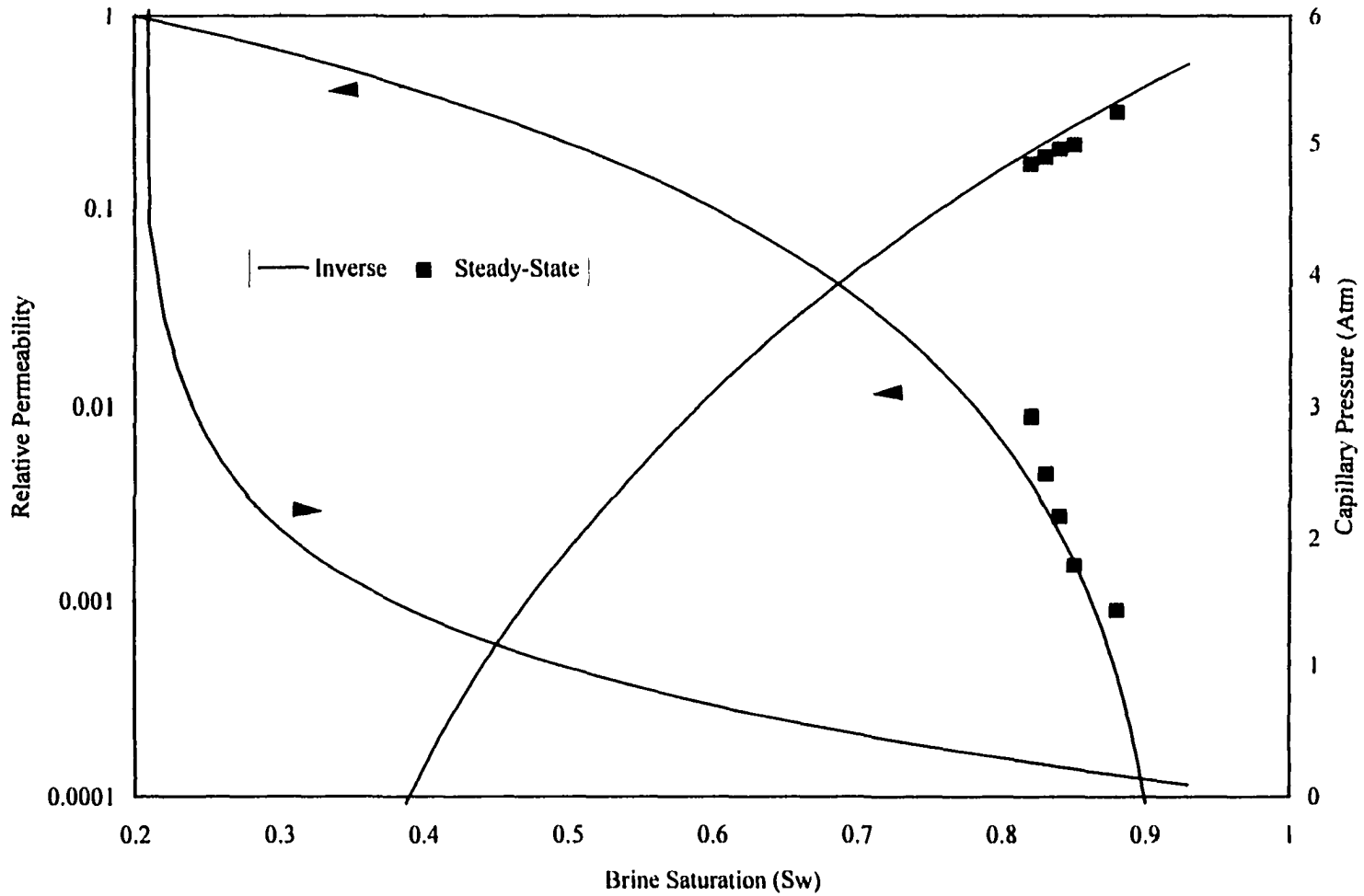


Fig. 7.43: Relative permeability and capillary pressure curves for nitrogen-water system.

CHAPTER VIII

CONCLUSIONS AND RECOMENDATIONS

The present study has demonstrated that a piece-wise functional representation of relative permeability and capillary pressure data from laboratory core fluid displacement data can be determined uniquely when the transient-state internal saturation profiles and the overall pressure differentials are used simultaneously for history matching. Global functional representations of relative permeability and capillary pressure data do not satisfactorily describe the flow functions. A discrete representation of the flow functions results in non-smooth functions.

A unique representation also requires that the number of estimated model parameters is less than or equal to the number of observable parameters and simulated annealing is a convenient method to achieve a global optimization for determining the best estimates of relative permeability and capillary pressure from laboratory core fluid displacement data.

An inverse model has been developed to determine relative permeability and capillary pressure curves from steady-state core flood tests. Instead of eliminating or minimizing the influence of capillary end effects, the capillary end effects have been used as an advantage to determine the relative permeability and capillary pressure curves. This interpretation method also reduces the required time frame to conduct tests. Relative permeability curvature of gas for non-Darcy flow has a higher curvature than Darcy's flow. Due to greater pressure dissipation in non-Darcy flow, the gas saturation develops more rapidly. Results indicate that non-Darcy flow is not negligible for estimation of relative permeability and capillary pressure curves particularly for gas/brine systems. The main difficulty in this method is the requirement of accurate saturation profiles by high resolution X-ray computer tomography, specifically at the ends of core.

However, for heterogeneous cores, the information on the permeability, porosity, initial water and residual oil saturation distributions along the core are also required.

NOMENCLATURE

a_i, b_i, c_i, d_i	cubic spline coefficients
A	cross sectional area (L^2)
B_w, B_o	formation volume factors of water and oil
J	objective function value
k	absolute permeability (L^2)
k_{rw}, k_{ro}	relative permeabilities of water and oil
k_{rw}^o, k_{ro}^o	end point relative permeabilities of water and oil
K_w, K_o	conductivities of water and oil (L^3T/M)
L	core length (L)
n_1, n_2, n_3	relative permeability and capillary pressure exponent
P	pressure ($M/L/T^2$)
$P_{initial}$	initial pressure ($M/L/T^2$)
$P_{specified}$	specified boundary pressure ($M/L/T^2$)
P_c	capillary pressure ($M/L/T^2$)
$P_{c,max}$	maximum capillary pressure ($M/L/T^2$)
q_w, q_o	volumetric productions of water and oil at standard conditions per unit time per unit reservoir volume(1/T)
Q	production rate (L^3/T)

S_w, S_o	saturations of water and oil
S_{wi}	initial water saturations
S_{wc}	connate water saturation
S_{or}	residual oil saturation
S_D	dimensionless saturation
t	time (T)
T	control parameter, temperature
u_w, u_o	darcy velocity for water and oil phases (L/T)
W_Q, W_p, W_s	weighting factors of production, pressure and displaced phase saturation data
x	distance (L)
z	vertical distance (L)
D	difference operator
m_w, m_o	viscosities of water and oil (M/L/T)
r_w, r_o	densities of water and oil (M/L^3)
g_w, g_o	specific weights of water and oil ($M/L^2/T^2$)
f	porosity

Subscripts and Superscript

c	data computed by finite difference method
k	time index for discrete sample values
i	space index for discrete sample values
m	measured data
s	standard condition

REFERENCES

Aarts, E.H.L., and Korst, J.H.M.: Simulated Annealing and Boltzmann Machines., Wiley, New York (1989).

Amyx, J.W, D.M. Bass, and R.L. Whiting: Petroleum Reservoir Engineering, McGraw-Hill Book Company., New York. (1960), p. 184-202.

Aziz, K. and A. Settari: Petroleum Reservoir Simulation, Applied Science Publisher Ltd., London (1979).

Bentsen, R.G., and Anli, J. : " A New Displacement Capillary Pressure Model," *Journal of Canadian Petroleum Technology,* Sept.-Oct. 1991, pp. 75-79

Bird, R.B., W.E. Stewart and E.N. Lightfoot : Transport Phenomena, Wiley, New York (1960).

Blick, E.F. and Civan, F. :" Porous-Media Momentum Equation for Highly Accelerated Flow," 1988 SPERE. (Aug.).

Blick, E.F., and Civan, F, "Porous Media Momentum Equation for Highly Accelerated Flow", SPE Reservoir Engineering, Vol. 3, No. 3 pp. 1048-1052, 1988.

Braun, E.D. and Blackwell, R.J.: " A Steady-State
Carter, R,D., Kemp, L.F. and Williams, D.:" Performance Matching with Constraints," Soc. Pet, Eng. J., (April 1974), 187-196.

Carter, R,D., Kemp, L.F. and Williams, D.:" Performance Matching with Constraints," Soc. Pet, Eng. J., (April 1974), 187-196.

Chardaire, C., G. Chavent, J. Jaffre and J. Liu: "Multiscale Representation for Simultaneous Estimation of Relative Permeabilities and Capillary Pressure", paper SPE 20501 presented at the 1990 Annual Technical Conf. and Exhibition, New Orleans, LA, Sept. 23-26, 1990.

Chardaire, C., G. Chavent, J. Liu and B. Bourbiaux: "Simultaneous Estimation of Relative Permeabilities and Capillary Pressure", paper SPE 19680 presented at the 1989 Annual Technical Conf. and Exhibition, San Antonio, TX, Oct. 8-11, 1989.

Chavent, G., Dupuy, M., and Lemonnier, P.:" History Matching by Use of Optimal Control Theory," Soc. Pet, Eng. J., (Feb. 1975) 74-86.

Chen, W.H., Gaqvalas, G.R., Seinfeld, J.H. and Wassermann, M.L.:"A New Algorithm for Automatic History Matching," Soc. Pet, Eng. J., (Dec. 1974) 593-608.

Christiansen, R. and Howarth, M.H. : "Literature Review and Recommendation of Methods for Measuring Relative Permeability of Anhydride from the Slado Formation at the Waste Isolation Pilot Plant (WIPP)," Report, SAND93-7074, Colorado School of Mines, July 1994.

Chung, M. and Catton, I.:" Multi-Dimensional Two-Phase

Flow in Porous Media with Phase Change", Heat Transfer, Houston, 1988, S.B. Yilmaz (Ed.), AIChE Symposium, New York, 1988, Vol. 84, No. 264, pp. 177-185.

Civan F. and R.D. Evans :" Relative Permeability and Capillary Pressure Data From Non-Darcy Flow of Gas/Brine Systems in Laboratory Cores," paper SPE 26151 presented at the 1993 SPE Gas Tech., Calgary, Alberta, Canada, Jun 28-30.

Civan, F. and Evans, R.D. :" Discussion of High Velocity in Porous Media," 1995 SPERE. (Nov.).

Civan, F. and R. D. Evans: "Non-Darcy Flow Coefficients and Relative Permeabilities for Gas/Brine Systems", paper SPE 21516 presented at the 1991 Soc. Pet. Eng. Gas Technology Symposium, Houston, TX, Jan. 23-25, 1991.

Datta Gupta, A., Vasco, D.W., and Long, J.C.S.:" Detailed Characterization of a Fractured Lime-stone Formation Using Stochastic Inverse Approaches," paper SPE/DOE 27744 presented at the 1994 symposium on improved oil recovery, Tulsa, OK, April 17-20.

Datta Gupta, A., Vasco, D.W., and Long, J.C.S.:" Detailed Characterization of a Fractured Lime-stone Formation Using Stochastic Inverse Approaches," paper SPE/DOE 27744 presented at the 1994 symposium on improved oil recovery, Tulsa, OK, April 17-20.

Dias, M. and A.C. Payatakes :"Network Models for Two-phase Flow in Porous Media Part 1. Immiscible

microdisplacement of non-wetting fluids," J. Fluid Mech. (1986) vol 164, pp. 305-336.

Dogru, A.H. and Seinfeld, J.H.:" Comparison of Sensitivity Coefficient Calculation Methods in Automatic History Matching," Soc. Pet, Eng. J., (Oct. 1981) 551-557.

Dullien, F.A.L.: Porous media: Fluid Transport and Pore Structure, Second Ed., Academic Press, San Diego (1992).

Eglese, R.W.: "Simulated Annealing: A Tool for Operational Research," European J. of Operational Research, (1990) **46**, 271-28

Ehrlich, R. and D.K. Davies: "Image Analysis of Pore Geometry: Relationship to Reservoir Engineering and Modeling," paper SPE 19054 presented at the 1989 SPE Gas Tech. Symp. ,Dallas, TX, June 7-9.

Eleri, 0.0, Graue, A., and Skauge, A.: " Steady-State and Unsteady-State Two Phase Relative Permeability Hystresis and Measurements of Three-Phase Relative Permeabilities Using Imaging Techniques", paper SPE 30764 presented at the 1995 Annual Technical Conf. and Exhibition, Dallas, TX, Oct. 22-25, 1995.

Enwere, M.P. and Archer, J.S.:" NMR Imaging for Core Flood Testing," SCA 9218 paper, 1992

Farmer, C. L.: "The Generation of Stochastic Fields of Reservoir Parameters with Specified Geostatistical

Distributions," Mathematics in Oil Production, Edwards, S.S. and King, P (eds), Clarendon Press, Oxford (July, 1988) 235-252

Farmer, C., Heath, D., and Moody, R.:" A Global Optimization Approach to Grid Generation," paper SPE 21236 presented at the 1991 SPE Symposium on Reservoir Simulation, Anaheim, CA, Feb. 17-20,

Farmer, C.L.: "The Mathematical Generation of Reservoir Geology",paper presented at the IMA/SPE European Conference on the Mathematics of Oil Recovery, Cambridge, July 25-27, 1989.

Farmer, C.L.: "The Mathematical Generation of Reservoir Geology", paper presented at the IMA/SPE European Conference on the Mathematics of Oil Recovery, Cambridge, July 25-27, 1989.

Fatt,I.:" The Network Model of Porous Media III. Dynamics Properties of Networks with Tube Radius Distributions", Trans. AIME, 207, 164-177.

Firoozabadi, A. and K. Aziz: "Relative Permeabilities from Centrifuge Data", *J. Can. Pet. Tech.* (Sept.-Oct., 1991) **30**, 5.

Heiba, A.A., M. Sahimi, L.E. Scriven and H.T. Davis : "Percolation Theory of Two-Phase Relative Permeability," SPE Res. Eng. (1992) 7, 123.

Helset, H.M., J.E. Nordtvedt, and S.M. Skjaveland: "Relative Permeabilities from Displacement Experiments with Full Account for Capillary Pressure," SPE Reserv. Eva. & Eng. (1998) April, 92.

Huang D. D and M. M Honarpour: "Capillary End Effects in Coreflood Calculations," *J. Pet. Sci. Eng,* (1998) **19**, p. 103-117.

Jones, L.G., Blount, E. M. and Glaze, O.H. :"Use of Short Term Multiple Rate Flow Tests to Predict Performance of Wells Having Turbulence," paper SPE 6133 presented at the 1976 Annual Technical Conf. and Exhibition, New Orleans, LU Oct. 3-6, 1976.

Jones, S.C. :" Using the inertial Coefficient, b To Characterize Heterogeneity in Reservoir Rock," paper SPE 16949 presented at the 1987 Annual Technical Conf. and Exhibition, Dallas, TX Sept. 27-30 1987.

Kadi, K.S. :" Non-Darcy Flow in Dissolved Gas-Drive Reservoirs," paper SPE 9301 ..

Kerig, P.D. and Watson, A.T.: "A New Algorithm for Estimating Relative Permeabilities from Displacement Experiments", *Soc. Pet. Eng. J.* (Feb. 1987) 103-112.

Khatib, Z.I., and S. Vitthal : "Use of Effective Medium Theory and 3-D Network Model to Predict Matrix Damage in Sandstone," paper SPER 19649 presented at the 1989 Ann. Meeting of the SPE, San Antonio, TX Oct. 8-11.

Kirkpatric, S., Gelatt, C.D., and Vecchi, M.P.: "Optimization by Simulated Annealing," Science. (1983) **220**, 671-680.

Kirkpatrick, S.: "Percolation and Conduction," Reviews of Modern Physics (1973) 45, 574

Koplik, J., and T.J. Lasseter : "Two-phase flow in random network models of porous media," SPE 11014, 1982.

Koplik, J.: "Creeping flow in two-dimensional networks," J. Fluid Mechanics, 119, 1982,pp. 219-247.

Koplik, J.: "Creeping Flow in Two-Dimensional Networks," J. Fluid Mech. (1982) 119, 219.

Lake, L.W.: Enhanced Oil Recovery, Prentice-Hall, Inc., New Jersey (1989).

Lin, C.-Y., and J.C. Slaterry : "Two-dimensional randomized network model for two-phase flow through porous media," A.I.Ch.E. J., 28, 1982, pp. 311-323.

Linda, R. Petzold :"Automatic Selection of Methods for Solving Stiff and Nonstiff Systems of Ordinary Differential Equations," SIAM J. Sci. Stat. Comput. **4** (1983), pp. 136-148

Long, J., Doughty, C., Hestir, K., and Martel, S.:" Modeling Heterogeneous and Fractured Reservoirs with Inverse Methods Based on Iterated Function Systems,"

Reservoir Characterization III, B. Linville (ed.), Pen Well Publishing Co., Tulsa, OK (1993).

Long, J., Doughty, C., Hestir, K., and Martel, S.:" Modeling Heterogeneous and Fractured Reservoirs with Inverse Methods Based on Iterated Function Systems," Reservoir Characterization III, B. Linville (ed.), Pen Well Publishing Co., Tulsa, OK (1993).

Lui, X., Civan, F. and Evans, R.D. :" Correlation of the Non-Darcy Flow Coefficient," *J. Can. Pet. Tech.* (Dec., 1995) **34**, 10.

Lvine, S. and D.L. Cuthiell :" Relative Permeabilities in Two-phase Flow Through Porous Media: An Application of Effective Medium Theory," Jour. Can. Pet. Tech, Sept.-Oct. 1986.

M.L.:"A New Algorithm for Automatic History Matching," Soc. Pet, Eng. J., (Dec. 1974) 593-608.

MacAllister, D.J., Miller, K.C, Graham, S.K. and Yang, C-T.:" Application of Xray CT Scanning to the Determination of Gas-Water Relative Permeabilities," paper SPE 20494 presented at the 1990 Annual Technical Conf. and Exhibition, New Orleans, Sept. 23-26.

Maini, B,B., Kokal, S. and Jha, K.:" Measurements and Correlations of Three-Phase Relative Permeability at Elevated Temperatures and Pressures, paper SPE 19677 presented at the 1989 SPE Annual Technical Conf. and Exhibition, San Antonio, TX, Oct. 8-11.

Marle, C.M.,: Multiphase Flow in Porous Media, Gulf Publishing Co., Houston. (1981).

Metropolis, M., Rosenbluth, M., Rosenbluth, A., Teller, A., and Teller E.: "Equation of State Calculations by Fast Computing Machines," J. Chem. Phys. (1953) **30**, 1087-1092.

Mitlin, S. V., McLennan J. D., and Green, G. S.: Simultaneous Determination of Two-Phase relative Permeability and Capillary Pressure of Porous Rocks from Steady-State Flow Experiments: Accounting for Gravitational Forces and Fluid Compressibility," *J. of Colloid and Interface. Sci.*, , No. 204, pp. 205-213, 1998.

Mohanti, K.,K. and J.S. Salter :"Multiphase Flow in Porous Media: II. Pore-Level Modeling," paper SPE 11018 presented at the 1982 Ann. Meeting of the SPE, New Orleans, LA, Sept 26-29.

Ning, X, and Holditch, S. A.: "The Measurement of Gas relative Permeability for Low permeability Cores Using a pressure Transient Method," paper SCA 9013 presented at the Fourth Ann. SCA Tech. Conf., Dallas, TX, August 15-16, 1990.

Nolen, J. S. and Berry, D.W.:" Tests of stability and time step sensitive of semi implicit reservoir simulation techniques," Trans. SPE of AIME, **253** (1972), pp. 253-266.

Noman, R. and Archer, J.S. :" High-Velocity Gas Flow in Liquid-Saturated Porous Media and its Visualization," *J. Can. Pet. Tech.* (May-June, 1988) **27**, 3.

O'Meara Jr. D.J. and Crump, J.G.: "Measuring Capillary Pressure and Relative Permeability in a Single Centrifuge Experiment," paper SPE 14419 presented at the 1985 SPE Annual Technical Conference and Exhibition, Las Vegas, NV, Sept.22-25.

Ouenes, A., and Saad. N.:"A New Fast Parallel Simulated Annealing Algorithm for Reservoir Characterization," paper SPE 26418 presented at the 1993 SPE Annual Technical Conference and Exhibition, Houston, TX, Oct.3-6.

Ouenes, A., G. Fasanino, and R. Lee: "Simulated Annealing for Interpreting Gas/Water Laboratory Corefloods", paper SPE 24870 presented at the SPE Annual Technical Conference and Exhibition, Washington, D.C., Oct. 4-7, 1992.

Ouenes, A., Meunier, G., Pelce V., and Lhote, I. : "Enhancing Gas Reservoir Characterization by Simulated Annealing Method (SAM)," paper SPE 25023 presented at the 1992 European Petroleum Conference, Cannes, France, Nov. 16-18.

Panda, M.N., and Lake, L.W. : " Parallel Simulated Annealing for Stochastic Reservoir Modeling," paper SPE 26418 presented at the 1993 SPE Annual Technical

Conference and Exhibition, Houston, TX, Oct. 3-6.

Payatakes, A. C. Chi Tien and R. M. Turian :"A New Model for Granular Porous Media. Part I. Model Formulation; AIChE. J., 19, 58 (1973a)

Purcell, W.R.: "Capillary Pressures - Their Measurement Using Mercury and the Calculation of Permeability Therefrom," Pet. Trans. AIME 39 (1949).

Ramakrishnan, T.S. and Cappiello, A.:" A New Technique to Measure Statistical and Dynamic Properties of a Partially Saturated Porous Medium," *Chem. Eng. Sci.*, Vol. 46, No. 4, pp. 1157-1163, 1991.

Relaitis, G.V., Ravindran, A., and Ragsdell, K.M.: Engineering Optimization Methods and Application, John Wiley & Sons, Inc., New York (1983) 98.

Richardson, J.G., Kerver, J.K., Hafford, J.A. and Osaba, J.S.: " Laboratory Determination of Relative Permeability," *Trans. SPE of AIME,* (1952), pp.187-96.

Richmond, P.C. and Watson, A.T.:" Estimation of Multiphase Flow Functions from Displacement Experiment," *Soc. Pet. Res. Eng.* (Feb. 1990) 121-127.

Rossen, W.R. and A.T.A. Kumar : "Single and Two-Phase Flow in Natural Fractures," paper SPE 24915 presented at the 1992 Ann. Meeting of the SPE, Washington, DC, Oct 4-7.

Satik, C., Ambusso, W., Castanier, M.L., and Horne, R.N.:"A Preliminary Study of Relative Permeability in Geothermal Rocks," paper presented at 1995 Annual Meeting Geothermal Resources Council , Reno, NV, Oct 8-11, 1995.

Schulenberg, T. and U. Muller :"An Improved Model for Two-Phase Flow Through Beds of Coarse Particles", Int. J. Multiphase Flow, Vol. 13, No. 1, 87-97,1987.

Sen, M.K., Data, G.A., Stoffa, P.L., Lake, L.W., Pope, G.A.: " Stochastic Reservoir Modeling Using Simulated Annealing and Genetic Algorithm," paper SPE 24754 presented at the 1992 SPE Annual Technical Conference and Exhibition, Washington, DC, Oct. 4-7.

Sharma,M.M. and Y.C. Yortsos:" A Network Model for Deep Bed Filtration Processes," AIChE. J., 33, 1644-1653 (October 1987)

Sheldon, J. W., Zondek, B. and Cardwell, W. T, :" One Dimensional, Incompressible, Non-Capillary, Two Phase Fluid Flow in Porous Medium," Trans. SPE of AIME, **216** (1959), pp. 290-296.

Stewart, C.R. and Owens, W.W. :" A Laboratory Study of Laminar and Turbulent Flow in Heterogeneous Porosity Limestones," Trans. SPE of AIME, (1952), pp. 121-1

Stone, H.L and Garder, A. O., Jr. :" Analysis of Gas-Cap or Dissolved-Gas Reservoirs," Trans. SPE of AIME, **222**

(1961), pp. 92-104.

Szucs, P. and Civan, F.:"Multi-layer Well Log Interpretation Using the Simulated Annealing Method," J. Petr. Sci. & Eng., **14** (1996), pp. 209-220.

Tarantola, A.: Inverse Problem Theory, Elsevier Science Publishers, New York, (1987) 167

Toth, J.,Bodi, T.,Szucs, P. and Civan, F.: "Practical Method for Analysis of Immiscible Displacement in Laboratory Core Test," Transport in Porous Media, Kluwer, Academic Pub., (1998), **31**, p. 347-363.

Tutu, N.K., Ginsberg, T. and Chen, J.C. : " Interfacial Drag for Two-Phase Flow Through High Permeability Porous Beds,"

Ucan, S., F. Civan, and R. D. Evans : "Simulated Annealing for Relative Permeability and Capillary Pressure from Unsteady-State Non-Darcy Displacement", SPE paper No. 26670, proceedings of the 1993 SPE Annual Technical Conf. and Exhibition, Houston, TX, Oct. 3-6 1993, pp. 673-687.

Ucan, S., Civan, F. and Evans, R.D. :" Uniqueness and Simultaneous Predictability of Relative Permeability and Capillary Pressure by Discrete and Continuous Means," *J. Can. Pet. Tech.* (April., 1997) **36**, pp. 52-61.

Ucan, S. and Civan, F. : "Simultaneous Estimation of Relative Permeability and Capillary Pressure for Non-

Darcy Flow Steady-State," SPE paper No. 35271, proceedings of the 1996 SPE mid-continent Gas Symposium, Amarillo, TX, Apr. 28-30 1996, pp. 155-163.

S. Ucan : "Pore Scale Modeling", in Evans, R.D. and Civan, F.," Characterization of Non-Darcy Multiphase Flow In Petroleum Bearing Formation", the final report, Under Contract No DE-AC22-90BC14659, U.S. Department of Energy, April, 1994.

Ward, J. S. and Norman, N. R. :" Capillary Pressure and Gas Relative Permeabilities of Low-Permeability Sandstone," SPEFE. (Sept. 1987) 345-355.

Wattenberger, R. A. and Ramey, H.J.:" Gas Well Testing with Turbulence, damage and wellbore storage." *Trans. SPE of AIME,* 243, pp. 877-87 (JPT)

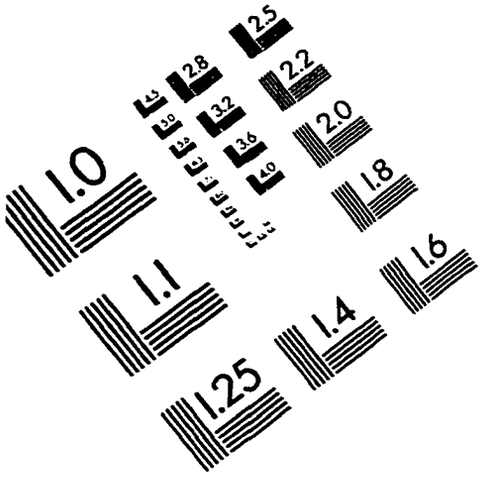
Whitney, D.D. and Evans, R.D. :"The Influence of Temperature, Effective Stress and non-Darcy flow on the Fracture Flow Capacity of Propped Fractures," proceedings of Symposium International Rock of Great Depth, Pau France, Aug. 28-31, 1989.

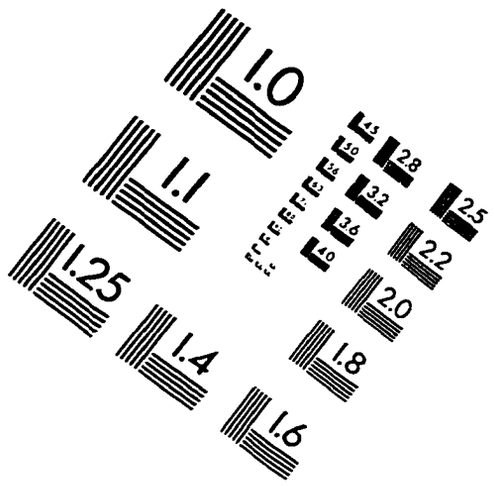
Yuan, H. H.: "Resolving Pore-Space Characteristics by Rate Controlled Poresimetry," SPE Formation Evaluation Journal (March 1989) 17-24.

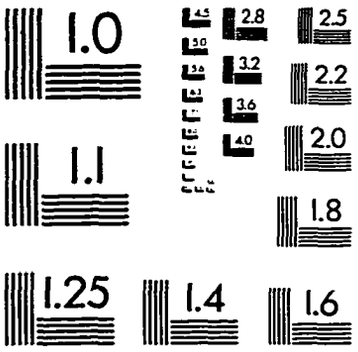
Zhou, C.D., Gao, C.Q., Jin, Z.W., and Wu, X.L.:"A Simulated Annealing Approach to Constrained Nonlinear Optimization of Formation Parameters in Quantitative Log

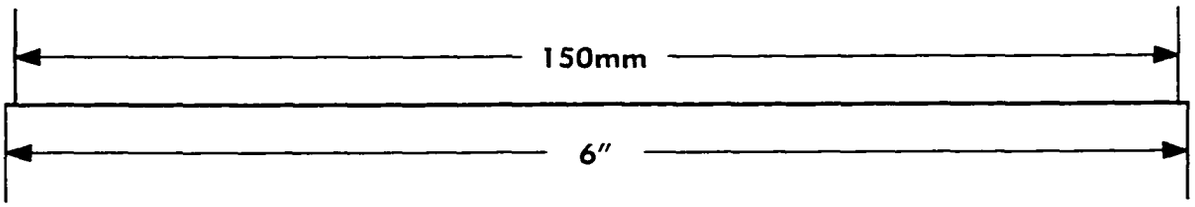
Evaluation," paper SPE 24723 presented at the 1992 SPE Annual Technical Conference and Exhibition, Washington, DC, Oct. 4-7

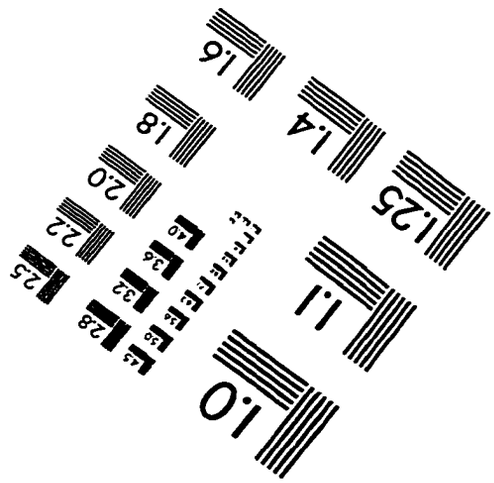
IMAGE EVALUATION
TEST TARGET (QA-3)

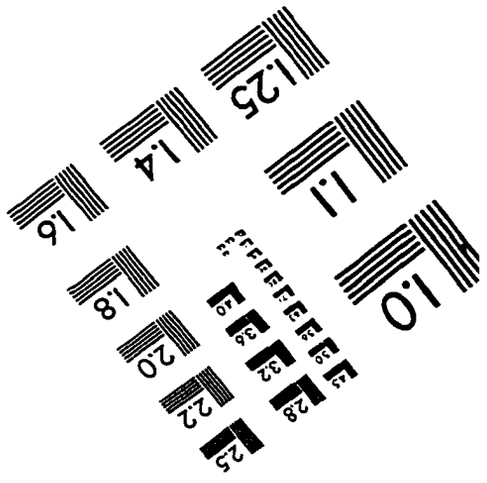












APPLIED IMAGE, Inc
1653 East Main Street
Rochester, NY 14609 USA
Phone: 716/482-0300
Fax: 716/288-5989

© 1993, Applied Image, Inc., All Rights Reserved